UNIVERSITA' DEGLI STUDI DI

MILANO - BICOCCA

Facoltà di Scienze MM. FF. NN

Corso di Dottorato in Biotecnologie Industriali

XXIV ciclo

DESIGN OF SMART BIOMATERIALS

PhD Student: Laura Russo

Supervisor: Prof. Laura Cipolla

PhD Coordinator: Prof. Marco Vanoni

2011

"Don't play what's there. Play what's not there"

Miles Davis

"Il Carbonio. E' di nuovo tra noi, in un bicchiere di latte. E' inserito in una lunga catena, molto complessa, tuttavia tale che quasi tutti i suoi anelli sono accetti al corpo umano. Viene ingoiato: e poiché ogni struttura vivente alberga una selvaggia diffidenza verso ogni apporto di altro materiale di origine vivente, la catena viene meticolosamente frantumata, e i frantumi, uno per uno, accettati o respinti. Uno, quello che ci sta a cuore, varca la soglia intestinale ed entra nel torrente sanguigno: migra, bussa alla porta di una cellula nervosa, entra e soppianta un altro carbonio che ne faceva parte. Questa cellula appartiene a un cervello, e questo è il mio cervello, di me che scrivo, e la cellula in questione, ed in essa l'atomo in questione, è addetta al mio scrivere, in un gigantesco minuscolo gioco che nessuno ha ancora descritto. E' quella che in questo istante, fuori da un labirintico intreccio di sì e di no, fa sì che la mia mano corra in un certo cammino sulla carta, la segni di queste volute che sono segni; un doppio scatto, in su e in giù, fra due livelli d'energia guida questa mia mano ad imprimere sulla carta questo punto: questo."

Il sistema periodico - Primo Levi

Preface

The work described in this thesis was conducted from 2008, to 2011 in the Department of Biotechnology and Biosciences at the University of Milano-Bicocca, Italy, under the guidance of Prof. Laura Cipolla.

The work on Hybrid Materials (**Chapter 4**) was conducted from May until October 2010 in the Department of Materials at the Imperial College of London, United Kingdom, under the guidance of Dr. Julian R. Jones.

Manuscripts published to peer-reviewed journals:

1. Sugar-decorated hydroxyapatite: an inorganic material bioactivated with carbohydrates. L. Russo, E. Landi, A. Tampieri, A. Natalello, S.M. Doglia, L. Gabrielli, L. Cipolla, F. Nicotra. *Carbohydrate Research* 346(12), 1564-8. **2011** .

2. Diazo transfer on material surfaces: a novel method for azido functionalisation. L. Russo, S. Zanini, C. Riccardi, F. Nicotra, L. Cipolla. *Materials Today* 14(4), 164-169. **2011**.

3. Kdo: a critical monosaccharide for bacteria viability. L. Cipolla, L. Gabrielli, D. Bini, L. Russo and N. Shaikh. *Nat. Prod. Rep.,* 27, 1618-1629. **2010**.

4. Ultrasonic assisted Fischer glycosylation: generating diversity for glycochemistry, N. Shaikh, L. Russo, L. Cipolla, F. Nicotra. *Molecular Diversity,* 15:341–345**. 2010,**

5. Discovery and design of carbohydrate-based therapeutics. L. Cipolla, A.C. Araújo, D. Bini, L. Gabrielli, L. Russo, N. Shaikh. *Exp. Opin. Drug Discov*. 5 (8), 721-737. **2010**.

6. Molecular dynamics investigation of cyclic natriuretic peptides: Dynamic properties reflect peptide activity. E. Papaleo, L. Russo, N. Shaikh, L. Cipolla, P. Fantucci, L. De Gioia. *J. Mol. Graph. Model*. .28:834-841. **2010**.

7. Carbohydrate Mimetics and Scaffolds: Sweet Spots in Medicinal Chemistry. L. Cipolla, B. La Ferla, C. Airoldi, C. Zona, A. Orsato, N. Shaikh, L. Russo, F. Nicotra, *Future medicinal Chemistry*, 2:587-599. **2010**.

8. C-type natriuretic peptide: structural studies, fragment synthesis and preliminary biological evaluation in human osteosarcoma cell lines. N. Shaikh, L. Russo, E. Papaleo, P. Giannoni, L. De Gioia, F. Nicotra, R. Quarto, L. Cipolla. *Wiley Periodicals, Inc. Biopolymers (Pept Sci).* 94: 213–219. **2010**.

9. Carbohydrate scaffolds in chemical genetic studies. F. Nicotra, L. Cipolla, B. La Ferla, C. Airoldi, C. Zona, A. Orsato, N. Shaikh, L. Russo. *J. Biotechnol.* 144 (3):234-241. **2009**.

10. Solid-phase supported mimic of GDP-L-galactose. B. La Ferla, L. Russo, C. Airoldi, F. Nicotra. *Tetrahedron: Asymm. (20), 744-745.* **2009**.

Book chapters

1. Materials biofunctionalization for tissue regeneration. Laura Cipolla, Laura Russo, Nasrin Shaikh, Francesco Nicotra POLYMERIC BIOMATERIALS III ED, Vol. I Polymers as Biomaterials CRC Press, **2010**

2. Underexploited targets in LPS biogenenesis for the design of antibacterials Laura Cipolla,* Luca Gabrielli, Davide Bini, and Laura Russo CABI, Nosworthy Way, Wallingford OX10 8DE, UK. **2011**, Accepted.

3. Trehalose mimetics as inhibitors of trehalose processing enzymes. D. Bini, F. Cardona, L. Gabrielli, L. Russo and L. Cipolla. *Carbohydrate Chemistry*, **2012**, 1-44. DOI: 10.1039/9781849732765 Accepted.

Parts of this work were presented at conferences:

1. "Plasma coupled to chimica grafting: collagen functionalization for nano medicine applications". S. Panseri, L. Cipolla, L. Russo, S. Zanini, C. Riccardi, A. Russo, M. Marcacci, A. Fiorani, C. Gualandi, M. L. Focarete and F. Nicotra *TechConnect World Conference and Expo 2011*, June 13-16, **2011**, Boston, Massachusetts, U.S.A.

2. "Azido functionalization of material surfaces by diazo transfer reaction" L. Cipolla, L. Russo, S. Zanini, L. Gabrielli, C.Riccardi, F. Nicotra.. *Congresso Nazionale di Biomateriali SIB 2011*, 23-25 Maggio **2011**, Bari

3. "PCL grafting with monosaccharides". L. Russo, A. Gloria, R. De Santis, L. Cipolla, L. Ambrosio, F. Nicotra. (2011). *Congresso Nazionale di Biomateriali SIB 2011*, 23-25 Maggio **2011**, Bari (IT).

4. "Click chemistry between monosaccharides and inorganic biomaterial" L. Russo, L.Gabrielli, D. Bini, L. Cipolla, F. Nicotra. *5th Glycan Forum*, Berlin, March 10-12, **2011**

5. "Collagen and Nanofibrous Scaffold Functionalisation by Plasma coupled to chemical grafting" L. Cipolla, L. Russo, C. Lupo, S. Zanini, C. Riccardi, S. Panseri, A. Russo, M. Marcacci, A. Fiorani, C. Gualandi, M. L. Focarete and F. Nicotra. *24th European Conference on Biomaterials*. Dublin - Ireland **2011**.

6. "PCL Grafting With Small Biomolecules" L. Russo, C. Lupo, A. Gloria, R. De Santis, L.Cipolla, F. Nicotra. *24th European Conference on Biomaterials*. Dublin - Ireland 2011.

7. "Diazo transfer on material surfaces: a novel method for azido functionalisation". L. Cipolla, L.Russo, S. Zanini, D. Bini, C. Riccardi, F. Nicotra. *24th European Conference on Biomaterials*. Dublin - Ireland **2011**

8. "Silica/Peg sol gel process toward new hybrid materials". L. Russo, E. Valliant, L. Gabrielli, L. Cipolla, J.R. Jones. *24th European Conference on Biomaterials*. Dublin - Ireland **2011**

9. *"New silica/PEG hybrids for bone tissue engineering"*. J.R. Jones, L. Russo, E. Valliant, L. Cipolla. *Hybrid Materials* **2011**, 6-10 March, Strasbourg – France.

10. *"C-type natriuretic peptide for tissue engineering applications"*. L. Russo, N. Shaikh, L. Cipolla, F. Nicotra, R. Quarto, P. Giannoni, *14th IBS*, 14-18th September **2010**, Rimini.

11. "Hydroxyapatite three-dimensional scaffold: biofunctionalisation by plasma technology and biological evaluation". L. Russo, N. Shaikh L. Cipolla, F. Nicotra, C. Riccardi, S. Zanini, E. Landi, F. Valentini, A. Tampieri, R. Quarto, P. Giannoni, *14th IBS,* 14-18th September **2010**, Rimini.

12. "Preliminary evaluation of C-type natriuretic peptide and its fragments for tissue engineering applications" L. Russo, L. Cipolla, N. Shaikh, F. Nicotra, P. Giannoni, R. Quarto - Congresso Nazionale SIB camogli (GE) 24-26 May **2010**.

13. "Carbonated Hydroxyapatite Biofunctionalisation with Carbohydrates" L. Russo, N. Shaikh, L. Cipolla, F. Nicotra, M. Sandri, A. Tampieri. *2nd European Conference on Biomaterials*. Losanna, CH. Settembre **2009**.

14. "Covalent Biofunctionalisation of hydroxyapatite scaffolds *via* plasma technology". F. Nicotra, L. Russo, N. Shaikh, L. Cipolla, S. Zanini, C. Riccardi, R. Ziano, F. Valentini, E. Landi. *22nd European Conference on Biomaterials*. Losanna, CH. Settembre **2009**.

15. "Silanisation of Carbonate substituted Hydroxyapatite toward Covalent Biodecoration". - L. Cipolla, N. Shaikh, L. Russo, F.

Nicotra, E. Landi, A. Tampieri. *22nd European Conference on Biomaterials*. Losanna, CH. Settembre **2009**.

16.   "Chemoselective "glycosilation" of Biomaterials" - F. Nicotra, N. Shaikh, L. Russo, L. Cipolla. *Eurocarb 15 Symposium*. Vienna - Austria. Luglio **2009**.

17.   "Azidoalkyl and propargyl glycosides from unprotected monosaccharides towards chemoselective ligation". F. Nicotra, L. Russo, N. Shaikh, L. Cipolla. *Eurocarb 15 Symposium*. Vienna - Austria. Luglio **2009**.

18.   "GDP-L-Galactose Mimic for Affinity Chromatography"- B. La Ferla, L.Russo, C.Airoldi, F. Nicotra. *X Convegno – scuola sulla chimica dei carboidrati.* Certosa di Pontignano – Siena. Giugno **2006**.

19.   "Functionalisation of a hydroxyapatite three-dimensional scaffold by plasma technology and biological evaluation". L. Cipolla, L. Russo, N. Shaikh F. Nicotra, C. Riccardi, S. Zanini, E. Landi, A. Tampieri, F. Valentini, P. Giannoni, R. Quarto. *Congresso Nazionale SIB* camogli (GE) 24-26 May **2010**.

20.   "Synthesis of ligands for Carbohydrate processing enzymes of relevant biological interest". L. Gabrielli, S. Merlo, C. Airoldi, D. Bini, N. Shaikh, L. Russo, L. Cipolla, F. Nicotra. Italian-Spanish Joint Workshop Milano (Italy), 22 April **2010**.

21.   "Design of Smart Biomaterials". L. Russo, N. Shaikh, C. Airoldi, S. Merlo, E. Sironi, D. Bini, L. Gabrielli, L. Cipolla, F.

Nicotra. *Italian-Spanish Joint Workshop* Milano (Italy), 22 April **2010**.

Table of Content

Chapter 1

Chapter 2

Chapter 3

Chapter 4

Chapter 5

Chapter 6

6.   Materials and methods

Chapter 1

1. Introduction

Humankind's use of materials to augment or repair the body dates to antiquity, when natural materials such as wood were used in an attempt to structurally replace tissues lost to disease or trauma. Historically, selection of material was based on availability and the ingenuity of the individual making and applying the prosthetic. In the early part of the twentieth century, naturally derived materials began to be replaced by synthetic polymers, ceramics and metal alloys, which provided better performance, increased functionality and more reproducibility than their naturally derived counterparts. These advances led to a pronounced increase in the range of use and the efficacy of biomaterials, as a result of which millions of lives have been saved or improved by devices such as vascular stents, dental restoratives, artificial hips and contact lenses. On the basis of their application, biomaterials were defined as types of material used in a medical device, and the academic foundation of the field lay in materials science and classical engineering. Materials were desired to perform largely mechanical functions: to prevent biological rejection, which hampered device performance and patient health[1] , it was preferable that they be 'inert' and not interact with the biology of the host organism. Early research and fortuitous accidents linking materials chemistry to biological response provided a rational basis for developing new biomaterials.[2] The molecular biology revolution

of the 1970s and advances in genomics and proteomics in the 1990s and 2000s, however, significantly affected the ways in which biomaterials are designed and used. It is well known that a series of interactions occur between the surface of biomaterials and the biological environment after they have been implanted into the human body. Therefore, the biomaterials surface plays an extremely important role in the response of artificial medical devices to the biological environment.

The efficacy of artificial implants is determined mainly by their surface characteristics such as surface morphology, microstructure, composition, and properties. These properties alter adsorption of proteins which mediate the adhesion of desirable and undesirable cells[3]. Research on biomaterials surface has become one of the hottest topics in biomaterials and biomedical engineering. The highest score for a keyword in the World Biomaterial Congress in 2008 (WBC 2008) is Biomaterials Surface, indicating that the current research focus of the biomaterials community is aimed at understanding the fundamental processes at the interface between implant surfaces and surrounding living tissues. It is also generally agreed that human biology and nature should be considered in the design of functionalized biomaterials[4].

However, in nearly every case, these materials were adopted from other areas of science and technology without substantial redesign for medical use. Although these materials helped usher in new medical

treatments, critical problems in biocompatibility, mechanical properties, degradation and numerous other areas remain. To this end, scientists are creating new materials including those with improved biocompatibility, stealth properties, responsiveness (smart materials), specificity and other critical properties. Modern biomaterials science is characterized by a growing emphasis on identification of specific design parameters that are critical to performance, and by a growing appreciation of the need to integrate biomaterials design with new insights emerging from studies of cell–matrix interactions, cellular signalling processes, and developmental and systems biology[5].

1.1 Tissue engineering and the biomimetic approach

A variety of new materials are being synthesized from man-made building blocks, and being used to create devices for specific medical applications. Materials composed of naturally occurring (biologically derived) building blocks, including extracellular matrix (ECM) components, are being studied for applications such as direct tissue replacement and tissue engineering. The ECM, a complex composite of proteins, glycoproteins and proteoglycans, provides an important model for biomaterials design[6].
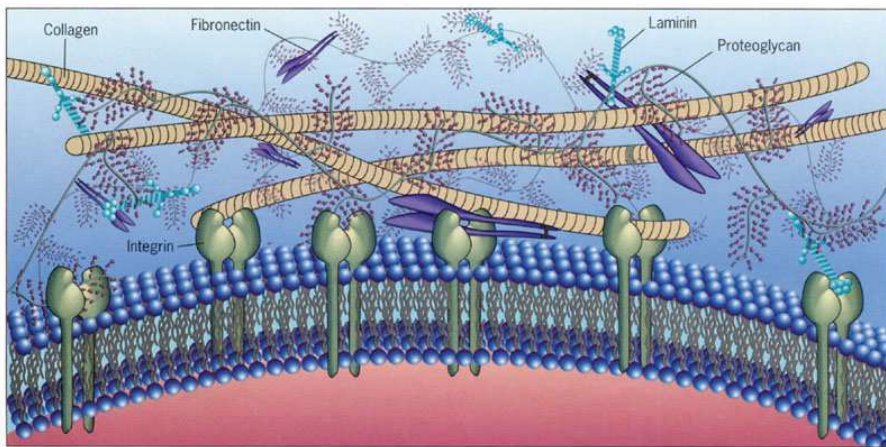
Figure 1.1 ECM components

ECM-derived macromolecules (for example, collagen) have been used for many years in biomaterials applications[5] and it is now possible to create artificial analogues of ECM proteins using recombinant DNA technology[7]. Tissue engineering is an advanced interdisciplinary field that encompasses the design of biomaterials for *in vivo* tissue regeneration where mimicking the natural extracellular matrix (ECM) is often pursued. The natural ECM supports organ and tissue structure and function, and also regulates basic cellular events like proliferation, growth, migration, differentiation, and survival. These functions are controlled through tissue-specific constituents, such as collagens, laminins, fibronectin or elastins, as well as functional molecules like growth factors or matricellular proteins, among others. Novel biomaterials should allow for the gradual endogenous remodeling of

4

native tissue leading to the replacement of implant material, manufactured to replace a missing biological structure, with fully functional ECM and cells that existed at the implant site prior to damage.

The critical point during *in vitro* tissue engineering is to at least partially recreate conditions that mimic the natural ECM environment for particular cell types in order to support their function. Since cell contact with the biomaterial surface significantly influences cell behavior and performance, trends in biomaterial designs lean towards bioactive materials that can modulate and control cell behavior. In recent years, biomaterial designs have focused on the exposition and incorporation of signaling molecules into scaffold materials rather than using them in a diffusive or soluble[8]. Among the most studied molecules are multifunctional proteins like growth factors[9,10,11,12] or cytokines,[13] while there are also reports on the incorporation of small molecules like neurotransmitters into scaffold materials (**Figure 1.2**).[14]
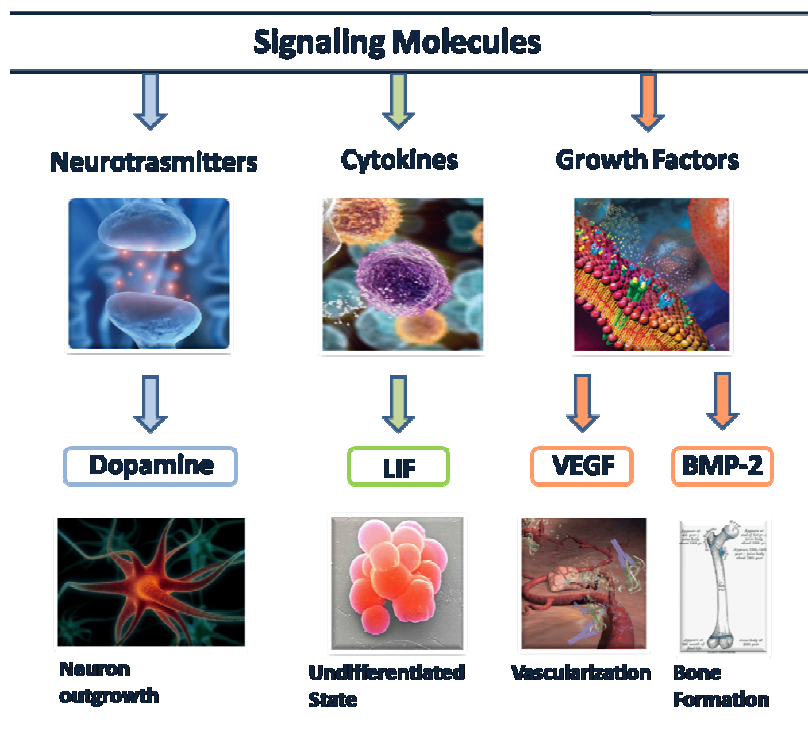
Figure 1.2. Examples of signaling molecules modulating cell behavior in bioactive materials for tissue engineering.

The outer membrane of a typical cell is covered by specific carbohydrate structures and a forest of at least six different receptor systems that can be activated by interactions with adjacent cells, ligands in the surrounding ECM, and secreted signaling molecules. Hundreds of different proteins play a role in the composite stimulation of cell receptors, which in turn determine a plethora of responses, including cell migration in the early embryo, coordinated

organogenesis, and wound repair throughout adult life[15], [16],[1718],[19]. Collectively, these extrinsic factors make up a highly defined and specialized cell microenvironment, which is essential for correct tissue development and continued function.

The ECM takes a variety of forms in different tissues and at different stages of development in the same tissue[20]. Diversity arises through combinations of specific molecular interactions between numerous isoforms, ratios, and geometrical arrangements of collagens, elastins, proteoglycans, and adhesion proteins such as fibronectins and laminins. This creates an environment that is replete with informational cues. In addition to this, a wealth of molecular mechanisms modulates the dissemination of this information[21].

1.2 New applications of functionalised materials: diagnostics and array technologies

Much of the preceding discussion has focused on the development of materials that display biological information, often in the form of peptide or protein domains, for the purpose of controlling cell and tissue behaviour. Various platforms of nanostructured mterials can be used in different aspects of medicine like diagnostics and therapeutics.

Nanoparticle technologies are significantly impacting the development of both therapeutic and diagnostic agents. At the

intersection between treatment and diagnosis, interest has grown in combining both paradigms into clinically effective formulations. This concept, recently coined as theranostics[22], is highly relevant to agents that target molecular biomarkers of disease and is expected to contribute to personalized medicine. Major classes of nanoparticles include, drug conjugates and complexes, dendrimers, vesicles, micelles, core–shell particles, microbubbles, and carbon nanotubes[23].

Nanotechnology has also found its use in diagnostic medicine as contrast agents, fluorescent dyes and magnetic nanoparticles (**Table 1.1**).

To date, nearly 30 nanotechnology-based products have been approved for clinical use, focused mainly on liposomal formulations and stealth polymer–drug conjugates. In addition to therapeutic nanoparticles for drug delivery, important topics include:

1. biomimetic nano- or micro-structured materials for tissue engineering and regenerative medical applications,
2. nanobiosensors, particularly those lab-on-chip-based systems for disease diagnosis at the point of care,
3. nano-probes for in vivo sensing/imaging, cell tracking and monitoring disease pathogenesis or therapy and
4. nanotechnology-based tools that accelerate scientific discovery and elucidation of basic biology[24].

Table. Some nanoparticles used for medical applications*				
Study phase	Product	Description	Use	Manufacturer
Preclinical	MRX 952	Nanoparticle preparation – to encapsulate camptothecin analogues	Tumours	IMA Rx Therapeutics
Preclinical	Targeted Nano Therapeutics (TNT)™ system	TNT with polymer coated iron oxide magnetic particle	Solid tumours	Triton Biosystems
Preclinical	AuroLase™	Gold nanoshell	Head and neck cancer	Nanospectra Biosciences Inc
Preclinical	Dendrimer-Magnevist*	PAMAM dendrimer	MRI imaging agent	Dendritic Nanotechnologies Inc
Phase 1	VivaGel*	Dendrimer based microbicide gel	HIV prevention	Starpharma Pty Ltd
Phase 1	INGN 401	Nanoparticle formulation of tumour suppression gene FUS1	Lung cancer	Introgen Therapeutics Inc
Phase 1&2	Cyclosert-Camptothecin – IT 101	β-Cylcodextrin polymer drug delivery system	Solid tumours	Calando Pharmaceuticals
Phase 2	VivaGel*	Dendrimer based microbicide gel	HSV prevention	Starpharma Pty Ltd
Phase 2	MRX 815	Nanobubble technology	Treatment of intravascular clot	IMA Rx Therapeutics
Phase 3	Combidex* / Ferumoxtran 10	Iron oxide nanoparticle	MRI contrast agent	AMAG Pharmaceuticals
Marketed	Abraxane*	Albumin bound taxane particles	Non small cell lung cancer	Abraxis Oncology
Marketed	AmBisome*	Liposomal preparation of amphotericin B	Fungal infection	Astellas Pharma US
Marketed	Doxil*	Liposomal doxorubicin	Ovarian tumour	Ortho Biotech

* Information obtained from respective company webpage on internet
ª Available at Nanotechnology Characterization Laboratory Webpage at *http://ncl.cancer.gov/*

Table 1.1 Nanotecnology-based products approved for clinical use

1.3 On the chemical nature of materials

It is sensible to consider today's optimal meaning of 'biomaterial' from two different perspectives, the first being concerned with the evolution of materials science and the wide range of materials options that have opened up during the last decade or so, and the second being the evolution of heath care technologies.

Dealing first with materials science, the classical view of a material has been 'a substance of which things are made'. Materials scientists were taught that there were three primary types of material, metallic, being based on the metallic bond, ceramic, based on ionic bonds and

9

polymeric, based on covalent bonds. In addition there were hybrids, which could either be entirely synthetic, usually referred to as composites which typically would be combinations of ceramics and polymers, or the natural equivalents of these composites, including bone, wood, and ivory. Obviously each of these categories contained many subdivisions. The metallic materials included pure metals and alloys, ceramics included glasses, glass–ceramics and carbons, the polymers included thermosets, thermoplastics, elastomers and textiles. As biomateriale science emerged, the conventional view of materials, as being tangible pieces of substances from which useful objects were made, prevailed. The stems of hip replacements were made of metals, artificial arteries were made of textiles, dentures and intraocular lenses were made of acrylic polymers; classical materials, classical technologies, classical concepts. However, these boundaries between material classes have now been eroded; those substances derived from clear, chemically defined primary interatomic and intermolecular bonds are being replaced by those of greater structural complexity that arise from quite different concepts, including those of nanotechnology and self assembly processes inspired by nature. Indeed it is one of the fundamental tenants that is driving nanoscience and nanotechnology that is at the heart of the revolution in materials science (or materials chemistry as it is so often called now), and that is the replacement of top down manufacturing by bottom up synthesis.

With hindsight it is obvious that we thought of materials as being substances of which things were made as long as and simply because, we visibly saw the objects being made by classical manufacturing or engineering processes. Let us consider a few of the constraints that would exist if we retained the concept that a material is a substance of which things are made. The first is that a material has to be a solid; in classical usage we do not make things of liquids and gases. The second is that, if something is made from this substance, we should be able to see it, or hold it. Thirdly, there is an implicit assumption here that the things which are made will be inanimate, the equivalent of being non viable in the first of the biomaterial definitions above. All of these positions now have to be challenged.

1.4 Functionalization strategies

Different biomedical devices and applications require different properties and functions of materials. Therefore methods to modify nanostructured materials to meet the needs of different biomedical systems are extremely variable.

The surfaces of nanostructured materials can be modified and functionalized with different reagents using different methods, including physical, chemical, or biological. Two things are often achieved by surface modification of nanostructured materials: 1)

enhanced solubility and stability of nanostructured materials in aqueous media and 2) new material functions and properties[25].

The surface modification of biomaterials with bioactive molecules is a simple way to make smart materials. To date, different strategies can be used for the introduction of biomimetic elements into synthetic materials:

a) Physical adsorption (van der Waals, electrostatic, affinity, adsorbed and cross linked),

b) Physical entrapment attachment (barrier system, hydrogel, dispersed matrix system)

c) Covalent surface immobilization, taking advantage of different natural or unnatural functional groups present both on the biomolecules and on the material surfaces (chemoselective ligation, via amino functionalities, heterobifunctional linkers, etc.).

The major methods of immobilizing a bioactive compound to a polymeric surface are adsorption via electrostatic interactions, ligand–receptor pairing (as in biotin–avidin), and covalent attachment (**Figure 1.3**).
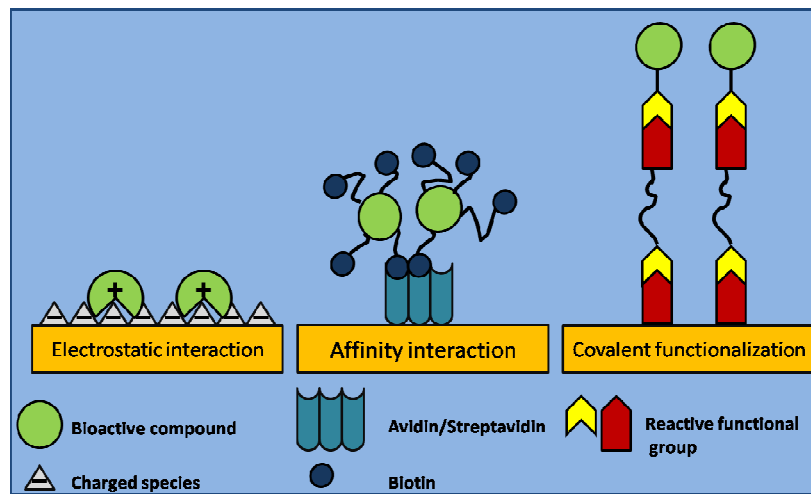
Figure 1.3 Different strategies for the introduction of biomimetic elements into synthetic materials

Physical methods, such as molecular coating (or adsorption), surface entrapment, and physical treating with plasma, ozone, or UV have emerged as leading strategies for surface modifications of nanostructured materials. Through physical modifications, functional molecules and entities, varying charges, or active chemical groups can be introduced onto the surfaces of nanostructured materials, leading to the functionalization and activation of the surfaces of materials. Physical modifications have obvious advantages, including ease of handling and mild interactions with biomolecules through little or no damage to their bioactivities. These methods, however, also exhibit certain limitations. For example, physical linkages are

often formed between the substrates and coatings using these strategies.

These physical linkages and interactions are considered to be weak compared to chemical bonds. Therefore, functional molecules and entities may detach from the surfaces of modified nanoparticles especially when certain serum compounds compete for active binding sites in physiological conditions; detachment is worsened by a competitive displacement of theses functional molecules and entities. Non-covalent adsorption is sometimes desirable, as in certain drug delivery applications[26].

Covalent immobilizations offer several advantages by providing the most stable bond between the compound and the functionalized polymer surface. A covalent immobilization can be used to extend the half-life of a biomolecule, prevent its metabolism, or allow continued bioactivity of indwelling devices[27].

Bioactive molecules (growth factors, ECM proteins, etc.) that are free in solution, as opposed to immobilized to the matrix, may induce significantly different biological responses. Growth factors are routinely added to cultures in vitro, and have been incorporated and released from polymeric systems with retention of bioactivity, as shown for neurotrophins, BMPs, and VEGF[28]. *In vivo*, these soluble factors can be released from the delivery site, and the relevant parameter is the duration over which therapeutic concentrations can

be maintained. Alternatively, bioactive molecules can be linked covalently to the scaffold, eventually in a reversible way or exploiting a degradable linking tether. For growth factor immobilization to fibrin, cell migration results in cell-activated plasmin degradation that can catalyze release of the factor. These scaffolds have been termed ''cell-responsive''[29] due to release of the factor upon cellular demand. Once released, these soluble factors can bind their receptors and initiate a signaling cascade.

Alternatively, immobilized biomolecules can ligate their receptors directly from the material surface; however, this type of interaction may not exactly replicate the signaling of soluble factors, as growth factor internalization can stimulate signaling pathways different from those activated at the surface. For example, neuronal growth factor NGF induces neurite outgrowth by signaling at the plasma membrane, yet promotes neuron survival when internalized[30]. Surface immobilization has been successfully used to attach several factors such as EGF[31], BMP-7[32], BMP-2[33], VEGF[34] , NGF[35], and NT-3[36] to a variety of natural and synthetic biomaterials. Signaling by these immobilized or locally released bioactive ligands may be more potent than signaling by soluble versions added directly to culture media[37]. These studies also demonstrate that the immobilization strategy must consider protein structure and active region topology, when designing suitable delivery systems in order to maximize bioactivity. Ultimately, some factors may be best delivered in a continuous

manner, while others benefit from direct attachment to the biomaterial substrate[38].

Different methods have been developed for covalent functionalization of biomolecules to diverse biomaterials. For covalent functionalization to an inert solid polymer, the surface must first be chemically modified to provide reactive groups (-OH, -NH$_2$, COOH, -SH) for a second functionalization step. When the material does not contain reactive groups, they can be generated by chemical and physical modification, on the polymer surfaces in order to permit covalent attachment of biomolecules. With this goal, a wide number of surface modification techniques have been developed, including plasma, ionic radiation graft polymerization, photochemical grafting, chemical modification and chemical derivatization.

For example peptides can react via the N-terminus with different groups on polymers (**Figure 1.4**). This is usually done by reacting an activated carboxylic acid group with the nucleophilic N-terminus of peptides. The carboxylic group can be activated with different peptide coupling reagent, e.g. 1-ethyl-3-(3-dimethylaminopropyl)-carbodiimide (EDC, also referred to as water soluble carbodiimide, WSC), dicyclohexyl-carbodiimide (DCC) or carbonyl diimidazole (CDI).

A) Carboxyl groups, preactivated via EDC and NHS,
B) amino groups, preactivated with DSC,
C) hydroxyl groups, preactivated as tresylate,
D) hydroxyl groups, preactivated as p-nitrophenyl carbonate.
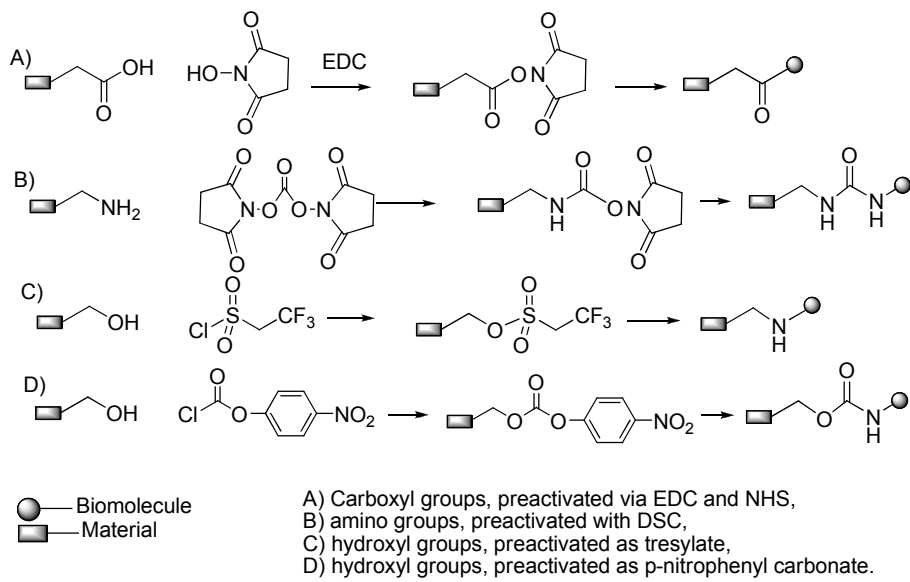
Figure 1.4. Coupling methods to different groups on materials.

In a more recent approach named chemoselective ligation (**Figure 1.5**), selected pairs of functional groups are used to form stable bonds without the need of an activating agent and without interfering with other functionalities usually encountered in biomolecules. Chemoselective ligation proceeds usually under mild conditions and results in good yields[39].
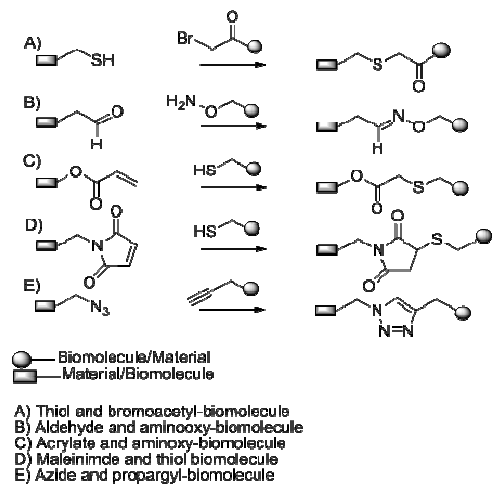
Figure 1.5. Chemoselective ligation methods.

A biomolecule may also be attached, with this coupling methods, via a spacer group, in order to give better access to the target receptor. One useful and biocompatible spacer is PEG that has been differently functionalized at two extremities[40]. Metal or ceramic surface may also be silanised, exploiting functionalized triethoxysilanes[41].

Chapter 2

2. Results and discussion – Materials

Decoration of nanostructured materials is relevant in a wide variety of applications, including novel tissue engineered scaffolds and devices, site specific drug delivery systems, non-viral gene carriers, biosensor and screening systems, and clinical bio-analytical diagnostics and therapeutics.[42] Through the modification of existing nanostructured materials one can control and tailor the properties of such materials in a predictable manner, and impart them with biological properties and functionalities to better suit their integration with biomedical systems. The functionalisation process can be performed by a variety of techniques, including plasma processes, that allows to tune surface properties of solids with negligible effect on their bulk[43].

The general aim of the project is the development of innovative materials for bone and cartilage tissue engineering, focusing on the design of smart biomimetic materials, fully integrating principles from cell and molecular biology able to directly regulate cell differentiation and metabolism. Materials equipped with molecular cues mimicking the structure or function of natural extracellular microenvironments are able to interact with surrounding tissues by biomolecular recognition[44]. Biomimetic materials should be capable of eliciting specific cellular responses and directing new tissue formation

mediated by specific interactions, which can be manipulated by altering design parameters. Smart materials should provide the opportunity for chemically linking biological signalling molecules such as peptides or small proteins, or carbohydrates, eliciting cell responses to help the healing process.

For tissue repair, biomaterials should have several properties to support viable repair. Firstly, the material must act as a support structure for cells and possess enough mechanical strength to protect the cells contained within it. Secondly, some level of bioactivity should be provided to accommodate cellular attachment and migration. Furthermore, the materials should be biodegradable and remodel as the new tissue forms and replaces the original construct. In this regard, the matrix should be non-toxic, non-attractive and non-stimulatory of inflammatory cells, and also non-immunogenic, which would be detrimental to tissue regeneration. Finally, the scaffolds should provide easy handling under clinical conditions, enabling fixation of the materials into the implant site. [45]

New smart materials were designed and synthetized to obtain innovative scaffolds useful in forming tissues with oriented mechanical and cellular properties. Furthermore, functionalized materials with various biochemical signals will influence MSCs behaviour *in vitro* enhancing the differentiation in chondrogenic and osteogenic cell lines and the matrix production and remodeling.

Hence the following issues have been taken into consideration for the design of smart biomaterials for bone and cartilage repair:

a) Materials: Natural Inorganic (i.e. Hydroxyapatite), Synthetic Organic (i.e. Polycaprolactone, Polypropylene), Natural Organic (i.e. Collagen) and composites (Hydroxyapatite-Polycaprolactone) as scaffolds.

b) Molecular cues: short peptides and biologically relevant glycidic structures, spacer arms to evaluate the influence of the distance from the material surface.

c) "Biodecoration" step: Study and design of biocompatible functionalisation strategies via covalent and spatial-oriented immobilization methods.

2.1 Hydroxyapatite

Ceramics are inorganic materials with crystalline structures that are brittle and porous. Common example of such materials include hydroxyapatite (HAp). Constituents mimicking natural bone have often been incorporated into biomaterial design to stimulate ossification. Calcium and phosphate ions are important components during the mineralization

phase of the ossification process. Materials composed of calcium phosphate such as HAp: $Ca_{10}(PO_4)_6(OH)_2$ and tri-calcium phosphate (TCP; $Ca_3(PO_4)_2$) are attractive candidates for bone substitutes.

HAp is a naturally occurring ceramic mineral found in bones. Synthetic HAp is widely investigated for potential bone tissue replacement due to its strength and biocompatibility[46]. It has been widely described the ability of bioceramics such as hydroxyapatite (HA) to form a bonding with the surrounding bone tissue. Since inorganic materials such as hydroxyapatite possess a paucity of reactive functional groups, biomolecular modification of these materials is still challenging.

We had at our disposal (Anna Tampieri group CNR Faenza) different HA samples: three-dimensional porous scaffolds or powder with different particle size. Depending on the HA sample, different approaches for HA functionalisation have been tested and are outlined in details in the next sections.

2.1.1 Hydroxyapatite 3-D: sample molecules

3D hydroxyapatite porous scaffolds were efficiently functionalized with sample molecules by covalent bonding of the carboxylic groups introduced by plasma technology followed by chemical grafting, thus demonstrating the applicability of plasma functionalisation for the immobilization of different (bio)molecules onto a 3D scaffolds of hydroxyapatite. The functionalized scaffolds resulted biocompatible, hence this method can be used as general method for biomolecules

attachment rendering hydroxyapatite bioactive for bone tissue regeneration uses.

Plasma polymerization of acrylic acid was used to modify macro/microporous hydroxyapatite scaffolds (HA), introducing COOH groups that were subsequently reacted with different compounds, in order to generate porous HA activated surfaces, bearing (bio)molecules linked to the scaffold via a covalent bond.

The compatibility of covalent bonding and plasma treatment of bioactive molecules was investigated through biological assay. Cell culture and growth kinetics assay of Human osteosarcoma MG-63 cells were evaluated using two differently functionalized surfaces (HA-COOH and HA-CONHTrp) and compared to standard untreated HA scaffolds.

2.1.1.1 Surface modification of HA 3D scaffolds by plasma polymerization

The deposition of stable pp-AAc (plasma–polymerised acrylic acid) coatings from AAc/Ar plasmas is well documented[47]. The use of diluted mixtures of acrylic acid in Ar allows the deposition of thin films with good retention of COOH functionalities. The carboxylic groups concentration in these pp-AAc layers, measured by means of ion-exchange reaction with a cationic dye (thionin acetate), was around 1 mmol/cm^3 [48]. The same plasma deposition conditions (AAc

23

and Ar flows, power input, total pressure) have been employed here for the coating of porous HA scaffolds. **Figure 2.1** shows an unmodified and a plasma treated HA sample after immersion in a thionin acetate solution and rinsing. The successful COOH functionalization is confirmed by the coloration of the plasma coated sample. In this case, the concentration of COOH groups, expressed as (moles of COOH)/(HA weight), ranges from 7×10^{-5} to 10^{-4} mmol/g. Thionin acetate assay allowed us to estimate also the penetration of the plasma deposition inside the porous structure of the HA scaffolds, that resulted to be poor, as expected.

Figure 2.1 Thionine acetate colorimetric assays on untreated HA (left) and plasma polymerised AAc-HA (right).

The HA-COOH scaffolds were also characterised by XRD analysis, in order to evidence possible undesired changes caused by plasma treatments in the HA material. XRD data showed no changes in the crystallinity as well as in the phase purity of the HA scaffold after the

plasma polymerization, as the unchanged value of the Ca/P molar ratio found by ICP confirmed (**Table 2.1**).

	Powder HA	Untreated HA scaffold	HA-COOH	HA-CONH-Dansyl	HA-COO-sugar	HA-CONH-Trp
Ca/P	1.69	1.67	1.67	1.67	1.67	1.67

Table 2.1. ICP determined Ca/P molar ratio for the differently functionalized HA porous scaffolds

### 2.1.1.2. Chemical modification of the plasma-functionalised scaffold with model organic molecules

Different classes of small organic molecules were chosen as model for the present study (**Chart 1**): a fluorescent label, such as the dansyl group (**2.1**), a monosaccharide derivative of D-galactose (**2.2**), and an amino acid (triptophane) (**2.3**).

Fluorescent probe:

dansyl hydrazine (**2.1**)

Carbohydrate:

2.2

Aminoacid:

Triptophane (**2.3**)
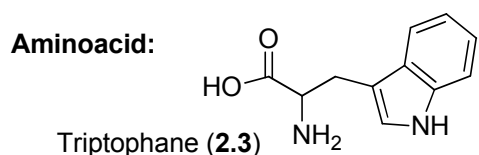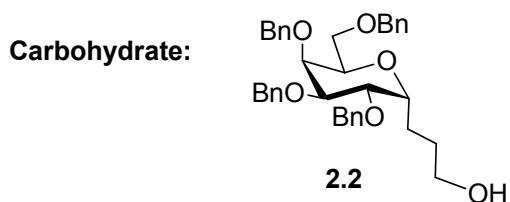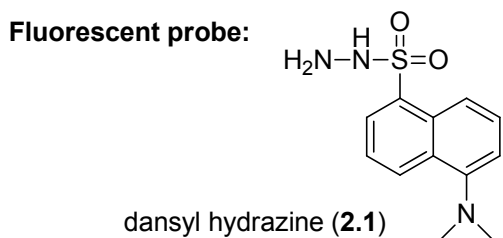
**Chart 2.1**. Model organic molecules used for the present study.

The dansyl derivative **2.1** was chosen in order to better understand the chemical reactivity of the carboxylic groups introduced by plasma deposition. In fact, we used the fluorescence of the dansyl group to prove the effective covalent bonding to the material *versus* the potential simple physical interaction with the porous scaffold. In addition, since biomolecules are usually involved in the regulation, adhesion, differentiation, proliferation, and activity of cells[49],

representative examples such as an amino acid and a carbohydrate derivative were chosen as models (**Chart 2.1**, compounds **2.2** and **2.3**).

The strategy adopted for biomolecules covalent bonding to plasma-treated HA (**Scheme 2.1**) consists in preparing a succinimidyl ester (-COOSuc)-terminated surface layer followed by reaction with the -NH$_2$ or -OH functionalised molecules using standard procedures. The -COOSuc surface is obtained by reacting HA-COOH grafted surfaces with *N*-hydroxysuccinimide (NHS), in the presence of a water-soluble carbodiimide such as 1-ethyl-3-(3-dimethylaminopropyl)carbodiimide (EDC)[50] for water soluble compounds (i.e. **2.3**), or dicylohexylcarbodiimide[51] for water unsoluble molecules (i.e. **2.1**, and **2.2**)[53].
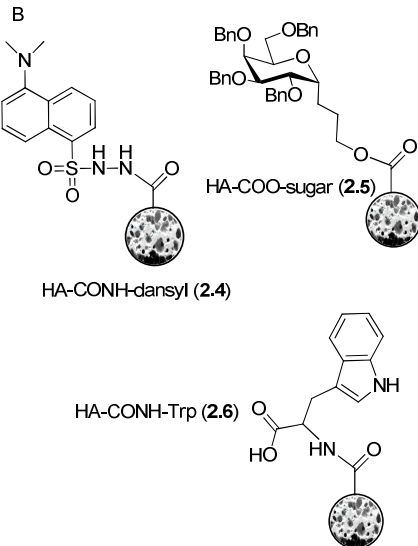
Scheme 2.1. A. Synthetic steps for the covalent bonding of sample molecules; B. Type of functionalizations of porous HA scaffolds achieved with the presented method.

2.1.1.3. Modification with the dansyl fluorescent label (2.1)

In order to investigate and control covalent bonding on plasma activated material surface the dansyl group was used as a small fluorescent probe. The dansyl group can be easily exploited as a very powerful complementary tool for surface analysis, in particular when it comes in very low concentrations[48]. Thus HA-COOH samples were derivatised with dansyl hydrazine, after preactivation of the carboxylic group (**Scheme 2.1**), to give the corresponding acyl hydrazide (**2.4, Scheme 2.1B**). For comparison, the same reaction was performed in the absence of the activating agents (DCC/NHS), in order to exclude the possibility of physical adsorbtion, which can be a possibility with porous materials. In order to determine the nature of the interaction between HA-COOH and dansyl hydrazine (covalent bond or physical entrapment) fluorescence microscopy analysis was performed on the two samples, respectively (**Figure 2.3**). For the reaction carried out without DCC, fluorescence emission spectrum shows a maximum at 518 nm. However, when DCC/NHS were used as coupling agents, a shift to 498 nm was observed; the emission features of the dansyl chromophore are known to be highly sensitive to the nature of their microenvironment, thus the observed hypsochromic shift is diagnostic of a different interaction with the material surfaces, suggesting the formation of a covalent bond between the dansyl group and the HA surface. These results show that the interaction of the dansyl probe in

29

the absence of DCC/NHS is produced by aspecific adsorption while, in the presence of the coupling agents, there is evidence of the formation of a covalent amide-type bond.
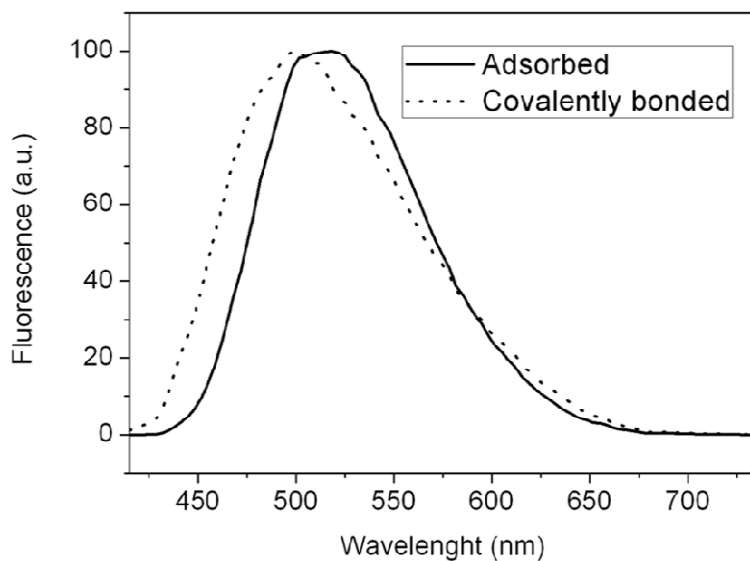

Figure 2.3. Fluorescence emission spectra of a) adsorbed dansyl hydrazine and b) covalently linked dansyl moiety.

2.1.1.4. Modification with biomolecules: a monosaccharide (2.2) and an aminoacid (2.3)

Small biological molecules, such as carbohydrates and aminoacids, are normally present and involved in the mechanisms that order complex biological systems. Carbohydrate-protein interactions

mediate a whole host of biological mechanisms, including those responsible for peptide conformation, enzyme activity, cell-cell recognition, cell adhesion, and cell development. Carbohydrates are involved in biological information delivery and due to their polyfunctional nature can be used for hydrophilicity and functionalisation tailoring of material surfaces, for example improving cell adhesion, or bioactivity; thus, the presentation of carbohydrates in an immobilized format can be of relevant interest.

At same breath proteins and peptides can be useful to elicit a desired and specific biological response, through immobilization of full protein or using biologically active motifs. Moreover it has been shown that amino acids can modify surface properties of a series of amino-acid-functionalized hydroxyapatite. In this context, in order to covalent biofunctionalise porous HA, via plasma technology, a carbohydrate mimetic (**2.2**) and a natural aminoacid (**2.3**) were used as model compounds, affording HA scaffolds **2.5** and **2.6** (**Scheme 2.1B**).

A *C*-glycosidic derivative of D-galactose was used as model monosaccharide. *C*-glycosides present several advantages over their *O*-glycosidic counterpart their structure is closely resembling the parent sugar, thus maintaining the biological information, but they lack the anomeric glycosidic bond which is usually subjected to degradative forces *in vivo*. Hence the *C*-glycosidic bond in place of the *O*-glycosidic one renders the linkage stable to enzymatic

31

degradation by glycosidases. Hence the *C*-glycosidic analogue of D-galactose possessing a suitable hydroxylic group for the coupling reaction with HA-COOH samples was synthesized in a few steps from the parent monosaccharide[52].

Both the functionalized scaffolds (that is **2.5** and **2.6**) were characterised by XRD, SEM, DTA.

XRD analysis showed no secondary phases besides apatite, thus the calcium phosphate material constituting the scaffold did not degrade after the chemical reactions. However, shoulders and peaks detected approximately in the range 290 - 400°C in the DTA curves (**Figure 2.4**) of the functionalized materials, during the heating in air, can be imputed to the degradation of organic material.
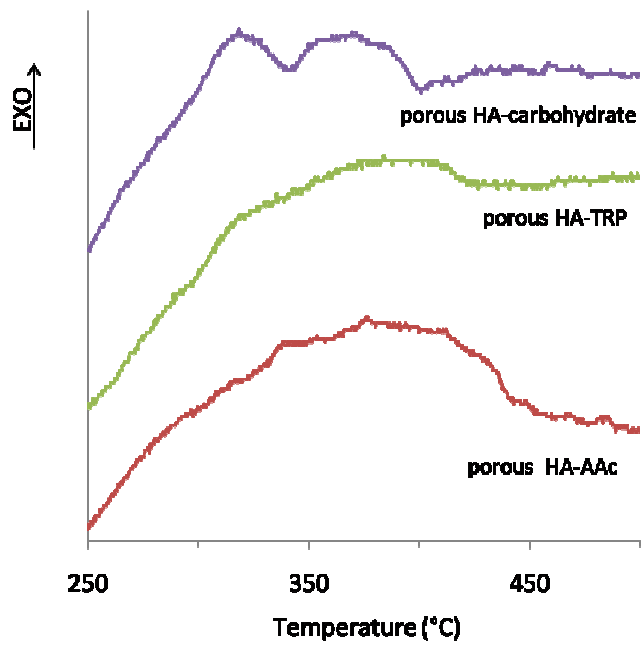
Figure 2.4. DTA curves for functionalised materials.

SEM images (**Figure 2.5**) evidence that the morphology of the HA porous scaffold was maintained after the functionalization treatments.
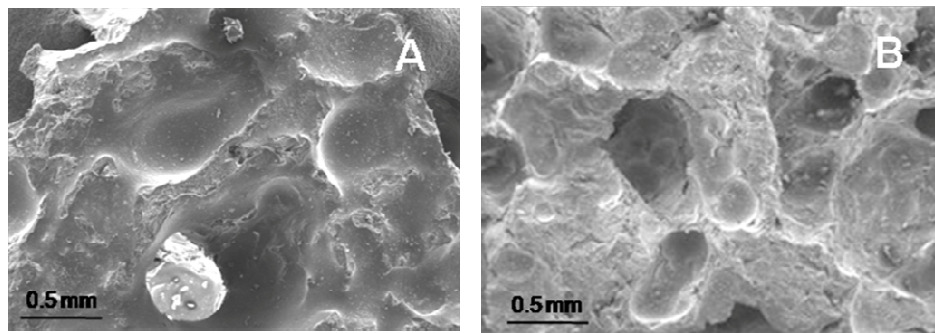
Figure 2.5. SEM image of a) functionalised HA scaffold **2.5**; b) unfunctionalised material.

The value of the Ca/P molar ratio found by ICP was unchanged (1.67) after treatment with carbohydrate and amino acid (scaffolds **2.5** and **2.6**) (see **Table 2.1**)

2.1.1.5. Biological Assay

Since the morphology and phase of hydroxyapatite scaffolds did not change upon plasma and chemical treatments, we proceeded with the evaluation of the biological compatibility of the functionalized scaffolds after plasma treatment (HA-COOH), and after functionalisation with triptophane (scaffold HA-CONH-Trp, **2.6**). Cell growth and kinetic assays were performed with MG-63 human osteosarcoma cells; 24-well multiwell petri dishes (Cellstar®; Greiner Bio-One; International PBI SA, Milano, Italy) were used as a reference growth surface, (Franceschi et al, 1985, Ahmed et al, 1994).

As expected, cell growth on plastic proceeded to a faster rate than on ceramic scaffolds, confluence being reached within day 5-7. In biocompatibility assays, MG63 displayed a preferential attachment to untreated HA, as testified by the alamar blue assay and by a higher number of stained cells at the onset of the experiments (**Figure 2.7** and **2.8**). However, upon culturing, all three surfaces (HA, HA-COOH and HA-CONH-Trp) allowed a progressive growth of the attached cells. Interestingly the growth curves displayed essentially the same trends, confirming that differences within the differently treated scaffolds were to be ascribed to the number of initially attached cells rather than to growth hindering (**Figure 2.6**). Differences in the number of attached cells are visible by direct imaging at early timings upon seeding (**Figure 2.7**). It should be noted that cell morphology does not seem altered in HA and Plasma/COOH modified surfaces, resembling a fibroblast-like shape. However, in HA-CONH-Trp scaffolds, some of the seeded cells acquire a polygonal shape, rather unusual for this line, evoking a possible stress and/or sufferance condition. At the end of the planned experimental timings, however, a rather uniform monolayer of cells can be detected on all surfaces (**Figure 2.8**). On all scaffolds a few cells had migrated onto the blank untreated surface, either by passing through the interconnected pores of the materials or by proliferating on the outer surfaces, although this effect was more evident in the HA-COOH or in the HA-CONH-Trp samples. Nonetheless, all cells detected onto the blank surfaces displayed a similar fibroblast-like morphology (**Figure 2.8**).

35

Interestingly bioactivated ceramic scaffolds retained a higher background on the seeding surfaces once stained with toluidine blue, possibly due to the chemical modifications induced on the treated surfaces. The same scaffolds, in fact, did not display such a background on the untreated blank surfaces (**Figures 2.7** and **2.8**).

Apart those cited, no additional differences were noted among cells attached onto the differently activated surfaces of the ceramic scaffolds thus supporting a substantial equivalence in the biocompatibility of the tested surfaces at later timings.
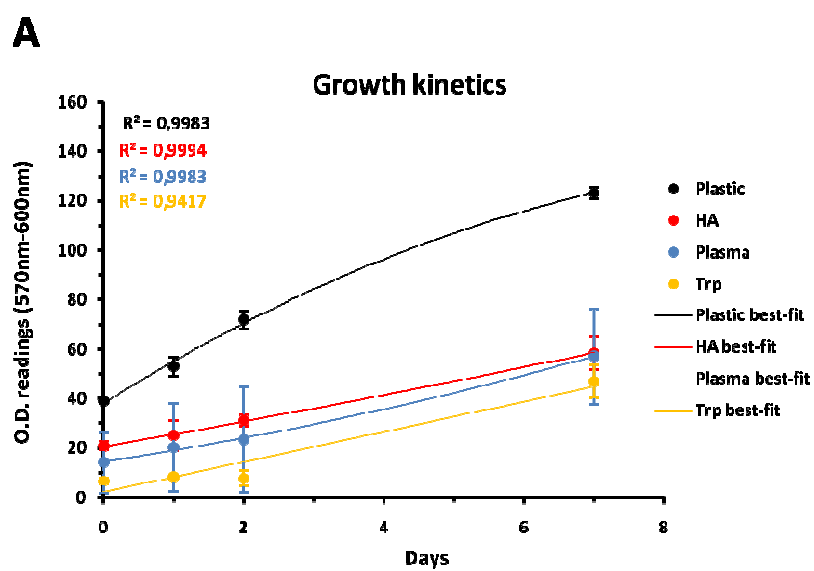
Figure 2.6: MG63 growth kinetics upon seeding onto ceramic scaffolds

Panel A: Growth curves of MG63 seeded on plastic (Plastic; black dots and line), on unmodified HA scaffolds (HA; red dots and line), on plasma/COOH-modified HA (Plasma; blue dots and line) or on plasma/Trp-modified HA (Trp; yellow dots and line). Data are the mean ± SD of three determinations on each of the three scaffolds for each seeding surface type at the indicated time-points . Correlation coefficient values (R^2) for each best fit curve are also depicted.
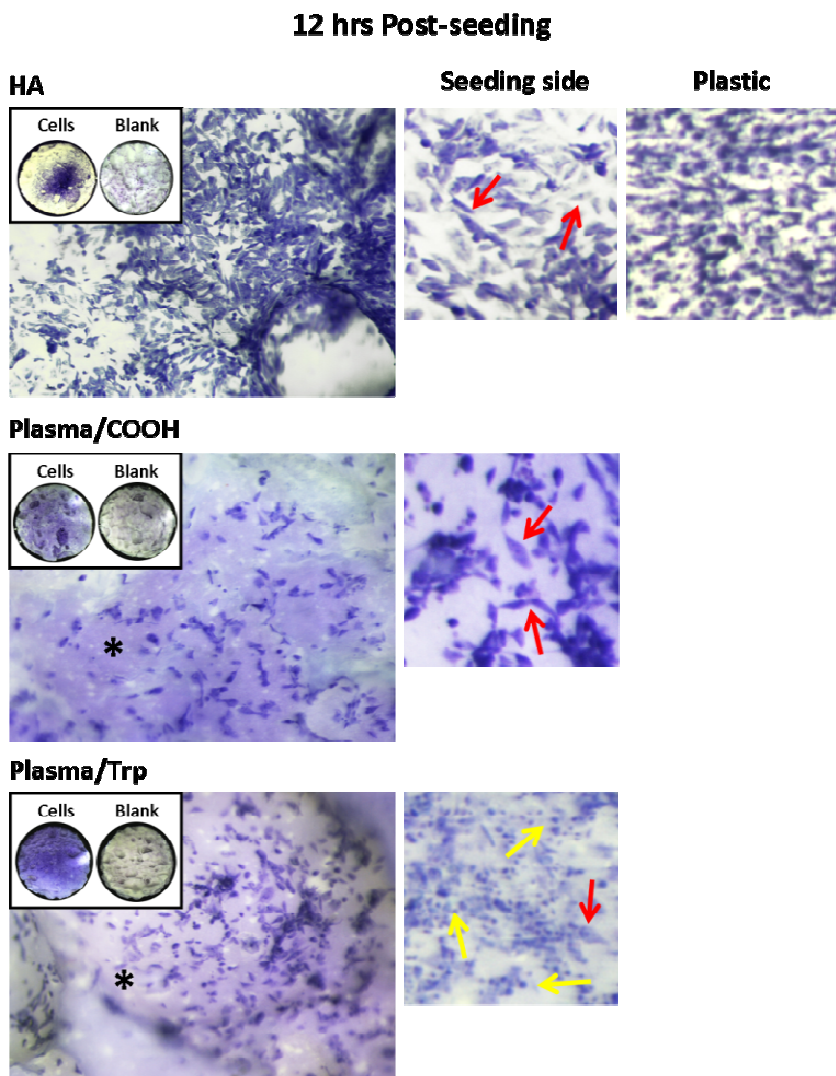
Figure 2.7 Cell detection on scaffold surfaces 12 hours post-seeding.

Toluidine blue staining of cells seeded onto the different scaffolds (HA, Plasma/COOH and Plasma/Trp) 12 hours post-seeding (time 0).

A larger number of attached cells is evident on HA samples. Inserts depict both surfaces, the cell seeded one (Cells) and the blank one (Blank) of a representative scaffold for each type. Larger magnifications evidence the fibroblast-like shape of attached cells (red arrows) or a more polygonal one(yellow arrows) on the cell-seeded surfaces (Seeding side). Persistence of a stained background is indicated by an asterisk (*) and was detected only in the bioactivated surface. Images, all depicted at the same magnification, are representative of results obtained for each scaffold type. A magnification of sub-confluent MG63 cells grown on plastic is depicted for reference (Plastic).
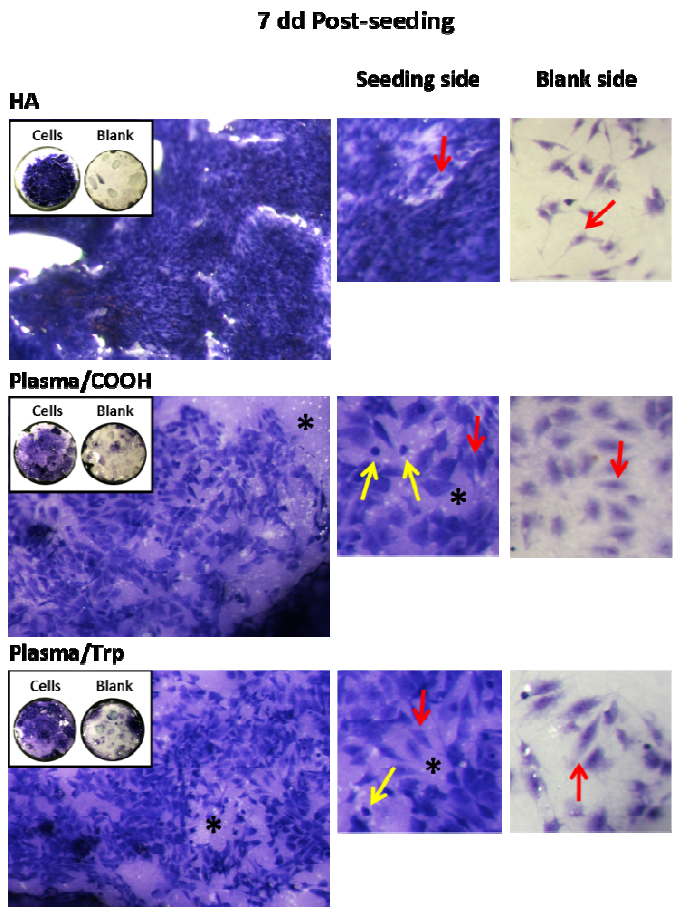
Figure 2.8 Cell detection on scaffold surfaces 7 days post-seeding.

As for figure 2.2, but depicted images refers to results obtained 7 days post seeding. Enlargements depicting cells on the untreated surfaces (Blank side) are also reported.

3D hydroxyapatite porous scaffolds were efficiently functionalized with sample molecules by covalent bonding of the carboxylic groups introduced by plasma technology followed by chemical grafting, thus demonstrating the applicability of plasma functionalisation for the immobilization of different (bio)molecules onto a 3D scaffolds of hydroxyapatite. The functionalized scaffolds resulted biocompatible, hence this method can be used as general method for biomolecules attachment rendering hydroxyapatite bioactive for bone tissue regeneration uses.

2.1.2 3-D Hydroxyapatite: C-Nautriuretic Peptide (CNP)

Using the same method HA 3-D has been functionalised also with CNP petides, to test biological response studying the osteogenic differentiation of mesenchymal cells on hydroxyapatite-decorated material. (**Scheme 2.2**).

3D hydroxyapatite porous scaffolds were efficiently functionalized with CNP by covalent bonding of the carboxylic groups introduced by plasma technology followed by chemical grafting. Plasma polymerization of acrylic acid was used to modify macro/microporous hydroxyapatite scaffolds (HA), introducing COOH. In order to ensure a spacing between HA surface and the CNP we used a commercial PEG arm, possessing an amino group at one available for HA-COOH

41

reaction and a carboxy group on the other side for the covalent bond to CNP.
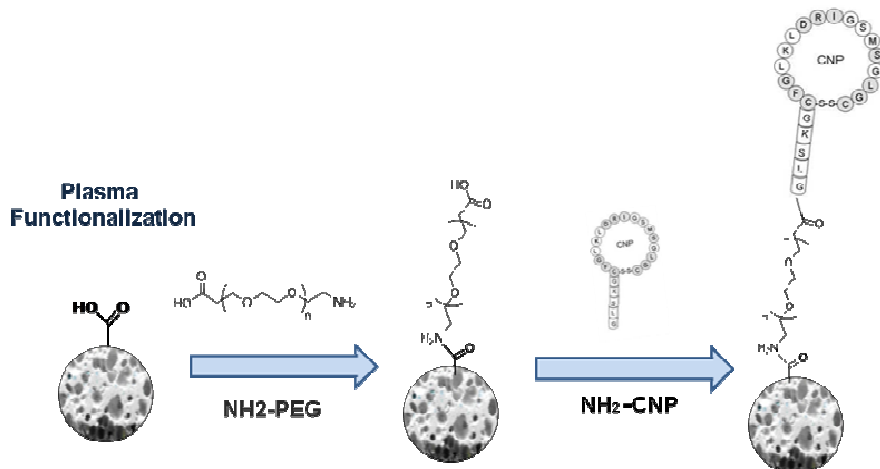
Scheme 2.2 3D HA scaffold functionalization

Bioceramic functionalisation has been performed by esterification reaction between the COOH groups of hydroxyapatite and NH_2 groups PEG, upon in situ activation of HA by -hydroxysuccinimide (NHS) and 1-ethyl-3-(3-dimethylaminopropyl)carbodiimide (EDC), in H_2O. After that, the HA was washed vigorously with MilliQ water. In order to avoid the non-specific adsorption of PEG on the HA surface, the samples were soaked in MilliQ water for 1 h at room temperature and then washed again, with MilliQ water. The obtained HA-PEG was than activated and used for the covalent linkage with CNP.

2.1.3 Hydroxyapatite granules - Pegylation

The effective immobilization of biomolecules on the surface of bioceramics is still challenging, due to the requirement of a sufficiently strong and specific affinity with the material surface, and of site-directed immobilization, and finally of maintenance of the biological activity. Most immobilization methods developed to date involve modification or coating of the inorganic material with appropriate substances in order to immobilize the proteins by physical adsorption via van der Waals, hydrophobic or electrostatic forces, or chemical bonding.[53]

Covalent linkage of bioactive molecules to material surface is a valid alternative strategy in order to allow a sufficiently strong and specific immobilisation of biomolecules with the surface itself; in addition covalent bonding may permit site-directed immobilization and preservation of specific conformation and exposition to control biological responses.

Thus, we envisaged the possibility of taking advantage of the hydroxyl groups of hydroxyapatite granules having dimensions in the range 400-600 microns [54] for the covalent linkage of a sample monosaccharide through a chemoselective ligation, via the azido-alkyne Huisgen cycloaddition, as illustrated in **Scheme 2.3**. As a preliminary test to assess the reactivity of hydroxyl groups of

hydroxyapatite, a simple reaction between HA and dansyl chloride was performed.

2.1.3.1. Hydroxyapatite granules functionalization and characterization

In order to assess the reactivity of HA, reaction with dansyl chloride was performed suspending HA granules in dry THF (2 mL) containing 0.25 M dansyl chloride and 5% triethylamine, and kept under stirring for 4 h (**Scheme 2.3A**).
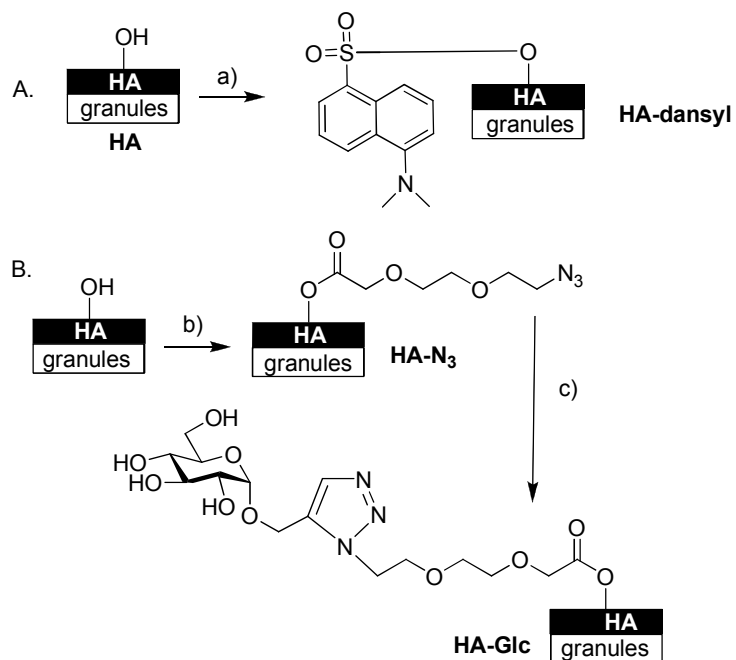
Scheme 2.3 HA functionalization

The dansyl functionalisation of HA was confirmed by UV analysis at 254 nm (**Figure 2.9**), and ATR Fourier transform infrared (FT-IR) spectroscopy (**Figure 2.10**).
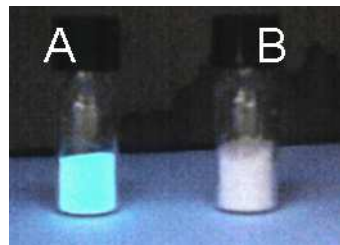

Figure 2.9. A. HA granules functionalised with the dansyl group; B) HA granules as negative control.

All the spectra reported in Figure 2 are dominated by the 1017 cm^{-1} absorption peak due to the phosphate (PO_4^{3-}) vibration of HA. Other absorption bands of HA are observed at 3570 cm^{-1} (stretching of structural OH), couple at 1455 and 1415 cm^{-1} (stretching of B-type carbonate), 962 cm^{-1}(phosphate), and at 872 cm^{-1} (bending of B-type carbonate). The spectrum of HA functionalized directly with dansyl cloride displays three evident peaks at 2979 cm^{-1}, 2946 cm^{-1} and 2880 cm^{-1} that are due to the CH_3 of the dansyl group. To better characterize the HA decoration, we performed the second derivative analysis of the measured spectra (a resolution enhancement mathematical procedure): in the case of HA-dansyl, the infrared

response of sulfonic ester leads to the well resolved peak at 1380 cm^{-1}. All together, therefore, these results underline the success of our hydroxyapatite biodecoration strategy.
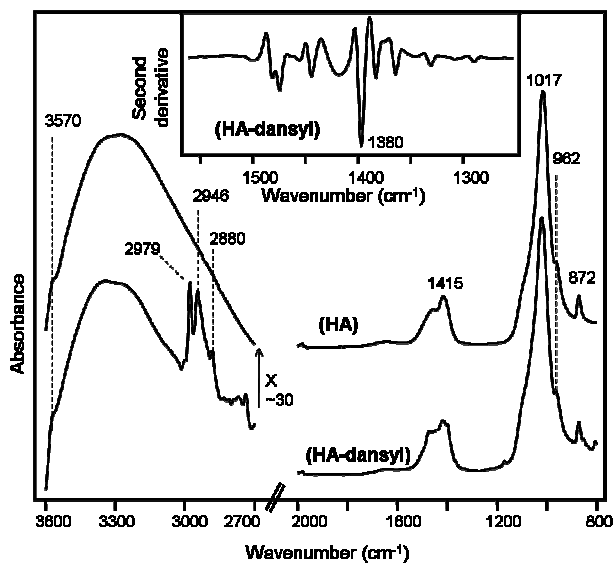

Figure 2.10. IR analysis of HA granules functionalised with the dansyl group (HA-dansyl) compared to unfunctionalised HA (HA).

With these results in our hands, we then proceeded for the chemoselective ligation of the carbohydrate moiety. In order to ensure a minimal spacing between HA surface and the monosaccharide we used a short PEG arm, possessing an azido group at one end for the Huisgen cycloaddition, and a carboxy group on the other side for the

covalent bond to the HA hydroxyls. Hence, the the triethylene glycol was desymmetrised first by monosubstitution with the azido group *via* the monomesylate **2.8**, (**Scheme 2.4**), as already described by Bertozzi et al., [55] then oxidised at the remaining OH by TEMPO, affording **2.10**.[56]
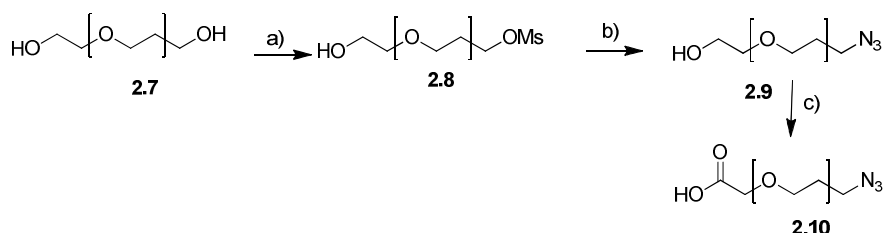
Scheme 2.**4** Preparation of the difunctional PEG linker.

Bioceramic functionalisation has been performed by esterification reaction between the OH groups of hydroxyapatite and COOH groups of the glycol, upon in situ activation of **2.10** by N,N,-diisopropylcarbodiimide (DIC), in dry THF (**Scheme 2.5**). Finally, the HA was added to the THF solution of activated **2.10**, and the suspension stirred for 12 h at room temperature. After that, the HA was filtered and washed vigorously with THF, MilliQ water and acetone. In order to avoid the non-specific adsorption of PEG on the HA surface, the samples were soaked in MilliQ water for 1 h at room temperature and then washed again, with MilliQ water and acetone.

The obtained HA-N$_3$ was submitted to Huisgen cycloaddition with an alkyne. The Huisgen cycloaddition[57], that is the 1,3-dipolar cycloaddition between azides and alkynes yielding irreversibly a stable 1,4-disubstituted 1,2,3-triazole offers several advantages for the biodecoration step of hydroxyapatite: i) the cycloaddition reaction is characterised by high versatility as well as high specificity and chemoselectivity in the presence of a wide variety of surrounding functional groups and solvents (ranging from both protic and aprotic organic solvent to water); ii) these reactions are featured by a high thermodynamic driving force (generally above 20 kcal mol^{-1}), thus allowing the use of mild reaction conditions and short reaction times, leading to quantitative coupling yields at room temperature;[58] iii) it guarantees the desired spatial orientation of the biomolecule on the material surfaces. Cu(I)-catalysed Huisgen-type cycloadditions have been employed in a variety of applications in the field of material science,[59],[60] such as the preparation of highly functionalized macromolecules[61] and the surface immobilization of (bio)macromolecules and polymers. [62,63] However, to the best of our knowledge, no examples of Huisgen cycloaddition have been employed to date for the "biodecoration" of bioceramics. As the alkyne partner, in order to give also biological relevance to the method, propargyl □-d-glucopyranoside was used as model substrate.

Hence, the propargyl □-glucoside was prepared by straightforward Fischer glycosylation catalysed by H$_2$SO$_4$ supported on silica gel and

48

ultrasounds on the unprotected monosaccharide[64] and coupled to the azido group by chemoselective click chemistry.

Click reaction was performed using 0.03 M stock solutions of propargyl 2-□-d-glucopyranoside, $CuSO_4 \cdot 5H_2O$ and sodium ascorbate in milliQ water. The HA-N_3 was suspended in the saccharide stock solution (2 mL), and a mixture of cupric sulfate solution (0.100 mL, 0.003 mmol, 5% in respect to the saccharide), and ascorbate solution (0.300 mL, 0.009 mmol, 15 mol % in respect to the saccharide) was added and stirred for 24 hours.

The "glycosylated" carbonated hydroxypatite HA-Glc was characterised by its ability to interact with glucose recognising lectins, that is Concanavalin A. Selective binding of Concanavalin A was confirmed for the "glucosylated" hydroxyapatite, when compared to the unfunctionalised one by FTIR spectroscopy (**Figure 2.11**). In figure 2.11 the FTIR spectra of hydroxyapatite HA, HA-Glc, and HA-Glc incubated with lectin were compared with that of the free lectin, in the 1450 cm^{-1}-1750 cm^{-1} spectral range. The functionalization of hydroxyapatite leads to an increased absorption in the 1700-1600 cm^{-1} region, where the protein Amide I band occurs. To better resolve the protein contribution, the second derivatives of the absorption spectra were performed. In particular, the two new peaks at ~1624 cm^{-1} and at ~1694 cm^{-1}, observed in HA-Glc only after incubation with lectin, can be assigned to the protein β-sheet secondary structures, in agreement with the FTIR spectrum of the free lectin.[65]
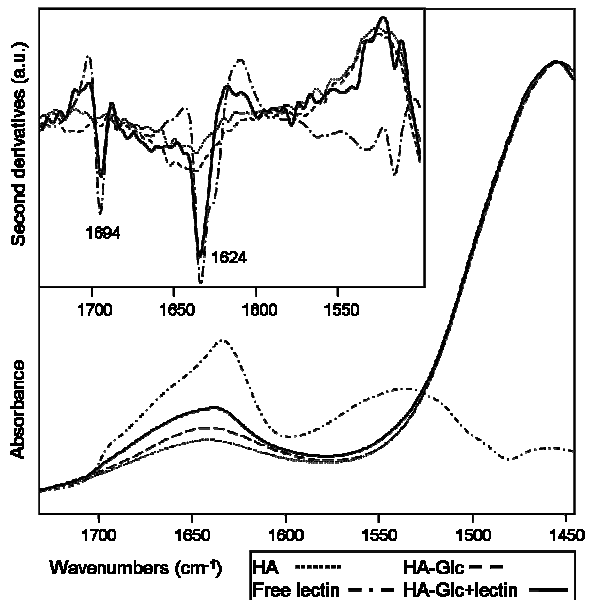
Figure 2.11. FTIR spectra of hydroxyapatite samples: plain HA (dotted line), of HA-Glc (dashed line), and of HA-Glc incubated with lectin (full line) are reported after normalization at the B-type carbonate stretching peak at ~1455 cm^{-1}. The absorption spectrum of free lectin (dashed-dotted line) is also reported for comparison. The second derivatives of the above absorption spectra are reported in the inset.

This methodology is a novel technique for the "biodecoration" of hydroxyapatite. The conjugation step, mediated by the Huisgen cycloaddition allows the chemoselective ligation of a model

50

monosaccharide to an inorganic biomimetic material; the method herein described can be extended to chemically defined short fragment of ECM polysaccharides (i.e. hyaluronic acid or heparan sulphate), thus improving the bioactivity of hydroxyapatite-based biomaterials for bone tissue regeneration.

2.1.4. Hydroxyapatite granules - Silanization

A different methodology has been proposed for the direct chemical functionalisation of HA. In fact, hydroxyapatite has been successfully biodecorated with carbohydrate derivatives, also via direct silylation of the hydroxyl groups of the apatite and subsequent covalent bonding with a suitably functionalized carbohydrate moiety (**Scheme 2.5**). As model carbohydrates perbenzylated *C*-glycoside derivatives of biologically relevant monosaccharides such as D-glucose, D-galactose and L-fucose were used. *C*-glycosidic derivatives possessing a carboxylic group for the coupling reaction to the aminopropylsilane-functionalised hydroxyapatite were synthesized in a few steps from the suitably protected natural monosaccharide (see **Chapter 3**).
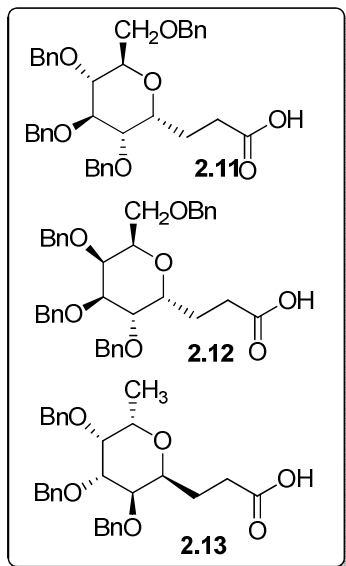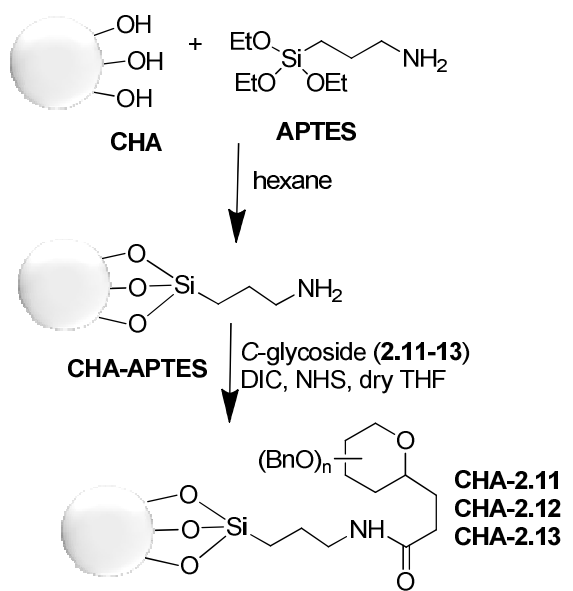
Scheme 2.5. Methodology for CHA functionalisation with carbohydrate C-glycosides.

In more details, the strategy for *C*-glycosides immobilisation (**Scheme 2.5**) involved: (i) grafting of aminopropyltriethoxy silane (APTES) onto the surface of CHA granules in dry hexane and (ii) reaction of the amino groups on the CHA surface with the activated hydroxysuccinyl esters from C-glycosides in dry THF as solvent.[6a]

In order to assess the degree of functionalization with the amino functionality, spectrophotometric analysis was performed, after silanisation of the hydroxyapatite with (3-triethoxysilylpropyl)carbamic acid 9H-fluorenylmethyl ester (Fmoc-APTES),[12] **Scheme 2.6**. The removal of the Fmoc group is usually achieved by treatment with piperidine in *N,N*-dimethylformamide (DMF). The mechanism of the Fmoc-deprotection reaction involves the formation of aromatic cyclopentadiene intermediates, which are rapidly eliminated to form dibenzofulvene, which is further scavenged by piperidine to form the Fmoc-adduct 1-((9*H*fluoren-9-yl)methyl) piperidine. This product strongly absorbs UV radiation at 289 nm, offering the potential to monitor the deprotection reaction by UV/visible spectroscopy, then quantitating the functional groups loading on CHA. Amino functionalisation of hydroxyapatite resulted 0.15 meq/g CHA.

C-glycosidic derivatives possessing a carboxylic group for the coupling reaction to the aminopropylsilane-functionalised CHA

(CHA-APTES) were synthesized in a few steps from the suitably protected natural monosaccharide (for experimental details see Supporting Information). Briefly, the ☐-allyl-*C*-glycoside was prepared by Sakurai reaction from the suitably protected parent monosaccharide;[13] then, the allyl *C*-glycosidic appendage was functionalized with a carboxyl terminus,[14] a suitable functional group for the condensation reaction with the CHA-APTES, by hydroboration (9-BBN), followed by oxidation to the corresponding carboxylic acid (TEMPO).[15] The carboxylic group was finally activated as succinyl ester (diisopropylcarbodiimide, *N*-hydroxysuccinimide) and then coupled to the amino group of CHA-APTES, in dry THF.
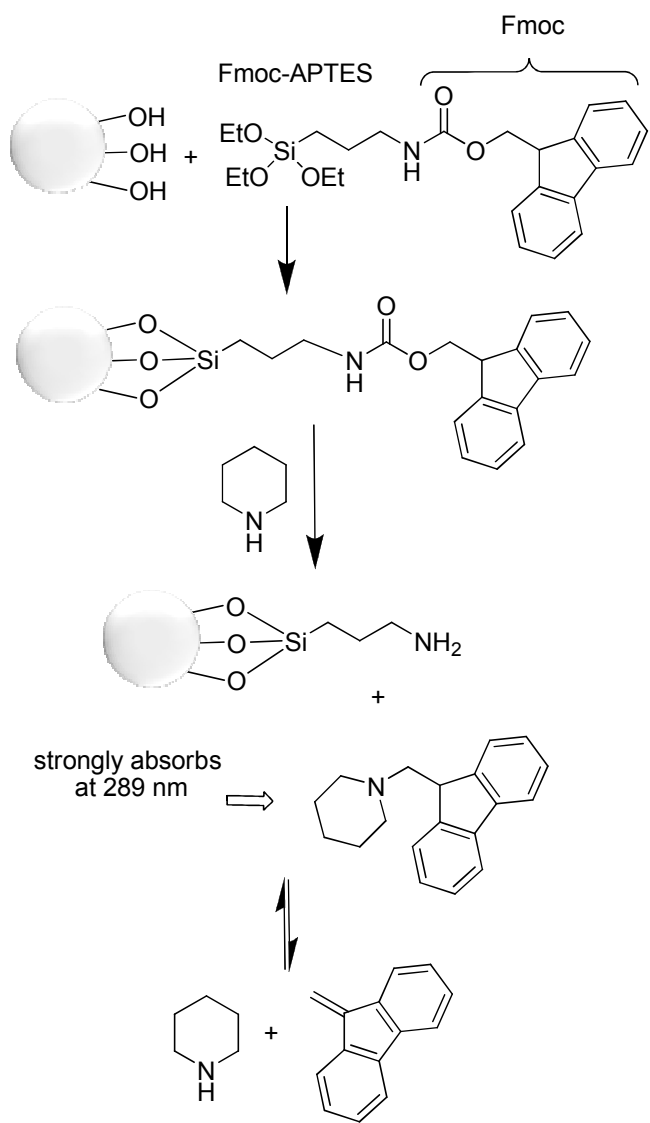
Scheme 2.6. Method used for the quantification of amino groups on HA surface.

2.1.4.1 Hydroxyapatite granules characterization

The CHA functionalized with carbohydrate derivatives was then characterized in order to determine (i) the chemical stability of the material upon chemical derivatisation and (ii) the effective biodecoration with carbohydrate derivatives.

In order to assess the stability of the material after chemical modifications, XRD analysis was performed and no phase change of the granules after functionalization could be detected: the material was still monophasic apatite. In addition, ICP analysis showed that the Ca/P molar ratio resulted substantially unaffected after chemical reactions. RX mapping of the elements performed by SEM-EDS analysis evidenced a homogeneous presence of Si, as for Ca and P, in the functionalized granules. The TG analysis of the unfunctionalised CHA granules in air detected a weight loss occurring up to 500°C imputable to dehydration of the absorbed and occluded water and to the removal of absorbed species.[16]

At higher temperatures carbonate ions decompose causing a weight loss due to CO_2 elimination, that allows to estimate the starting carbonation of the CHA granules as about 5.5 %wt. This value is in the range of the contents of the biological apatite (2-8 %wt).
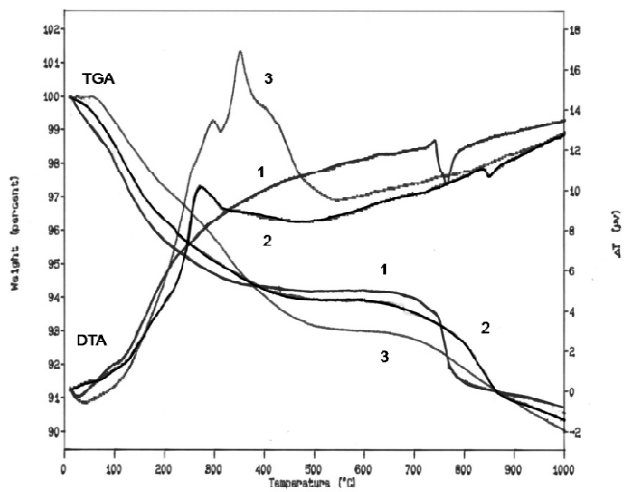
Figure 2.14 TGA analysisi of the HA samples: unfunctionalised CHA
(curve 1), CHA-APTES (curve 2) and biodecorated CHA (curve 3).

The STA analysis confirmed the presence of additional compounds
besides CHA in the functionalized material, since the TGA and the
DTA profiles changed moving from unfunctionalised CHA, to the
functionalized one (**Figure 2.14**). In particular DTA analysis
evidenced in both curves, 2 and 3 the presence of significant peaks in
the range of temperature 250-450°C imputable to the degradation of
organic phases. In particular, the peak centered at 270°C in curve 2
can be correlated to the degradation of the silane group (APTES) and
the multiple peaks in the range 250-450°C observable in curve 3 to the
presence of both, APTES and the linked carbohydrate moiety.

In order to further characterize the biofunctionalisation of CHA, that is in order to assess the effective biodecoration with carbohydrates Fourier transform infrared (FTIR) analysis were performed. In **figure 2.15** we report the infrared absorption spectrum of unfunctionalised CHA and those of the functionalized CHA, respectively with 3-aminopropyltriethoxysilane (CHA-APTES) and with C-glycosides **2.11-13**, conjugated to CHA *via* 3-aminopropyltriethoxysilane (spectra from CHA-1 CHA-3). All the spectra are dominated by the 1017 cm^{-1} absorption peak due to the phosphate (PO_4^{3-}) vibration of CHA. Other absorption bands of CHA can be observed in the spectra, as those due to the structural OH (3570 cm^{-1}), to phosphate (962 cm^{-1}), and to the B-type carbonate (couple at 1415 cm^{-1} and at ~1455 cm^{-1}, and the peak at 872 cm^{-1}).[16, 17] The presence of the typical peaks of the B-type carbonate confirmed that the carbonate ions are substituting in the phosphate site of hydroxyapatite.[16]
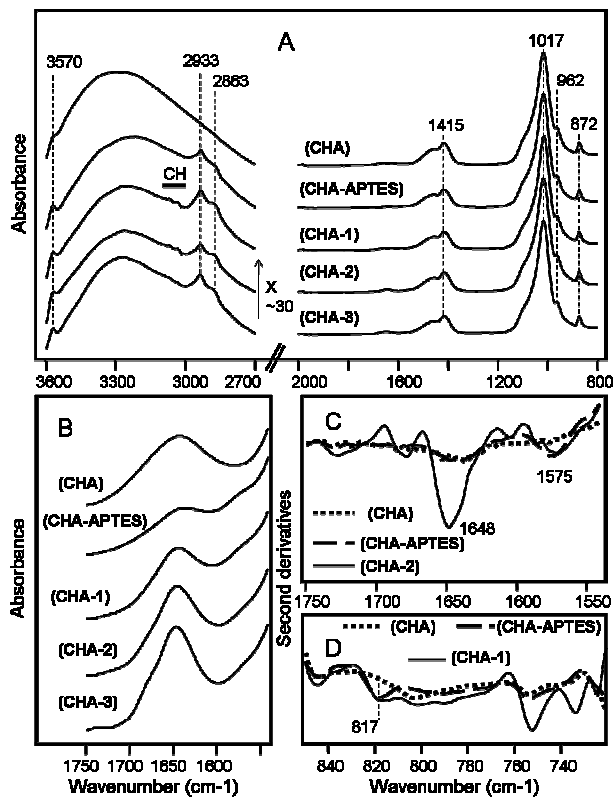
Figure 2.15 FTIR analysis of CHA samples. (A, B) ATR/FTIR absorption spectra of hydroxyapatite (CHA) and of functionalized CHA, respectively with 3-aminopropyltriethoxysilane (CHA-APTES) and with compounds **2.11-13** (CHA-2.11; CHA-2.12; CHA-2.13) showed in different spectral regions. (C, D) Second derivatives of the absorption spectra reported in (A, B) displayed in different spectral regions. Spectra are reported after normalization at the phosphate absorption at 1017 cm^{-1}.

For the characterization of the biodecorated materials, the spectral region 3100-2800 cm^{-1} where CH bonds absorption are usually found is of valuable interest. Indeed (Figure 2.15A), the functionalization with 3-aminopropyltriethoxysilane leads to the appearance of several new bands, including the 2933 cm^{-1} and 2863 cm^{-1} peaks that are due, respectively, to the asymmetric and symmetric CH_2 stretching. These bands are also present in the spectra of CHA biodecorated with derivatives **2.11**-**13** *via* 3-aminopropyltriethoxysilane. In addition, these last materials display absorption peaks in the region 3091-3033 cm^{-1} due to CH vibrations of aromatic rings present in the carbohydrate structure.

A more detailed inspection of the spectra discloses several additional features that further confirm the biodecoration of CHA. For instance, the formation of an amide bond between the silane group and the different compounds leads to a new absorption around 1650 cm^{-1} (**Figure 2.15 B**) due to the C=O amide stretching vibration.[18] To discard the possibility of carbohydrate absorbtion onto CHA, and fully confirm the bonding between the amine group of CHA-APTES and the *C*-glycosides carboxyl group, we performed the second derivative analysis of the measured spectra, which is a resolution enhancement mathematical procedure. Since the C=O amide band displays a reduced width compared to the CHA absorption in the same spectral region, in this way it is possible to clearly detect the formation of the new amide bond,[18] as can be seen in **figure 2.15 C**, where only the

CHA-2.12 is reported as example. The presence of an absorption component around 1575 cm^{-1} further confirms the formation of an amide bond. Indeed, this component – absent in the CHA spectrum - can be assigned to the NH$_2$ bending vibration in the case of CHA-APTES and to the NH bending (Amide II band) in that of CHA-2.12 (Fig. 2.15C). Similar results were obtained for the biodecoration with carbohydrates **2.11** and **2.13**.

Many other additional bands were also observed after biodecoration confirming the success of our procedure. For instance, the absorption in the 720-760 cm^{-1} region can be assigned to aromatic ring vibrations (Fig. 2.15D). We should also report that materials CHA-APTES, CHA-2.11, CHA-2.12 and CHA-2.13 display a component around 817 cm^{-1}, absent in CHA, that can be assigned to a vibrational –O-Si- mode.[19]

With all these data in our hands we can affirm that carbonated hydroxyapatite has been successfully biodecorated with carbohydrate derivatives. It should pointed out that classical organic coupling reactions have been applied for the covalent functionalisation of inorganic materials such CHA.

2.2 Polypropylene (PP) membrane as model system

The preparation of new or existing materials with tailor-made functionalities utilizing tough, efficient and orthogonal chemistry is

still challenging and will demand more and more the involvement of synthetic organic chemistry into materials science. "Click" chemistry[66] is a striking example of the organic chemistry contribution to material science[67,68]. A variety of click reactions have been reported[69], but the Huisgen 1,3-dipolar cycloaddition catalysed by copper (I) between azides and alkynes yielding irreversibly a stable 1,4-disubstituted 1,2,3-triazole[70] plays a particularly relevant role in organic synthesis and fulfils many requirements for the conjugation of polyfunctional molecules onto polymers by post-modification processes. In fact, this cycloaddition reaction is characterised by high versatility as well as high specificity and chemoselectivity in the presence of a wide variety of surrounding functional groups and solvents (ranging from both protic and aprotic organic solvent to water). These reactions are featured by a high thermodynamic driving force (generally above 20 kcal mol^{-1}), thus allowing the use of mild reaction conditions and short reaction times. The use of Cu(I) catalysts accelerates the process, leading to quantitative coupling yields at room temperature.[71] Cu(I)-catalysed Huisgen-type cycloadditions have been employed in a variety of applications in the field of material science[72,73], such as the preparation of highly functionalized macromolecules[74] and the surface immobilization of (bio)macromolecules and polymers [75,76].

In order to apply Huisgen cycloaddition to material science, suitable methods for azido groups introduction are needed. Several strategies

have been proposed for the preparation of azido-functionalized polymers[77,78]; among them we can mention a general strategy consisting in the (co)polymerization of halide functionalized monomers followed by nucleophilic substitution of the halide groups by sodium azide (NaN_3)[79,80]. Alternatively, the azido group can be introduced via epoxide opening by NaN_3 on the co-polymerised of glycidyl-containing monomers (i.e. glycidyl methacrylate)[81]. A second approach consists in the (co)polymerisation of azido-prefunctionalized monomers[12,13]. However, both approaches suffer from a strong limitation: the necessity of using only particular functionalized monomers (halide-, epoxide-, azido-functionalized), restricts the possibility of tailoring the chemical and physico-mechanical properties of the material, which could result, in this way, unsuitable for the desired application.

In the last years, plasma treatments have been gaining popularity as a versatile tool for surface modification of materials[82,83,84,85,86]. Plasma treatments can be used to introduce different functionalities onto inert surfaces (for example polyolefins); examples of plasma modifications include the introduction of COOH and OH functionalities through air[87, 88, 89, 90], O_2[91] or inert gases (Ar, He) plasmas[24,92] (in the latter case is the post-exposure to air of the treated materials which leads to the introduction of oxygen-containing functionalities), and the introduction of amines (through, for example, NH_3 plasmas). The use of plasma modification techniques has some major advantages. First

of all, they modify the surface of the materials without affecting their morphology and their physical and chemical bulk properties. Moreover, other techniques will often influence the mechanical properties of the outer layer of an implant. For example, wet chemical treatment of a surface will cause a partial degradation and scissions of the polymer chains at the surface, leading to a decrease of the mechanical strength and to a faster degradation. Another advantage is that plasma treatments enable to uniformly modify the materials surfaces, regardless of the geometry, and can be used on complex objects. Finally, the use of hazardous solvents can be avoided, as plasma is a solvent-free technique.

Chemically, two main strategies can be used for the introduction of an azido group on organic compounds. Traditionally, the introduction of azides has been achieved by nucleophilic attack of inorganic azide (usually NaN_3) on appropriate leaving groups. Recently, diazo transfer from triflyl azide (TfN_3) to primary amines has found wide use[93]. This approach was initially reported in the 1970s, and found large application since the 1990s. Since then, the diazo transfer procedure has been widely exploited, especially for the modification of biomolecules such as proteins, as recently demonstrated[94].

Both procedures (nucleophilic substitution and diazo transfer) can be readily applied to the majority of chemical structures. However, while the first approach has been extensively used in material science, to date to the best of our knowledge no examples of diazo transfer

processes have been reported for the preparation of azido-functionalized material surfaces.

Hereby we propose a novel and alternative strategy for the incorporation of azido functionalities onto polymeric materials coupling plasma technology and solution processed diazo transfer reaction. Thus the first step is solvent-free, whereas the second step is performed in heterogeneous phase in the presence of organic solvents. The approach allows for the introduction of the azido group downstream of the material preparation, preserving in this way its physico-chemical and mechanical characteristics which can be *a priori* tailored accordingly to the desired application. Obviously, this feature represents a great advantage in comparison with the above mentioned strategies for the insertion of N_3 functionalities. The method is widely applicable to polymers of different nature, since plasma allows the introduction of functional groups onto different materials, even on those not presenting reactive functional groups. The long term goal is to decorate *via* covalent immobilization any material with (bio)active molecules, an application that has seen rapid growth in the past decade in such industries as biomedical, textiles, microelectronics, bioprocessing, and food packaging, in addition to biosensing or bioseparation applications.[27]

Polypropylene is an interesting model system, since it is an organic material that does not possess any functional groups needed for bioconjugation of active molecules. Thus we envisaged the possibility

to use PP as a general model for setting up functionalisation conditions, that can be applied to any other biomaterial of interest. The whole process involves the surface plasma functionalization of a material with primary amino groups, followed by a diazo transfer reaction which converts the amino functionalities into azido groups, that can be exploited for further chemoselective reactions. Chemical reactivity of the azido functionalities was verified by subsequent "click" chemistry with a monosaccharide previously synthesised (**Scheme 2.6**).
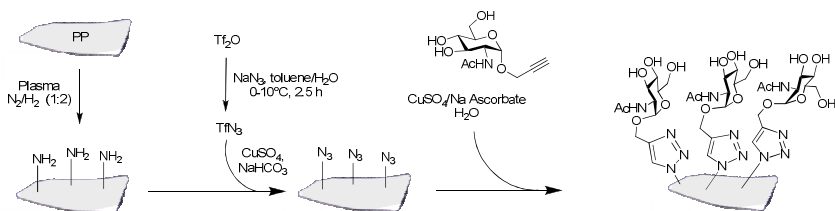
Scheme 2.6. Azido functionalization process

2.2.1 Strategy for azido functionalization of materials

As proofs of concept we then applied this novel methodology to polypropylene (PP). The whole process, illustrated in Scheme 2.6, involves the surface plasma functionalization of PP membranes with primary amino groups (-NH$_2$ groups), followed by diazo transfer reaction for the conversion of the amino functionalities into azido

66

groups. The amino functionalization of polyolefinic materials by means of plasma treatments has been successfully investigated in the past[95,96]. For this purpose, plasma treatments with NH_3 or N_2/H_2 mixtures and plasma polymerization of amine-containing monomers (such as allyl amine) are generally used. Literature demonstrates[31,32] that such kind of plasmas allow the creation of surfaces with an NH_2 surface density ranging from 0.5 and 1.5 groups/nm^2, as determined by fluorescence and colorimetric assays. PP membranes (0.2 μm pore size) were treated with an N_2/H_2 plasma and characterized to assess the introduction of primary amino groups, which can be easily detected with fluorescamine, a non-fluorescent compound that selectively reacts with primary amino groups yielding a fluorescent product (λ_{ecc}= 400 nm, λ_{em}= 475 nm). Hence, we dipped untreated and plasma-treated membranes in a 9×10^{-4} M solution of fluorescamine in acetone (reaction time 10 minutes).[97] After rinsing and drying of the samples, the insertion of amino functionalities was assessed by fluorescence. Figures. 2.16a and 2.16b show, respectively, an untreated and a plasma-treated PP membrane after immersion in the fluorescamine solution. Photographs were acquired under UV irradiation, using a laboratory lamp emitting at 366 nm. The strong fluorescence of the modified membrane (**Figure. 2.16b**) confirms the amino functionalization owing to the plasma treatment.
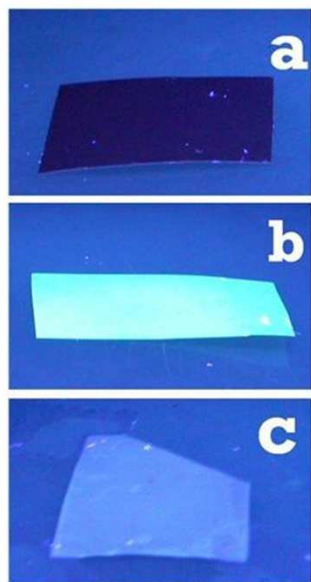
Figure 2.16. UV irradiation of polypropylene membranes

The conversion of the amino groups into azido functionalities was performed by diazo transfer reaction mediated by freshly prepared triflyl azide[28]; the amino functionalised PP membrane was suspended in milliQ water containing $NaHCO_3$, $CuSO_4 \cdot 5H_2O$, triflic azide in toluene, and methanol. The total volume of the solvents was such as to fully cover the membrane, and the ratio was H_2O/ toluene/MeOH 1/1.7/6.7 in order to have a monophasic solvent mixture. ATR/FTIR spectroscopy (**Figure 2.17**) confirms the formation of azido groups on the surface of the PP membranes. The adsorption band at 2104 nm is unequivocally assigned to the stretching vibration of the azido groups. Furthermore, a decrease of the band related to the amino

functionalities is observed. The conversion reaction is almost complete, as confirmed by the small residual fluorescence detected on azido-functionalized membrane dipped in a fluorescamine solution. In order to prove the effective diazo transfer reaction, a blank test was performed dipping a crude PP membrane, i.e. without amino groups, in the triflyl azide solution; IR analysis did not show azide signals that could be ascribed to diffusion of the reactants inside the membrane
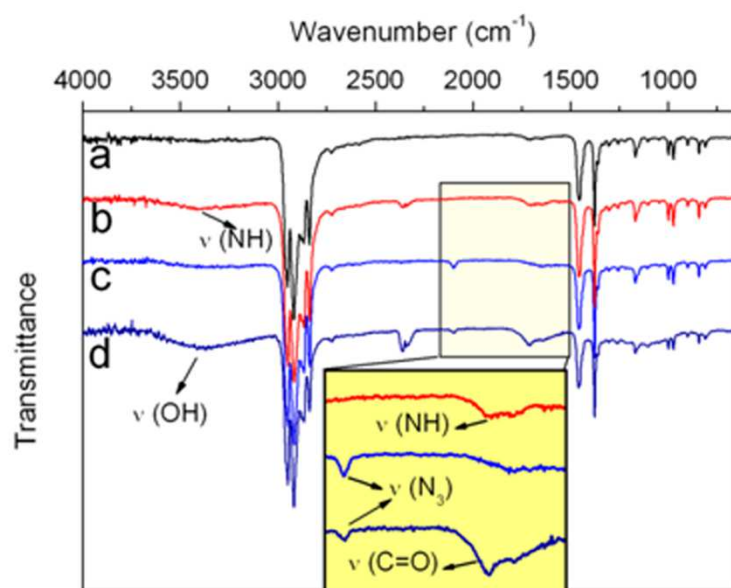

Figure 2.17 ATR/FTIR spectroscopy

To further confirm the presence of the azido functionality, XPS analysis was also performed (Figure 2.18). N_2-plasma treated surfaces present several and diverse nitrogen-containing functionalities, including primary amines, amides, urethanes etc.[32]. The best fit of the N1s peak allows to estimate that the amine group (which are known to have a characteristic single peak at 399.3 eV)[98] accounts for 27% (**Figure 2.18**, blue area) of the total nitrogen-containing functionalities (black peak). The typical peaks indicating the presence of the azido functionalities (i.e. around 400 and 404 eV binding energies),[99] are very close to the other nitrogen-containing functional groups, but despite the presence of several nitrogen-containing species, XPS allowed us to detect the presence of the azido functionalities (Fig. 3b, blue area): the appearance of the peak at 403.4 eV (ascribed to the electron deficient central nitrogen of the azido group)[35] is indicative of azido group presence; on the other hand the second peak due to the electron-rich nitrogen of the azide results overimposed to the peaks due to the other nitrogen-containing groups.
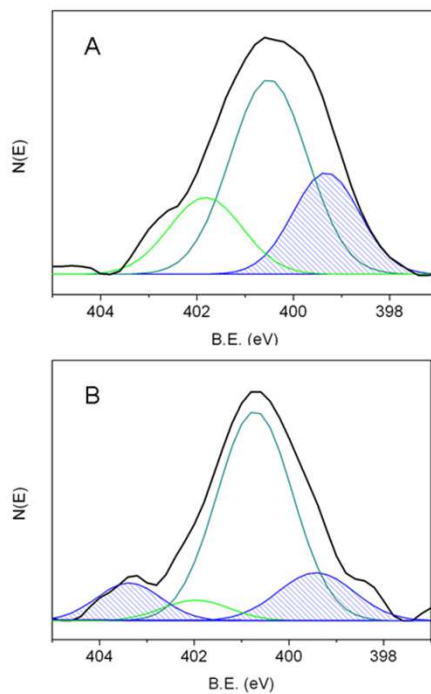
Figure 2.18 XPS analysis

The obtained azido-functionalyzed material was submitted to click coupling with an alkyne. As the alkyne partner, in order to give also biological relevance to the method, propargyl 2-acetamido-2-deoxy-☐-d-glucopyranoside (**Scheme 2.7**) was used as model substrate. Carbohydrates are an excellent platform for material functionalization for several reasons. First, carbohydrates can be used to tailor the material (bio)properties, for example improving cell adhesion[100], or bioactivity[101]; in addition since they possess polar groups (i.e.

hydroxyl and amino/acetamido groups) they can be used to modify the hydrophilicity of the material surface to which they are grafted.

However, since carbohydrates are polyfunctional molecules, novel and effective approaches for carbohydrate immobilization onto solid surfaces by chemoselective reactions are highly desirable. The chemoselective approach is recently finding wide application in glycomic studies[102], that is the study of the carbohydrate-protein interactions involved in several biological mechanisms, including viral infection, cancer metastasis, peptide conformation, enzyme activity, cell-cell recognition, cell adhesion, and cell development. The presentation of carbohydrates in an immobilized format facilitates many of such studies, allowing the preparation of carbohydrate glycochips[103] for the screening of carbohydrate arrays[104]. In this respect, alkynyl glycosides, which are suited for the chemoselective Huisgen cycloaddition, are particularly interesting since they can be easily obtained from the free parent saccharide, in excellent yields and purity.[105]

Propargyl 2-acetamido-2-deoxy-□-d-glucopyranoside is an interesting model substrate, since it is a relevant monosaccharide involved in many biological phenomena, and, in addition, it possesses the acetamido functionality at C-2, that can be exploited as probe for ATR/FTIR surface characterization of the functionalised PP. The PP-N_3 surfaces were submitted to copper(I)-mediated Huisgen cycloaddition in water. ATR/FTIR spectra (**Figs. 2.17c** and **2.17d**)

72

confirms the success in the coupling reaction. In fact, a decrease of the adsorption band at 2104 nm (stretching vibration of the azido groups) can be observed, together with the appearance of new bands at 3020-3750 cm^{-1} and 1708 cm^{-1} that can be ascribed to the stretching vibrations of OH and C=O groups (of the acetamido functionality) of the coupled monosaccharide, respectively.

In order to further confirm the cycloaddition reaction, contact angle measurements were performed prior and after the coupling reaction. The azido-functionalized surface is hydrophobic (contact angle = 122°±4°). Instead, the carbohydrate-functionalized surface, as expected, is hydrophilic (contact angle = 74°±7°). This result represent a further evidence of a successful cycloaddition on the modified PP membranes. (**Figure 2.19**)
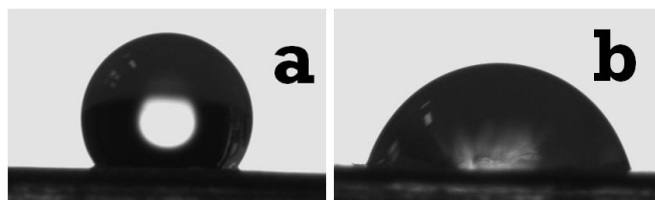

Figure 2.19 Photographs of water drops putted on differently modified PP membranes. (a) azido-functionalized membrane; (b) carbohydrate functionalized membrane by click coupling.

Finally, the morphology of the material before and after surface modifications was investigated by scanning electron microscopy

(SEM), that does not evidence any major changes of the membrane structure and porosity (**Figure 2.20**).


Untreated PP-membrane   Modified PP-membrane
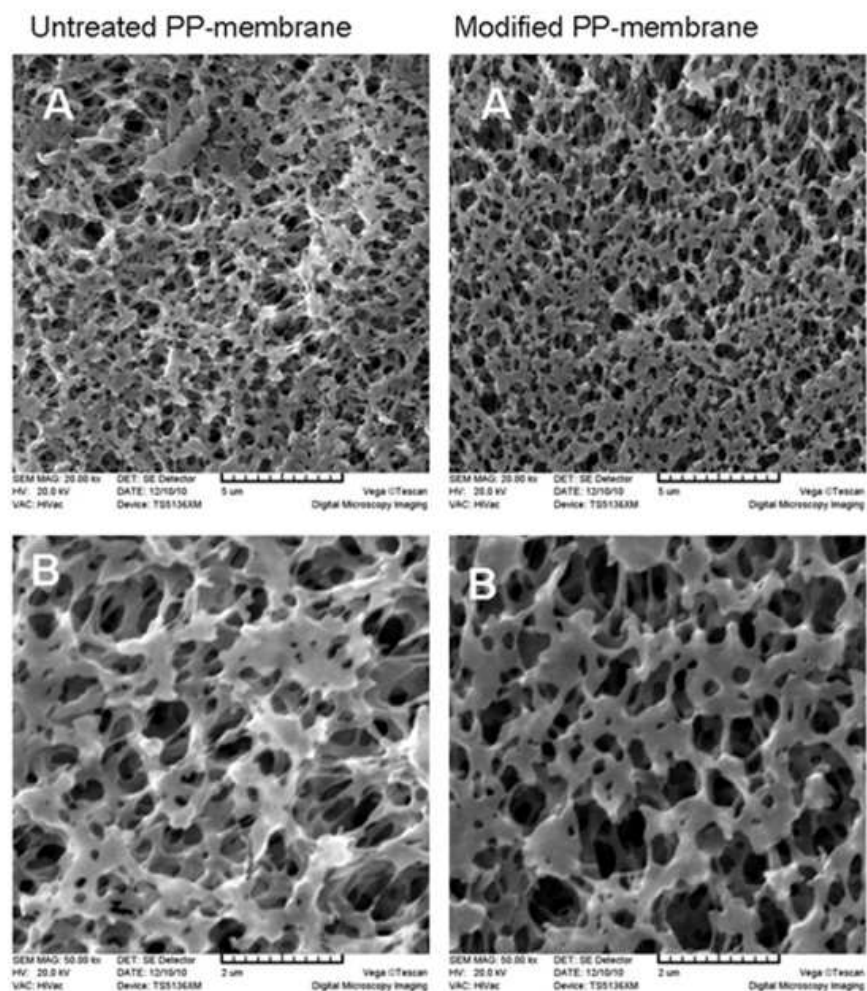
Figure 2.20. SEM analysis

2.3. Polycaprolactone (PCL)

PCL is another relevant implantable biomaterial, with good mechanical properties and slower degradation rate. It is extensively used as sutures, adhesives and scaffolds in tissue engineering.

Biodegradable synthetic materials such as poly(ε-caprolactone) (PCL), has been used as scaffolds to support the regeneration of bone in tissue-engineered applications. However, as any other synthetic polymer it does not present molecular motifs for cell biological recognition, and therefore it is unable to cross-talk with living cells; moreover it is highly hydrophobic, and this feature can mine the interaction with body fluids and cells. On the basis of these considerations, biomimetic approaches have been developed, in order to produce bioactive materials able to promote and enhance cell attachment. New funtionalities were covalently introduced onto a PCL surface by the reaction between amino groups of different molecules and the ester groups of PCL. While aminolysis reactions with 1,6-hexandiamine is a classical method for PCL functionalisation[106], we therein propose the use of different biomolecules that can be used both for aminolysis and at the same time add biological cues to the material surface.

The different approaches used for PCL functionalisation are described in the following sections.

2.3.1. PCL: a one step procedure

We investigated the possibility of PCL bioactivation by one-step procedure of polymer aminolysis to graft bioactive molecules on the polymer surface. PCL substrates were manufactured through melting-molding and molding-solvent casting techniques. Aminolysis on PCL substrates/scaffolds was then performed with an amino sugar (**Scheme 2.7**).
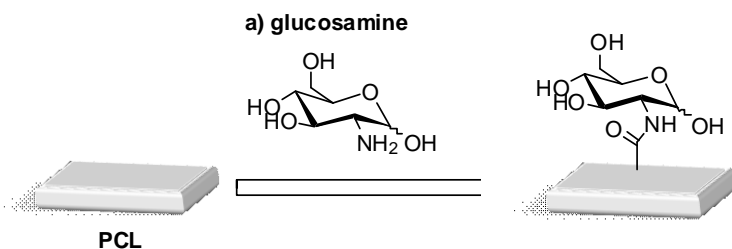
Sceme 2.7. Surface modification of PCL with glucosamine

The novel biofunctionalised PCL substrates were then characterised in terms of morphological, mechanical and biological properties. In particular mechanical properties of surface-modified and unmodified PCL samples were investigated using the small punch test setup (ASTM F 2183) (Figure 2.21), which covers the determination of the mechanical behavior by small punch testing of miniature disk

specimens, in order to evaluate the effect of the functionalization/bioactivation process on the mechanical behavior.

**Figure 2.21.** Experimental setup used to perform small punch tests.

The results obtained from small punch tests performed on surface-modified and unmodified PCL samples have highlighted that the functionalization/bioactivation does not alter the mechanical performances (Table 2.2).

Materials	Peak Load (N)
Unmodified PCL	29.0 ± 2.1
Surface-modified PCL	27.5 ± 3.2

Table 2.2. Results obtained from small punch tests: peak load reported as mean value ± standard deviation.

2.3.2 PCL: functionalization via linker

New functional groups were covalently introduced onto a PCL surface by the reaction between amino groups of linkers and the ester groups of PCL. By aminolysis with 1,6-hexanediamine, free amino groups were introduced onto the PCL membrane surface. Moreover aminolysis reaction was performed also by cysteine with the introduction of SH group useful for the chemoselective linkage of small biolecules and a carboxy group for calcium coordination (**Scheme 2.8**). Introduction of new functionalities will be useful for cell adhesion and covalent linkage of biomolecules to induce proliferation and differentiation.
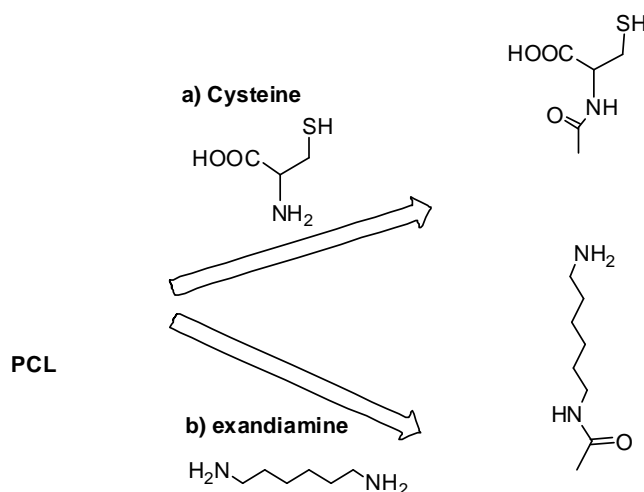
Scheme 2.8. A) Cysteine reaction; B) Exandiamine reaction

The novel biofunctionalised PCL substrates were then in terms of mechanical properties. In particular, small punch tests (ASTM F 2183) was performed on Cystein functionalised PCL. The results obtained from small punch tests performed on surface-modified and unmodified PCL samples have highlighted that the functionalization/bioactivation does not alter the mechanical performances (**Table 2.3**).

Materials	Peak Load (N)
Unmodified PCL	29.0 ± 2.1
Surface-modified PCL	28.1 ± 2.7

Table 2.3 Results obtained from small punch tests: peak load reported as mean value ± standard deviation.

2.4. Collagen

Collagen is the major component of articular cartilage, it is responsible for the compressive and tensile strenght of the tissue and universally applied as biomaterial in regenerative medicine because of its unique biocompatibility. Collagen accounts for 30% of all body proteins in mammalian species and it is found to be highly

conserved.6 It is composed of three protein chains wrapped around each other in a tight triple helix, which arrange with other helices via secondary interactions to form a thermally reversible hydrogel.[46]

For cartilage repair, biomaterials should have several properties to support viable repair. Firstly, the material must act as a support structure for cells and possess enough mechanical strength to protect the cells contained within it, withstanding *in vivo* forces during joint movement. Secondly, some level of bioactivity should be provided to accommodate cellular attachment and migration. Furthermore, the materials should be biodegradable and remodel as the new cartilage forms and replaces the original construct. In this regard, the matrix should be non-toxic, non-attractive and non-stimulatory of inflammatory cells, and also non-immunogenic, which would be detrimental to tissue regeneration. Finally, the scaffolds should provide easy handling under clinical conditions, enabling fixation of the materials into the implant site. [45]

Collagen is universally applied as biomaterial in regenerative medicine because of its unique biocompatibility.

2.4.1 Collagen film modification

To study and design collagen based smart materials we produced a collagen film subsequently modificated by plasma deposition strategy

with the introduction of carboxylic and amino groups on the surface of material.

Characterization of film surface properties such as surface hydrophilicity and roughness was made by contact angle measurement (**Figure 2.22**) and atomic force microscopy (**Figure 2.23**), respectively. Contact angle analysis revealed that the surface hydrophilicity significantly increased after the treatments. In addition, AFM characterization showed an increase in surface roughness through plasma treatments. An enhanced roughness is considered as a beneficial factor in adhesion processes, since it is a consequence of surface etching and functionalization[107]
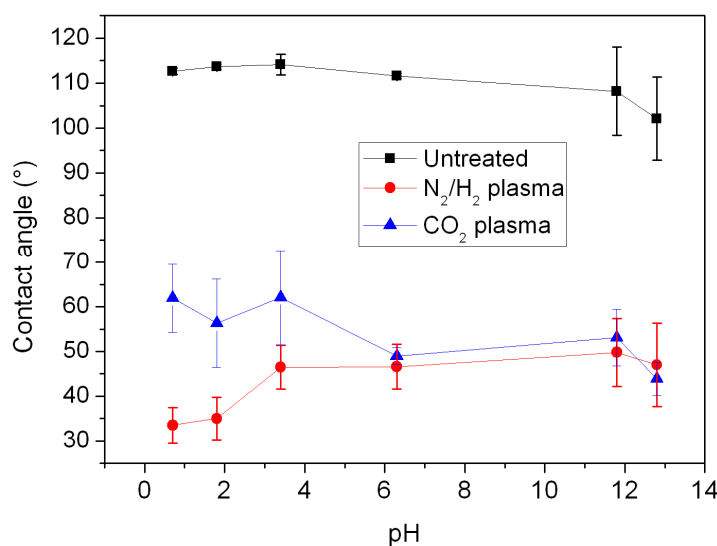

**Figure 2.22** Contact Angle Measurement
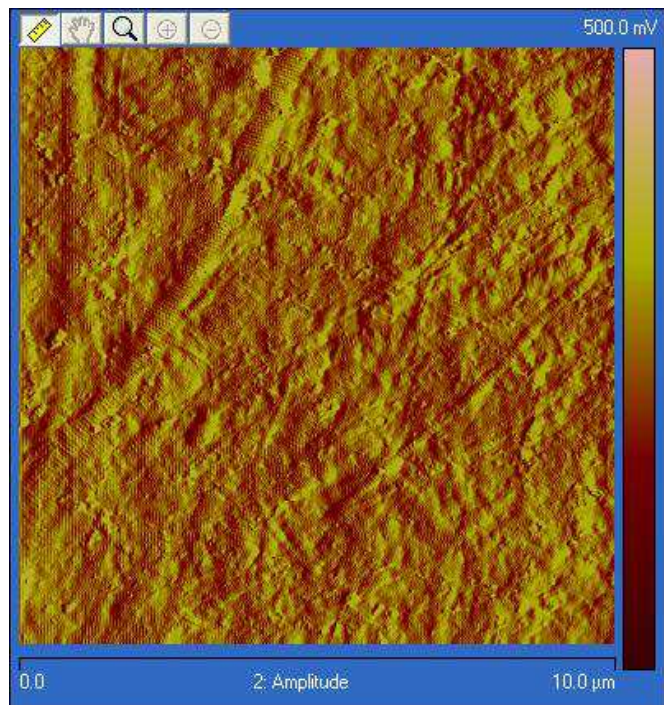
Figure 2.23 AFM analysis

In order to further characterize the collagen membrane, the plasma treated-collagen membranes were reacted with a fluorescent probe via a covalent bond, in order to quantify the carboxylic groups introduced by plasma deposition (**Scheme 2.9**). As a result, strong fluorescence of both the modified collagen film and the unmodified collagen was obtained. The possible explamnation for this result is that the dansyl hydrazine is reacting also with the functional groups of side-chain of amino acids of the protein, thus giving a very strong background that covers the fluorescence signal due to the plasma functionalisation that

82

is known to be quite low. We still have to find a suitable method to quantify the functional groups inserted by plasma technique.
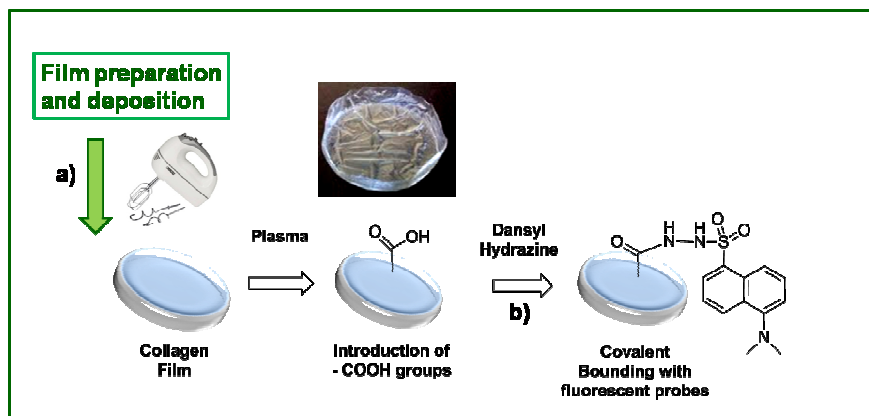
Scheme 2.9. Collagen film and functionalization model

However, surface modifications of collagen films and fibrous scaffolds could be evaluated by means of contact angle measurements and labeling with fluorescent probes. Contact angle measurements allow us to assess the changes in the surface energy and in the acid/base surface character of the collagen scaffolds following to the plasma treatments (**Figure 2.24**).
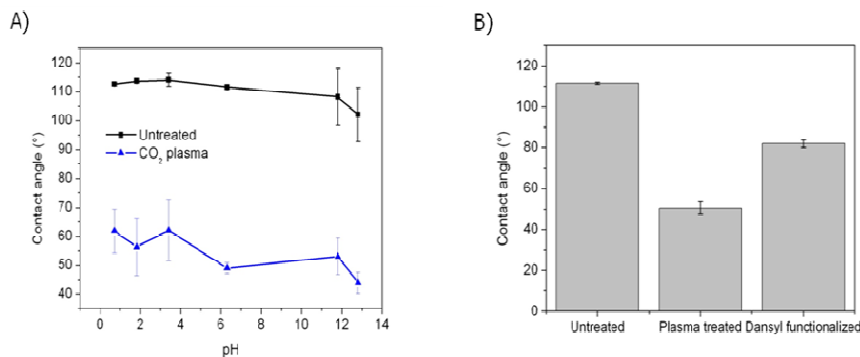
Figure 2.24 Contact Angle: A) Untreated and Plasma treated collagen films. B) Untreated, Plasma treated and dansyl hydrazine functionalizated collagen films.

2.4.2 Biological assay

Collagen films functionalized by plasma technology with the carboxyl group -COOH and the amino group -NH$_2$ were assayed *in vitro* for osteoblast proliferation, attachment, viability and morphology at 1, 3 and 7 days after seeding. Human MG-63 Osteoblast-like cells were used. Non-functionalized collagen films were used as control.

Analysis of cell proliferation

Quantification of metabolically active cells was performed for each time point, by use of the MTT assay. Results demonstrate an increase in cell proliferation from day 1 to day 7 for all collagen films (**Figure 2.25**). No statistically significant difference was identified between

control collagen film and -COOH or -NH$_2$ functionalized films for any of the time points, indicating that functionalized films perform equally well as non-functionalized films to what regards osteoblast proliferation.
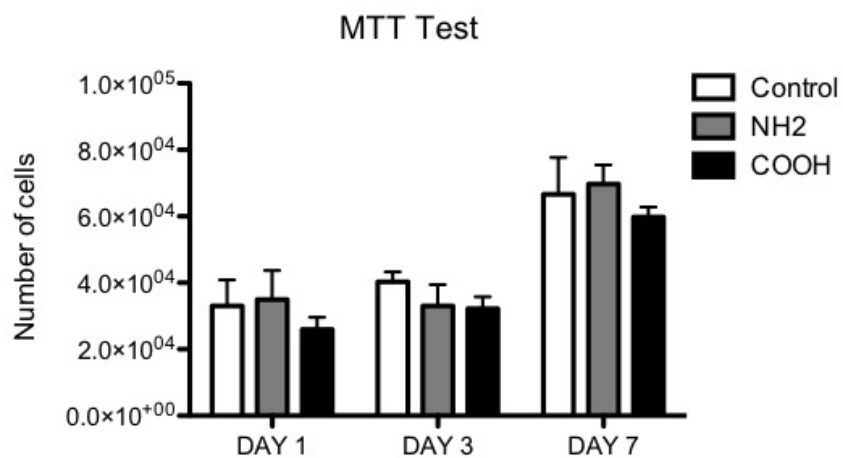
**Figure 2.25** MTT assay

Analysis of cell viability, spreading and morphology

The Live/Dead assay was performed on each collagen film at the indicated time points. Results show no difference in cell viability, with a high number of live cells and limited number of dead cells for control and functionalized scaffolds (Figure 2.26 A,B,C), indicating high biocompatibility for all collagen films.

Phalloidin was used as a specific marker for actin filaments, which allowed the analysis of cell morphology and cell spreading on the material surface. No difference was observed between cells seeded on control and on collagen functionalized with carboxyl and amino groups, for any of the time points (**Figure 2.26D**). Moreover, cell morphology was visualized by scanning electron microscopy at 1, 3 and 7 days after seeding and again, no difference was observed between collagen films (**Figure 2.26E,F**).
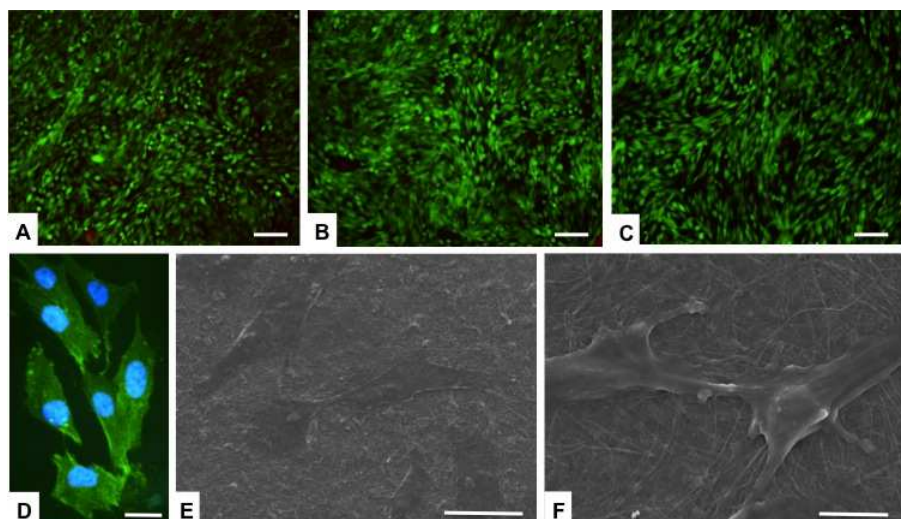

Figure 2.26 Live/Dead assay

Overall, these results demonstrate that the *in vitro* behaviour of collagen films functionalized with either -COOH and -NH$_2$ groups is

identical, with no difference to non-functionalized collagen film. All three present high osteoblast biocompatibility.

Chapter 3

Study, design and synthesis of biomolecules

Different classes of biomolecules have been used in combination with different materials and different functionalisation strategies in order to develop new biomaterials.

3.1 C-Nautriuretic Peptide (CNP) and short motifs

Natriuretic peptides are a family of structurally related but genetically distinct hormones/paracrine factors that regulate blood volume, blood pressure, ventricular hypertrophy, pulmonary hypertension, fat metabolism, and long bone growth.[108] These peptides were given a number of different names such as atrial natriuretic factor, cardionatrin, cardiodilatin, atriopeptin, and atrial natriuretic peptide (ANP); the latter description is most often used today. In addition to ANP, B-type natriuretic peptide (BNP), which was originally called brain natriuretic peptide[109] and C-type natriuretic peptide (CNP)[110,111] were subsequently purified from porcine brain extracts based on their ability to relax smooth muscle. Moreover, Dendroaspis natriuretic peptide (DNP) was isolated from the venom of *Dendroaspis angusticeps* (the green mamba snake).[112] However, the gene for DNP has yet to be identified in the human genome. DNP present high sequence homology with the previous ones, as depicted in **Figure 3.1**.

A- and B-type natriuretic peptide are secreted from the cardiac atria and ventricles, respectively. ANP signals in an endocrine and paracrine manner to decrease blood pressure and cardiac hypertrophy. BNP acts locally to reduce ventricular fibrosis. C-type natriuretic peptide (CNP) primarily stimulates long bone growth but likely serves unappreciated functions as well.

All natriuretic peptides are similar in primary amino acid structure, containing a 17-residue disulfide ring (**Figure 3.1**), and are the products of separate genes.[113]

The natriuretic system in mammals consists of the above mentioned peptides type A-, B-,and C-, and three receptors mediating their biological activity, NPR-A, NPR-B, and NPR-C.[6, 114] They are also known as GC-A (guanylyl cyclase A) , GC-B (Guanylyl Cyclase B), and the clearance receptor, or as NPR1, NPR2, and NPR3, respectively. The GC-A receptor, which preferentially binds ANP and BNP, and the GC-B receptor, whose cognate ligand is CNP, are coupled to guanylyl cyclase, producing cGMP as a secondary messenger. NPR-A and NPR-B represent two of the five transmembrane guanylyl cyclases found in humans.[115] The third natriuretic peptide receptor, NPR-C, has no guanylyl cyclase activity or any known intrinsic enzymatic activity and binds all three NPs with similar affinity. To date, no specific endogenous ligand has been identified for NPR-C, and it is thought to act mainly as a clearance receptor, although other roles have been proposed.[116]

The significance of the CNP/GC-B/NPR-C axis in longitudinal bone growth is now widely recognized,[117,118,119] while the functional consequences of the CNP/GC-B/NPR-C axis on osteoblasts are still unknown.

Natriuretic peptides have therapeutic potential[120] and have already found application into the clinics, especially ANP and BNP. Measurement of serum BNP levels is used in the clinic as a diagnostic indicator for heart failure, and synthetic analogues of both of these peptides have been approved in some countries for the treatment of heart failure;[121] trials are underway to determine the most effective use of these peptides. Concerning CNP, recently a patent appeared on its application in the treatment of skeletal dysplasia.[122]

We obtained preliminary results regarding an ongoing research project focused on the study of the effect of different fragments of CNP on osteogenesis and chondrogenesis compared to the full length peptide. At first, sequence similarity among the NPs class and a conformational investigation by molecular dynamics simulations of CNP in comparison to ANP and BNP were carried out[123].

The primary sequence of CNP was aligned to the other NPs known sequences and to the C-terminal fragment of the osteocrin peptide, which has been recently shown to present homology to NPs and to interact with the NPR-C receptor (Figure 1).[124] Extensive structure-activity studies of NPs have converged on the idea that the residues

within the cyclized loop are largely, responsible for receptor selectivity.[1]


```
           1          10
           .          .
CNP        CFGLKLDRIGSMSGLGC
ANP        CFGGRMDRIGAQSGLGC
BNP        CFGRKMDRISSSSGLGC
DNP        CFGHKIDRINHVSNLGC
Ostn-1     .FGSPLDRLSAG.....
Ostn-2     .FGIFMDRIGRN.....
```
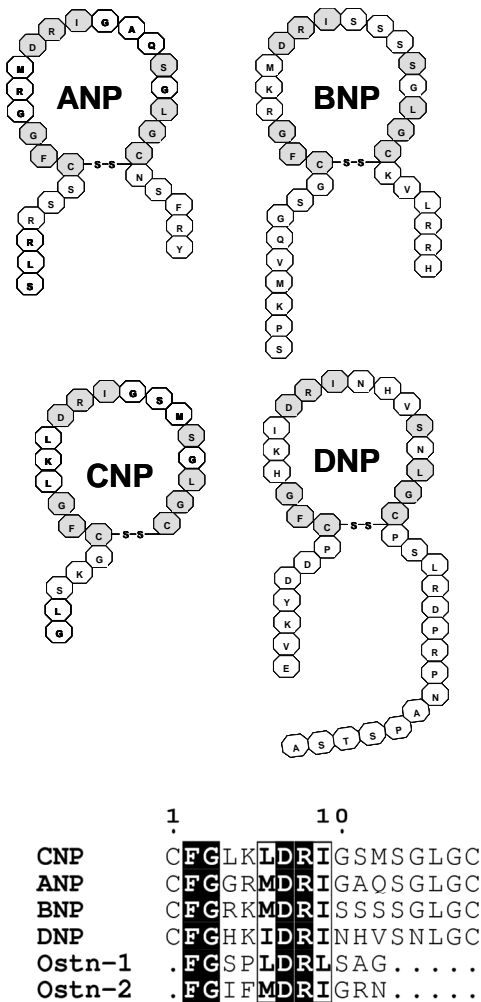
Figure 3.1. Structures of natriuretic peptides (shaded circles indicate identical amino acids; each ring structure is stabilized by a disulphide bond) and multiple sequence alignment of NPs. The multiple sequence

alignment has been carried out by ClustalW2 (http://www.ebi.ac.uk/Tools/clustalw2). For sake of clarity, only the sequences of the cyclic portion of the NPs have been considered. Ostn-1 and Ostn-2 are the sequences of the C-terminal proteolytic fragments of osteocrin peptide.[17]

3.1.1. Computational studies

Therefore we focused on the analysis of the cyclic portion of the peptides. From the sequence alignment of NPs, it turns out that ANP and BNP present higher similarity when compared to CNP (**Figure 3.1**). In particular, differences between CNP and ANP/BNP are located mainly in two regions of the cyclized loop (4-6 and 10-12). The action of the three main members of the NP family (ANP, BNP and CNP) is mediated through their cell-surface receptors, NPRs. In particular, NPR-A and NPR-B transduce the NPs signal through a large cytoplasmic domain and they are specific for ANP/BNP and CNP, respectively. The differences in the cycle primary sequences between ANP/BNP and CNP can reflect differences in the activity and specificity for different NPRs.

Conformational study of NPs in solution

The X-ray structure of NPs used as initial structure for MD simulations are derived by the complexes between the receptor NPR-C and the peptides. No intramolecular stabilization of the peptides

92

were observed in these complexes, suggesting that they are not stable solution structures. In fact, the structure of the free peptides rapidly diverged during MD simulations from the bound-conformations (**Figure 3.2**).

Therefore, to better characterize the conformations assumed from the peptides in solutions, cluster analysis of mainchain rmsd matrices were carried out and the average structures from the main populated clusters were reported in **Figure 3.2.** Several conformations are explored during the simulations indicating a high flexibility of the peptides.
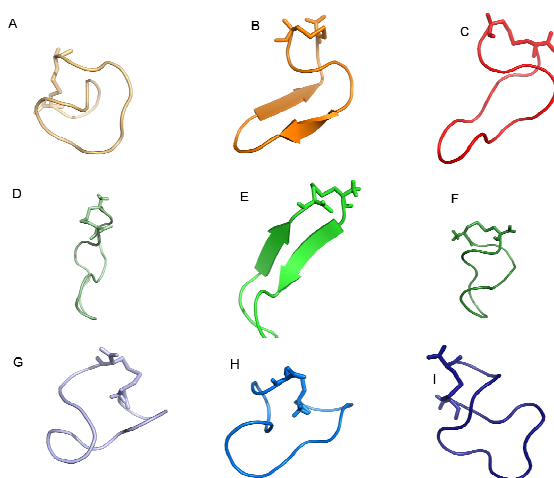

Figure 3.2. Average structures from cluster analysis of peptide simulations. The average structures from the three-main populated clusters of ANP (A-C), BNP (D-F) and, CNP (G-I) simulations are shown.

Moreover it turns out that transient formations of beta-strand structures are observed only in ANP (**Figure 3.2B**) and BNP (**Figure 3.2E**) simulations. They involve some of the ANP and BNP typical residues, such as the polar ones at position 17, replaced by methionine in CNP (**Figure 3.1**).

The high conformational variability of the peptides is also confirmed by analysis of rmsf as flexibility index (**Figure 3.3**). The Cα rmsf per residue indicates the intensity of fluctuation of each residue with respect to the average structure. Coherently with the high conformational variability of the peptides, the rmsf profiles for each residue are characterized by significantly high values, indicating the absence of stable secondary structure elements. Moreover, the rmsf profiles of ANP and BNP present a higher similarity than rmsf profiles of CNP, suggesting that the dynamics of peptides with different specificity for NP receptors are strictly different.
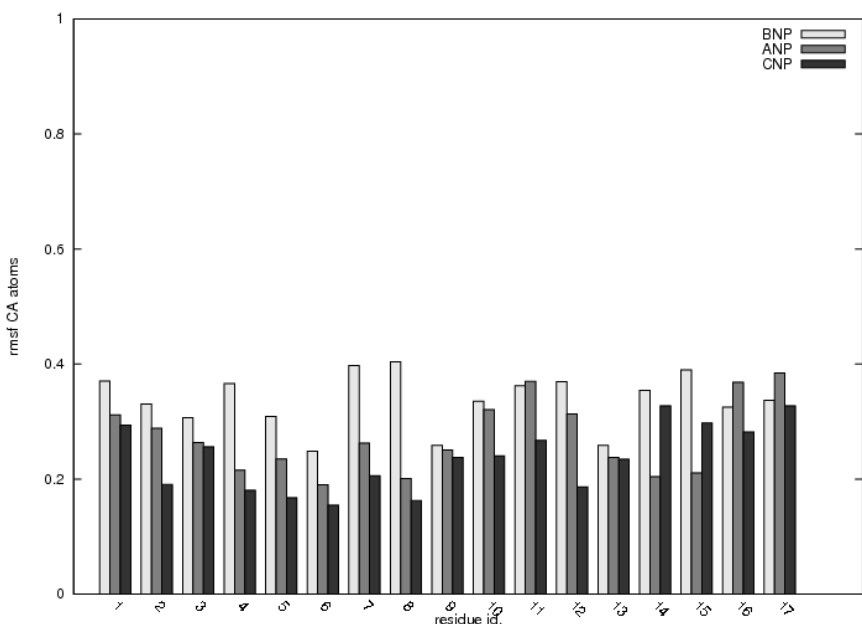
Figure 3.3. Rmsf as a flexibility index. Cα rmsf per residue calculated on peptide simulations discarding the first 3 ns of each simulation.

In summary, none NP structure corresponding to the bound conformation to the NPRs can be isolated during the simulations in agreement with the hypothesis that NP bound conformations are not stable in solution and that induced-fit mechanisms are involved in the formation of NP-NPR complexes.

The differences in activity and NPR specificity of CNP and ANP/BNP seems to be correlated to different amino acid composition of the cyclized loop, different flexibility patterns and free conformations

(**Figure 3.2**) explored during the simulations. Additional detailed conformational studies will be deeply addressed elsewhere[125].

These observations prompted the study of the biological activity of significant fragments of CNP, with particular regard to the 14-17 region of the peptide, in which differences in the amino acid composition seem to be strongly correlated with conformational properties, activity and specificity of the three NPs (op. seems to be determinant for different conformational properties, activity and specificity of the three NPs).

3.1.2 Synthesis

Since it's not clear whether the full-length form of CNP is the only active molecule or if short fragments can exert biological effects, we started our study with the synthesis of a very short sequence, $I^{14}GSM^{17}$ (Peptide **1**), containing one of the two putative sequences responsible for the biological activity, which are not conserved in the natriuretic peptide family. In addition, we also prepared a mimetic where the fully conserved isoleucine is changed into glycine, that is $G^{14}GSM^{17}$ (Peptide **2**). The peptides were synthesised manually using standard Fmoc chemistry protocols. The two fragments were then evaluated in three different osteosarcoma cell lines, using the full length CNP peptide (CAS number 127869-51-6, Calbiochem USA) as control.

3.1.3 Biological assays

Peptides were preliminary tested for their ability to influence cell growth of human osteosarcoma cell lines, since the CNP peptide was previously shown to be involved in endochondral ossification and bone formation.

Growth kinetics were assessed at three different peptide concentrations (455 nM, 45.5 nM or 4.55 nM) for peptide **1**, peptide **2** and CNP on three human osteosarcoma cell lines, MG-63,[126] Saos-2,[127] and HOS.[128] Control cells, cultured in the absence of peptide, were assessed in parallel. Results are shown in **Figure 3.4**, for the minimum concentration tested.

Peptides displayed different effects upon the cell type used. All peptides slightly reduced proliferation of MG-63 cells already after 5 days of culture (data not shown), peptide **2** being the most active after 7 days (−27% with respect to controls). By converse, in SAOS-2 cells, proliferation was increased, although to a relative extent, with peptide **1** inducing the maximal effect (+31%). A similar induction was obtained in HOS cells, but only when peptide **2** was added to the growth medium (Figure 3.4).

Peptide administration (4,55 nM): effects on cell growth after seven days of culture
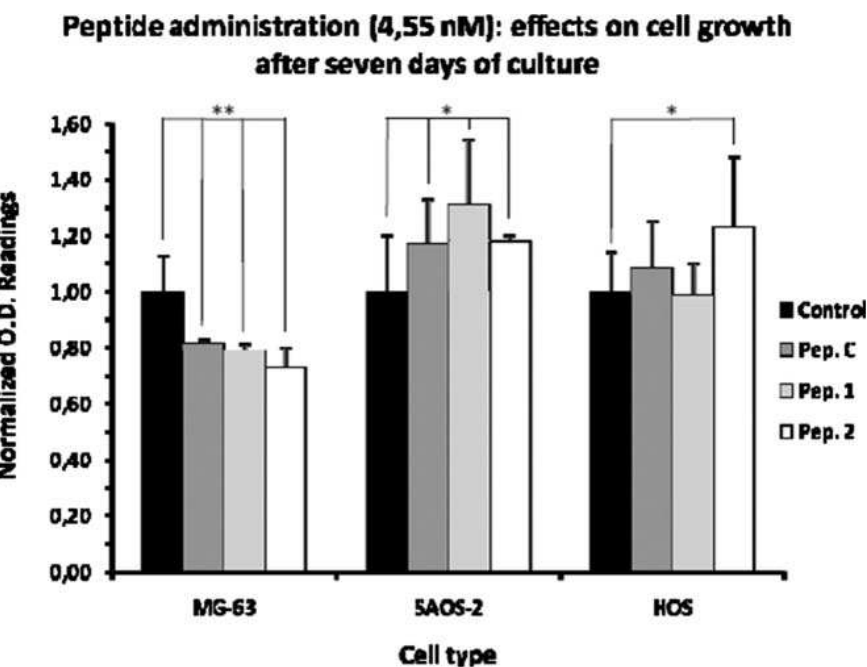
Figure 3.4. Effects of the administration of the peptides under testing on the growth kinetics of MG-63, SAOS-2 and HOS cells; depicted results refer to data obtained exposing cells to peptides at the concentration of 4.55 nM for seven days. Results are normalized to control values for each cell type used. Each data point represents the average of six determinations performed in two different experiments. Error bars depict standard deviation values (n=6); *: $p<0.05$; **: $p<0.001$ (p values refer to control vs. treated cells).

Cell cycle arrest and activation of bone matrix proteins transcription are sequential events that lead to osteoblast differentiation.[129] Any variation of the cell proliferation rates, then -although limited- may be

98

of interest, particularly considering that those are human osteoblast-like tumor cell lines, with relative high growth rates. In addition, osteogenesis is associated with reduction of the proliferative bursts and cell differentiation: the former may depend upon the availability of a properly assembled hyaluronan-rich matrix,[130] while the latter coincides with increased alkaline phosphatase activity,[131] osteocalcin biosynthesis and matrix component deposition.[22, 132] However the proliferative and differentiative potentials of bone precursors change during osteogenesis. In living bone, in fact, osteocytes derive from pre-osteoblasts and osteoblasts after polarization,[133] a process that allows bone growth through a concerted control of proliferation (needed to generate new cells) and differentiation (needed to induce the cells to produce matrix and become resident in it). Pre-osteoblasts are normally proliferating cells and typically express osteogenic transcription factors, later down-regulated in the osteoblast/osteocyte stages. Collagen I/III, osteopontin and osteonectin, fibronectin, tenascin C and thrombospondins are also expressed. However, from the stage of osteoblast, osteocalcin and bone sialoprotein become expressed, while type III collagen is down-regulated. In this light, then, a reduced proliferation of MG-63 cells upon CNP treatment is in accordance with the proposed role for the peptide in the osteogenic differentiation of cartilage and bone precursors.[134,135] On the contrary, in SAOS-2, proliferative events and matrix deposition are contemporary and possibly controlled through cell morphology and tensegrity by molecular components of the matrix itself [136]; this event

99

may partially explain the results obtained exposing SAOS-2 or HOS cells to the tested peptides, where cell proliferation was slightly increased. The used cell lines, in fact, -although not derived from the same tumor source- could be related to slight "different stages" of the osteoblastic differentiation, being SAOS-2 and HOS cells in a more immature one, possibly displaying a lesser dependency upon matrix production and a higher proliferative potential. Moreover, it should be remembered that other studies, have tributed opposite effect to the administration of the same molecule to different osteoblast-like cells: it was reported that anti-tenascin antibodies reduced alkaline phosphatase activity and type I collagen production in UMR-106, ROS-17/2.8 and SAO-2 cells lines. However proliferation was slightly increased only in SAOS-2 cells, while it was inhibited in the other two,[28] indicating that more than one single stimuli was probably needed to overcome the proliferative potential of SAOS-2. The relevance of the cell "responsiveness", when in different stages, is also evidenced by the CNP administration to an osteogenic cell line (ROB-C26) that maintains potentials for differentiating into myoblasts, osteoblasts and adipocytes. The effects of the peptide were clearly different when the same cells were primed toward the separate lineages. [137] In our settings, however, the effects of the peptides could be minimized by the cells used, already addressed toward an osteoblast-like phenotype. The peptides osteogenic potential could be fully exploited using human skeletal progenitor cells, such as bone marrow stromal cells, particularly considering that the receptors for

the natriuretic peptides have already been detected in the chicken, mouse and rat cell counterparts.[29, 138, 139,] As a whole, the proliferation results, although limited, are in accordance with previous work, reflect the cells' osteogenic potential and indicate that full length CNP can be successfully substituted by biologically-effective synthetic peptides. Indeed the molecular mechanisms underlying their action are yet to be disclosed.

3.2 Carbohydrates

Carbohydrates make up a substantial portion of the biomass on earth, mostly in the form of structural polysaccharides such as cellulose from plants and chitin from arthropods and fungi. All the known living organisms also display an array of free or covalently linked carbohydrates collectively known as glycans[140]. Oligosaccharide structures present a high level of diversity introduced by the occurrence of the two anomeric variants at each glycosidic linkage and by the presence of five potential attachment points (hydroxyls) per sugar unit, affording highly complex linear or branched different glycan structures, mediating a great deal of biological information (glycocode). Despite the increasing knowledge about natural glycan diversity, the deciphering of information content for the glycocode is still challenging. Glycotechnology still needs the development of simplified and sound synthetic methods to facilitate not only analysis

of proteins for carbohydrate-binding activities, but also elucidation of their ligands, for example with the use of glycoarrays.

3.2.1. Propargyl Glicosides

Small biomolecules, such as carbohydrates are normally present and involved in the mechanisms that order complex biological systems. Covalent functionalization on biomaterial surfaces is a efficient approach in order to obtain an improvement of material biocompatibility and, controlled biological responses. The chemoselective method of choice is the reaction between a triple bond and an azide (defined click chemistry).

In this respect, the direct synthesis of unprotected glycosides possessing suitable functional groups that can be further manipulated by chemoselective reactions is becoming a relevant tool in bioorganic chemistry[141]. The alkyne triple bond or the azido group have become functional groups of increased interest due in part to the recent discovery of chemoselective ligation reactions between the two as reaction partner, such as the "click" chemistry[142] which has found great application. These groups are easily introduced, are chemically stable, and do not react with common organic reagents or other functional groups generally found in biomolecules. Triazole formation between the azido and the triple bond functionalities is irreversible and usually quantitative. In addition, this reaction benefits

102

from extremely mild reaction conditions. Thus, the potential for this reaction to modify a wide range of functionally complex substances, such as carbohydrates, is significant. In addition, the unique properties of this reaction appears transferable to surface-bound reactants and will likely provide access to a growing variety of novel "biodecorated" surfaces[143].

Glycoconjugation exploiting the click chemistry requires the functionalization of carbohydrates with alkynes or an azido group. The simplest method to do that is the glycosylation of unprotected sugars with propargyl or azidoalkyl alcohol. Hence improved and simplified methods for the synthesis of azido- or alkynyl carbohydrate derivatives are highly desirable.

Most common methods for the synthesis of glycosides involve the reaction promoted by suitable activators of a glycosyl donor, that is a fully protected saccharide with a leaving group at the anomeric position (i.e. peracetylated glycosyl halides or trichloroacetimidates), and a glycosyl acceptor frequently containing only one free hydroxyl group[144]. The synthetic sequence is then followed by final deprotection steps to the desired glycoside. A valuable alternative is glycosylation on unprotected sugars. Fischer glycosylation has been used for decades for the synthesis of simple alkyl (methyl, ethyl, allyl) and aryl glycosides from free sugars[145]. The reaction is usually catalysed by acids and refluxed in the alcohol acceptor as solvent. This procedure for Fischer glycosylation has a few disadvantages,

including the use of strong mineral acids, a large excess of alcohol and high temperature/long reaction times, which often lead to by-product formation. Plusquellec and co-workers proposed the direct *O*-glycosylation of reducing sugars in the presence of ferric chloride affording furanosides in good yields using organic co-solvents such as THF or dioxane[146]. In the presence of $BF_3 \cdot Et_2O$ alkyl □-pyranosides were obtained but in moderate yield.

Recently, glycosides having 2'-azidoalkyl and propargyl aglycons[147] have become synthetic intermediates of increased importance in chemoselective ligation reactions, hence their synthesis should be simple and rapid.

In this paper we propose an improved procedure for Fischer glycosylation towards propargyl and 2'-azidoethyl glycopyranosides using H_2SO_4–silica as catalyst[148] plus ultrasounds, as illustrated in Figure 3.5.. This procedure is exemplified with most biologically relevant 2-acetamido-2-deoxy-monosaccharides, such as *N*-acetylglucosamine, *N*-acetylgalactosamine and *N*-acetylmannosamine. In order to show high applicability of the procedure, the glycosylation was tested also on a sample disaccharide, such as lactose.
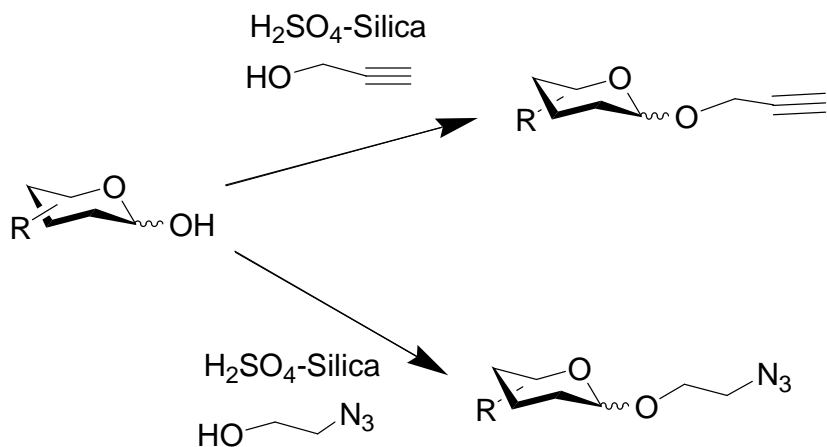
Figure 3.6. H_2SO_4-Silica catalyzed glycosylation of free sugars

Ultrasound-assisted Fischer glycosylation has been already proposed[149], but this methodology has not been used in combination with silica supported H_2SO_4 as the catalyst yet. In these conditions the glycosylation reaction proceeds in short times (15 mins-2 h) depending on the substrates, with the only exception of lactose, which requires 12 h, while d-galactose requires the shortest reaction time (15 mins). Longer reaction times observed for lactose are in agreement with other reported procedures, and are probably due to lower solubility product of the disaccharide in the acceptor alcohol. In this last case, we didn't get much improvements on reaction times, compared to already reported procedures, but we observed better yields. Results are summarised in **Tables 3.1** and **3.2**. In general, it

should be noted that the success of this methodology depends on the solubility of the reacting sugar in the acceptor alcohol.

Table 3.1 Propargyl glycopyranosides from free sugars
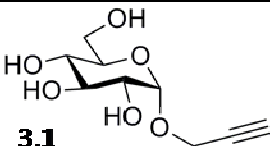
Product	Reaction time	Yield	Ratio (α/β)
3.1	30 mins	85%	10:1
3.2	15 mins	80%	10:1
3.3	30 mins	90%	1:0
3.4	30 mins	90%	1:0
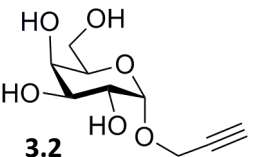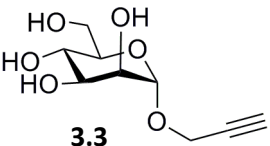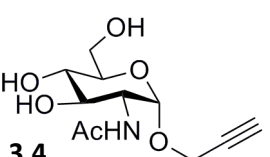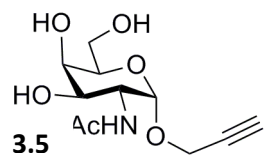
3.5   30 mins   85%   1:0
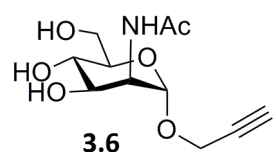
3.6   30 mins   85%   1:0
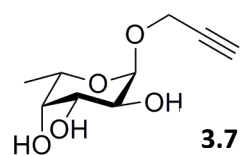
3.7   2 h   82%   1:0
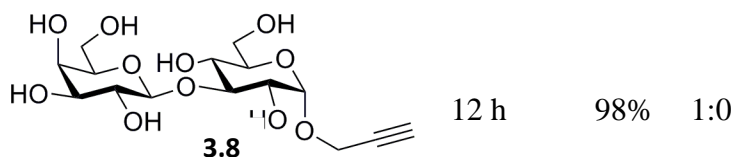
3.8   12 h   98%   1:0

Table 3.2 2'-Azidoethyl glycopyranosides from free sugars
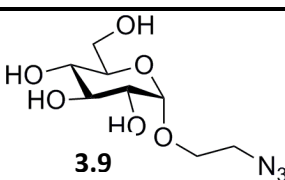
Product	Reaction time	Yield	Ratio ($\square/\square$)
3.9	30 mins	90%	20:1
3.10	30 mins	70%	10:1
3.11	30 mins	80%	1:0
3.12	30 mins	75%	1:0
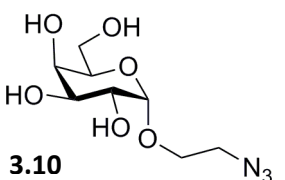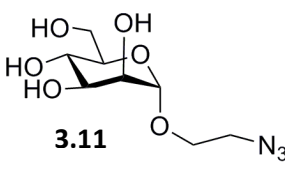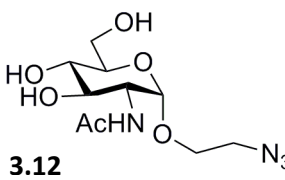
3.13	30 mins	78%	1:0	
3.14	30 mins	85%	1:0	
3.15	2 h	75%	2:1	
3.16	12 h	75%	1:0	
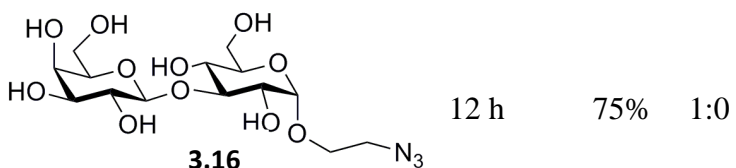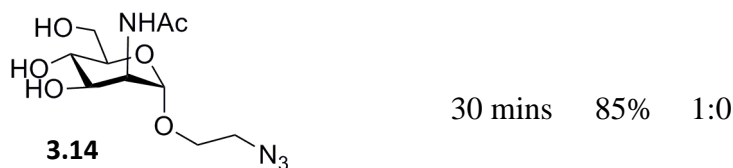
In all tested cases the reaction proceeds with production of the □-glycopyranoside as the dominant product, corresponding to the most thermodynamically stable anomer; total consumption of the starting material (except for lactose) and no significant by-products were observed, thus the yields were usually high.

Glycosides **3.1-3.15**, **3.7**, **3.9-3.13** and **3.15**-**3.16** have been previously characterised and NMR data are in perfect agreement with those already reported. Compounds **3.6, 3.8** and 3.**14** were unknown in the literature and full characterisation as their peracetylated derivatives is given in the experimental.

Ultrasound assisted Fischer glycosylation catalysed by sulphuric acid supported on silica gel was then used an efficient method for the preparation of 2'azidoalkyl and propargyl glycopyranosides, that have been used for material functionalysation by chemoselective strategies.

3.2.2 C-Glycosides

C-glycosides present several advantages over their *O*-glycosidic counterpart: their structure is closely resembling the parent sugar, thus maintaining the biological information, but they lack the anomeric glycosidic bond which is usually object of degradative forces *in vivo*.
C-glycoside derivatives of biologically relevant monosaccharides such as D-glucose, D-galactose and L-fucose were synthetised. *C*-glycosidic derivatives possessing a carboxylic group for the coupling reaction to the materials were synthesized in a few steps from the suitably protected natural monosaccharide. The □-allyl-*C*-glycoside was prepared by Sakurai reaction from the suitably protected parent monosaccharide; then, the allyl *C*-glycosidic appendage was

functionalized with a carboxyl terminus, by hydroboration (9-BBN),
followed by oxidation to the corresponding carboxylic acid (TEMPO)
(**Scheme 3.1-3.2**).
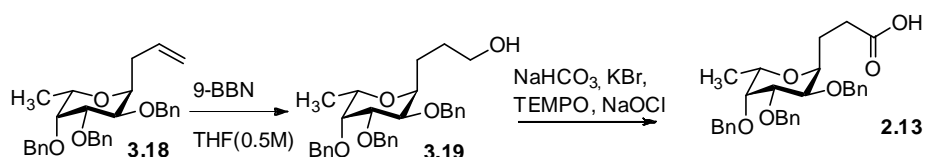
Scheme 3.1. Synthesis of galactose and glucose *C*-glycosides
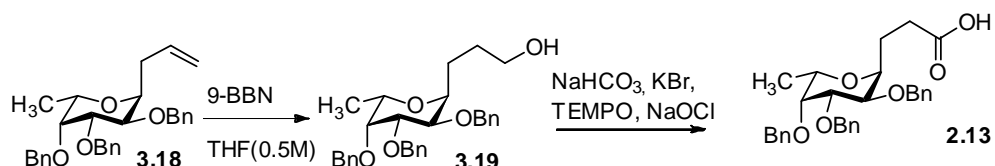
Scheme 3.2. Synthesis of Fucose C- Glycosides

The C-glycosides therein synthesised have been conjugated to
complementary functional groups suitably introduced on different
biomateriale.

Chapter 4

4. Result and discussion- Design, synthesis and characterization of hybrid materials for bone tissue engineering

Bone grafts are commonly used to regenerate bone in defect sites resulting from disease or trauma but there is clinical need for artificial materials that will be readily available and reduce pain and recovery time for the patient. An optimum synthetic bone graft substitute should fulfil several criteria. It should[150]:

(1) resorb at the same rate as the bone forms,

(2) be biocompatible and products of resorption should not be toxic,

(3) be osteoconductive and osteogenic,

(4) exhibit mechanical properties similar to the host trabecular bone,

(5) act as a template for three-dimensional bone tissue growthwith interconnected macroporous network.

If the scaffold is too large for blood vessels to penetrate all of the pore network, the scaffold should also possess angiogenic properties or tissue engineering approaches of growing vessels within the scaffold prior to implantation may be necessary. Synthetic constructs for bone regeneration have been made from inorganic and organic materials One example of an inorganic construct for bone regeneration is the sol–gel derived bioactive glasses. Jones et al. developed macroporous bioactive glass foams that can form an HCA layer after 72 h of

112

immersion in SBF. The same foams were also shown to have a compressive strength of smax ¼ 2.3 MPa, which is in the compressive strength range of human trabecular bone.7 However, they were brittle owing to their glassy nature.

Composites of inorganic and organic components are a promising way forward in overcoming the lack of toughness in inorganic materials and lack of strength in organic materials[151].[152]

To improve toughness, hybrid inorganic-organic materials with interpenetrating networks (IPN) of silica and organic polymer are being devloped[153].[154] The potential advantage of IPNs over conventional composites are that there is potential for control of mechanical properties and degradation rate of the material trough interface control[155],[156]

Homogeneously dispersed organic–inorganic hybrids can be obtained by increasing the interfacial interactions between both components via the formation of hydrogen bonds or covalent bonds, by using coupling agents to bridge between the polymer and the silica.

The aim of this part of the work performed at Imperial College (London, UK) under the supervision of Dr. Julian R. Jones has been the fabrication of a tailored hybrid with reduced brittleness compared to a bioactive glass. Polyoxyethylene bis(amine)/bioactive silica hybrids with composition 35 wt% organic and 65 wt% *silica* were synthesised using a sol–gel technique. Polyfunctional amines are one of the most popular curing agents that are commonly used to fabricate

a wide class of thermosetting organic polymers based on the epoxy-amine system. The reaction between epoxy and amino groups in order to obtain homogenous materials have been the object of extensive research in industry[157158].

4.1 Design and preparation of new hybrid materials

Organic and inorganic compounds, used in the polymer functionalization and during the sol-gel process are summarized in **Figure 4.1.** The synthetic procedure is summarised in **Figure 4.2**. The hypothesis for covlaent coupling is that the polyoxyethylene bis(amine) (dPEG) contains two amino terminal groups available for the covalent functionalisation with the epoxy group of a coupling agent, glycidopropyltrimethoxysilane (GPTMS). When in solution with –COOH or –NH$_2$ groups, the epoxy ring (glycidol group) of GPTMS can open (nucleophilic attack) and a bond forms between the coupling agent and the polymer, leaving the dPEG functionalised with a short chain molecule with a trimethoxysilane group on the end of the short chain. The inorganic sol was prepared by the hydrolysis of the silica precursor tetraethyl orthosilicate (TEOS) in acidic conditions in a separate beaker. When the functionalised polymer is added into the sol–gel process, the methoxysilane groups hydrolyse; forming three silanol groups, which can undergo condensation with silanol groups of the hydrolysed TEOS, forming Si–O–Si linkages between the functionalised polymer and the silica network.

GPTMS   dPEG   TEOS
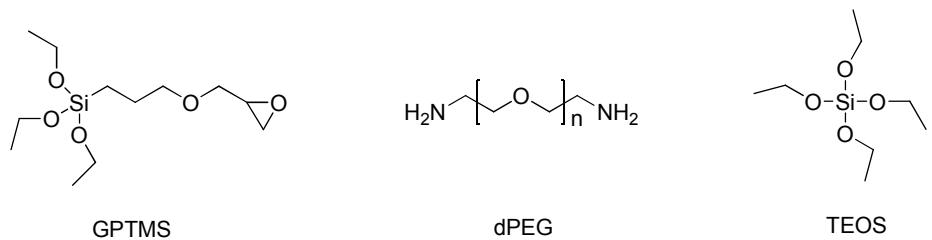
Figure 4.1 Organic and inorganic compounds. Polimer functionalization: GPTMS (glycidopropyltrimethoxysilane) and dPEG (polyoxyethylene bis(amine)). Sol-gel process TEOS (trietoxysilane) . Two different ratios of functionalisation (dPEG:GPTMS 1:2 and 1:4) were employed for the fabrication of the material. The hybrid sol was poured into teflon moulds and were sealed and aged at 40° C and dried at 60°C.
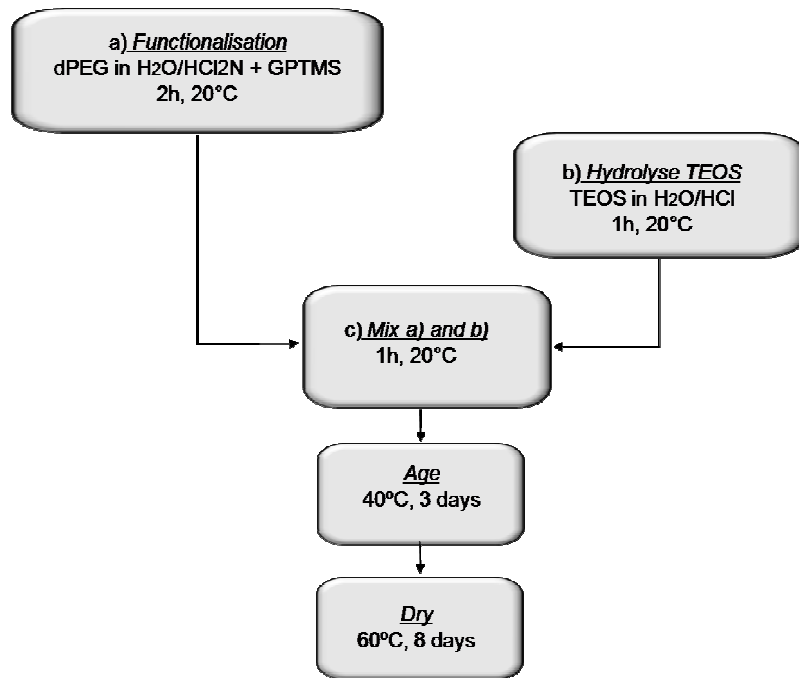
Figure 4.2 Flow chart showing the reaction and processing steps involved in the synthesis of the hybrid material.

PEG-based hybrid networks with alkoxysilane groups were prepared by epoxy-amino reaction and subsequently addition of hydrolysed TEOS, to obtain two different hybrid materials. The degree of functionalisation of the organic network was easily controlled by the amine/epoxy molar ratio.(Figure 4.2). The novel hybrid materials were then characterized in terms of morphology and mechanical properties. Transparent crack-free materials were obtained. FTIR

spectra (**Figure 4.3**) of dPEG and a hybrid of GPTMS/TEOS (without covalent coupling) were compared to spectra of the dPEG/ silica hybrids with two degrees of coupling (dPEG:GPTMS ratios of 1:2 and 1:4).
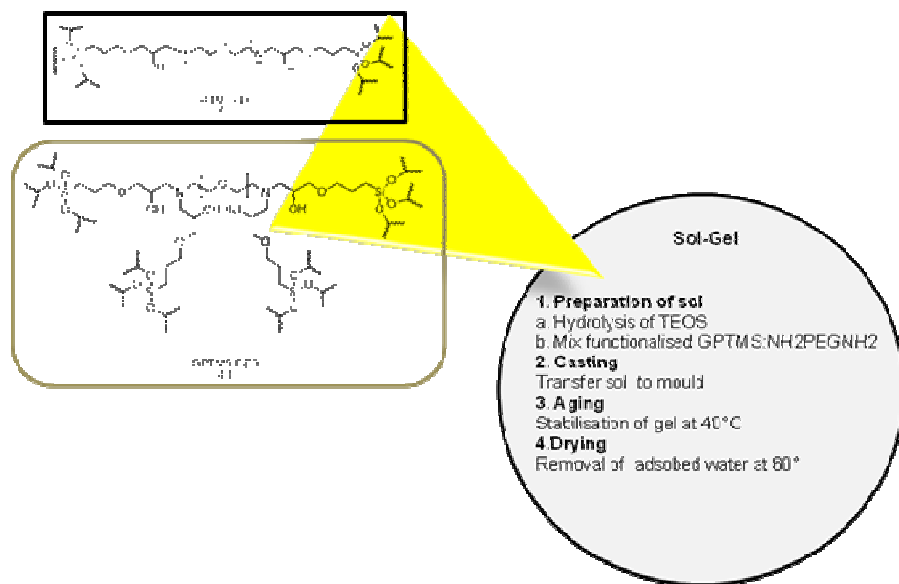
Figure 4.3 Hybrid 1:2 and 1:4 in sol-gel process

4.2 Characterization

In the FTIR spectrum presented in Figure 4.4 the vibrational modes due to Si–O–Si asymmetric stretching are observed at approximately 1,070 and 1,200 cm–1. Additional peaks are seen at 790 cm–1 (for symmetric Si–O–Si stretching vibration) and at 450 cm–1 (for Si–O–Si bending modes).

117

Figure 4.4 shows also vibration bands from the main silica network content in the hybrid samples are between 400 and 1250 cm^{-1}. The additional absorption band observed around 1070 cm^{-1} can be ascribed to the organic modification of the silica matrix and, in particular, to the C-O and C–C bonds. Other signals are between 1350 and 1500 cm^{-1} that can be observed like C-N stretch signals in dPEG and hybrids samples.

The primary amino groups of the dPEG which appear at 1640 cm^{-1} is not showed in the hybrids, which suggests that these groups be involved in covalent bound withepoxygroup of GPTMS.[159][160].
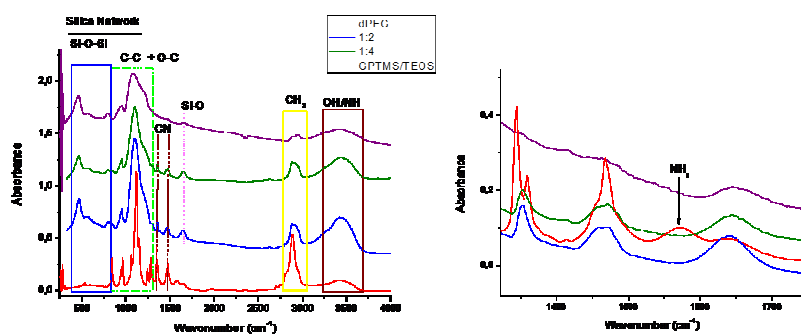
Figure 4.4 FTIR spectra of dPEG, 1:2 and 1:4 hybrids and GPTMS/TEOS sample

The hybrid materials exhibit substantially better mechanical behaviour than conventional glasses for bone regeneration applications. Compressive strength of the samples was 30 MPa These results

compare to a compressive strength of 87 MPa and a strain to failure of 2.75% for a sol-gel silica glass monolith (**Figure 4.5).**
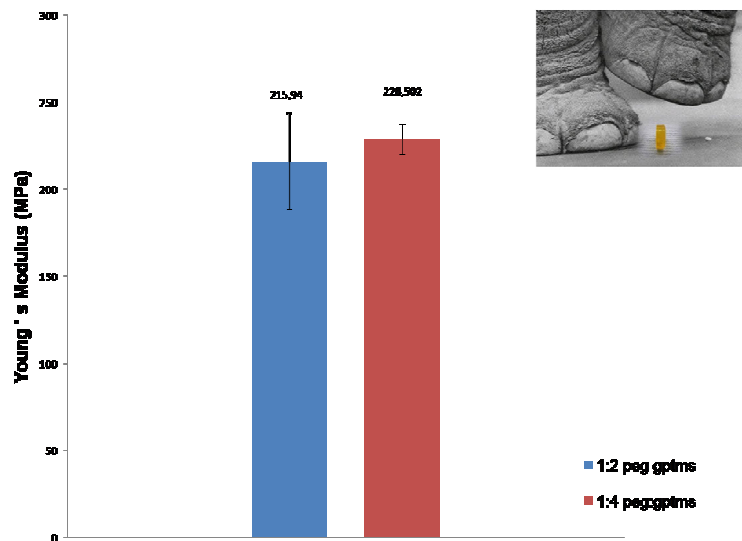
Figure 4.5. Young's Modulus obtained by compression test of A) 1:2 and B) 1:4 hybrids.

In general, the mechanical properties values showed low standard deviations, which affirms that the both dPEG:GPTMS:TEOS materials are chemically homogeneous. Mean strain to failure was 10%. The transparent nature of the monoliths also indicate homogeneity (**Figure 4.6).**

Changing the covalent coupling had no significant effect on the mechanical properties for these materials. This could be due to the low molecular weight of the dPEG (1500 mw)

The fracture surfaces of 1:2 and 1:4 hybrid materials were compared using SEM (**Figure 4.6**). The 1:4 hybrids exhibited a fracture surface indicative of brittle fracture (Figure 4.6b), very similar to a glass. However the 1.2 hybrids has a more ductile mode of failure (Figure 4.6a), although the fracture surface would still be considered brittle compared to plastic failure in polymers.
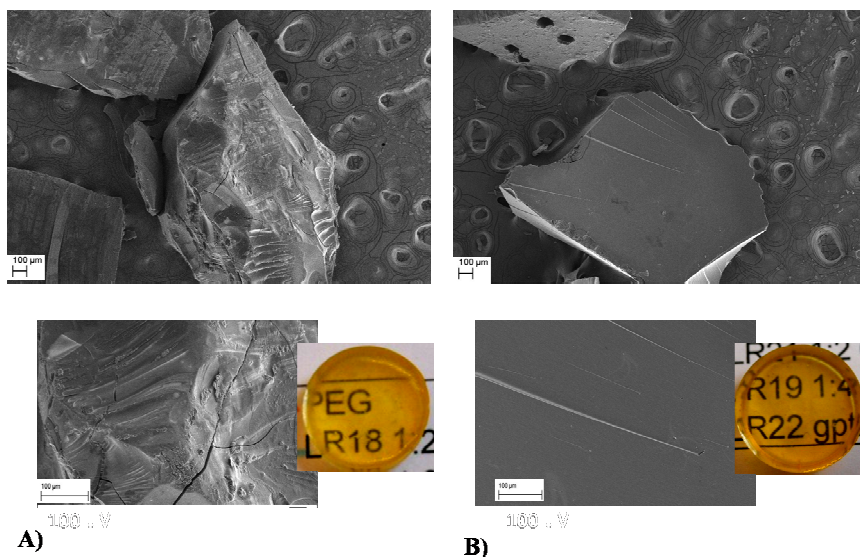
Figure 4.6. SEM photomicrographs of hybrids **A)** 1:2 **B)** 1:4 hybrids.

4.3 Reactivity of gptms as a function of pH

Silica-based hybrid organic–inorganic materials prepared by sol–gel chemistry exhibit unique chemical and physical properties. (3 glycidoxypropyl)trimethoxysilane (GPTMS)-based networks represent an archetype of this class of substances, with a vast range of applications.

Compared to other chemical elements, silicon is one of the most convenient and productive element for the preparation of theorganicallymodified alkoxides required for the design and synthesis of hybrid organic–inorganic materials. A plethora of reasons speak in favour of the peculiar character of silicon, among which the transparency, thermal and chemical stability of Si-O-Si networks, and the 'sweet chemistry' involved in their synthesis[161] are just a few. Generally speaking, the polycondensation reaction of alkoxysilanes results in a variety of structures, ranging from monodisperse silica particles to polymer networks, depending of the reaction conditions involved[162]. In addition, copolymerisation of alkoxysilanes of different functionalities makes it possible to tailor the ultimate material structure and performance.

Properties of the micro heterogeneous hybrids materials depend, to a good extent, on an interphase interaction determining the morphology. Strong interactions, for instance, leads to a reduction of the size of inorganic domains in the organic medium and often improve the properties. Therefore, organofunctional trialkoxysilane monomers are

used to prepare hybrid polymers and are employed as coupling agents, mainly in coating materials. (3-glycidyloxypropyl)trimethoxysilane (GPTMS) is an organofunctional alkoxysilane monomer that can undergo both the sol–gel polymerisation of the alkoxy groups and curing of the epoxy functionality to form a hybrid network with covalent bonds between organic and inorganic phases[163]. In order to control and set hybrid materials synthesis the GPTMS behaviour has been investigated in relation to pH conditions, at pH 2, 5 and 7 by solution liquid NMR. For different values of pH the system became too gelly that liquid NMR was not applicable to this study. However, the data collected till now clarify some points of the reactivity of GPTMS.
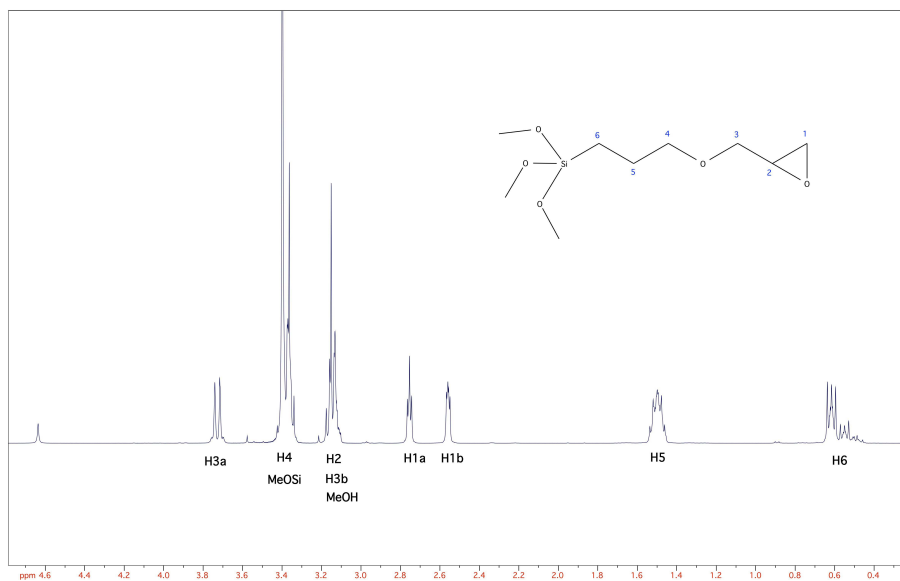
During the hydrolysis of the epoxidic ring, the signals of H1a and H1b disappear and they move to lower fields, so they have been used to estimate the percentage of epoxide's hydrolysis, giving value 2 to each integral of the H5 and H6 signals.

The rate of hydrolysis increases from pH 7 to more acidic pH.

The reactions have been checked for 3 days and the data are collected in the following graph (Figure 4.7).
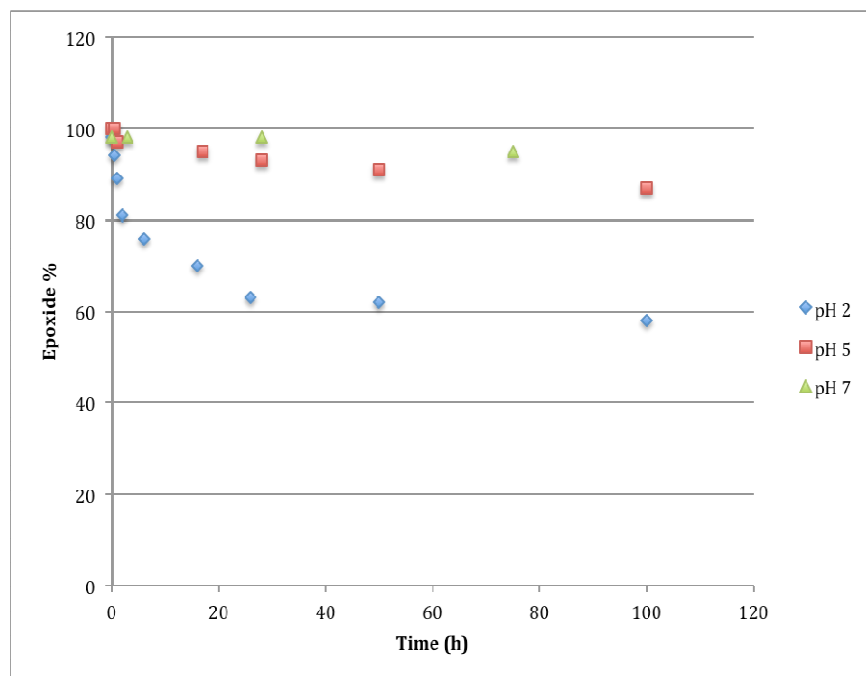
Figure 4.7. Hydrolysis of epoxidic ring

At neutral pH (no catalytic H^+ or OH^- are present) the hydrolysis is very slow, in fact after 3 days only 5% of the epoxide has been hydrolysed.

At pH 5 the acidic catalysis is slightly present, so the hydrolysis increases and after 3 days 13% of the epoxidic rings are opened.

At pH 2 the hydrolysis is more accentuated, with a strong decrease in the first 24, reaching 42% of hydrolysed epoxide after 3 days.

After 4 days the three solutions look clear, with no precipitation and the NMR peaks are still sharp confirming that the compounds are completely soluble in water and the gelification process is not started yet.

At basic pH (9 and 11) the gelification process becomes important; at pH 9, at t_0 an epoxide hydrolysis of 14% can be observed. After a few minutes the gelification started and then a white precipitate appeared, giving very broad NMR signals.

At pH 11 the gelification is so much faster that even at the t_0 is not possible to record a ^{1}H-NMR spectra with sharp peaks. After the addition of GPTMS into the basic solution, the gelification is immediately visible.

If for the basic solutions the ^{1}H-NMR spectra alone can't give us much information, the ^{13}C-NMR spectra could be more interesting.

125
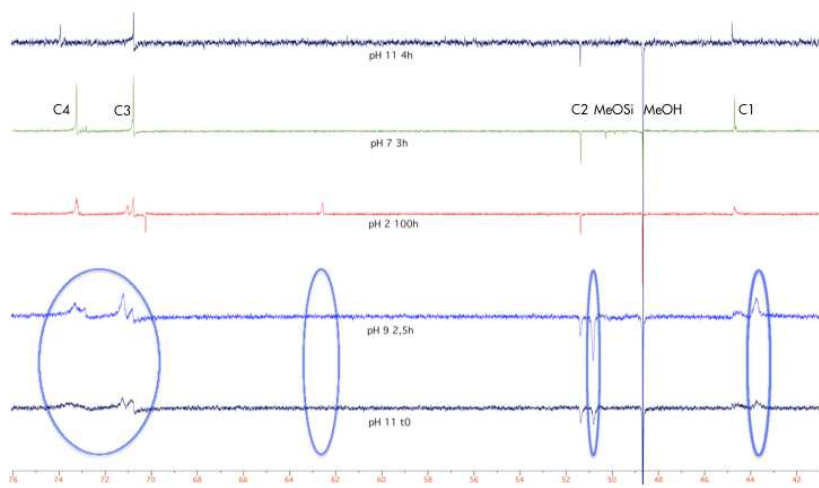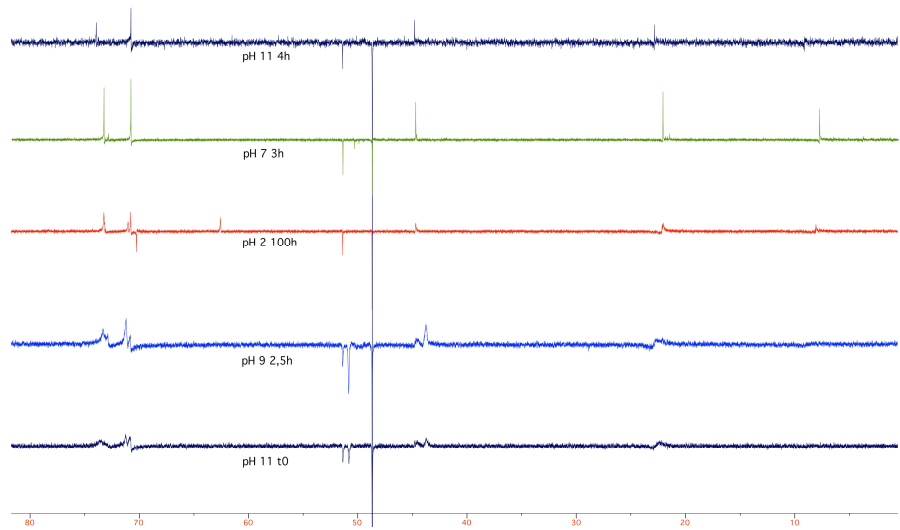
In the presence of a gel system, also the carbon signals appear much broad, but it's still possible to observe that at pH 11 (t_0) and at pH 9 (2,5 hours), the epoxidic ring is opening and new signals are appearing in the reaction system. These signals are not present in the GPTMS hydrolysis reaction recorded at acidic pH, thus suggesting that a different reaction is taking place.

In details the C1 is shifting from 44.66 ppm to 43.77 ppm, while in acidic conditions it's at 62.7 ppm.

The C2 is shifting from 51.4 to 50.8 ppm while at acidic pH it's at 70.29. It's important to observe that the NMR spectrum at pH 11, after 4 hours, when most of the GPTMS is in solid phase, doesn't show any hydrolysis of the epoxide ring. Moreover the peaks are much sharper, indicating that we are detecting only the small amount of GPTMS that didn't participate to the gel system and it's still completely soluble. Thanks to these observations we can assume that the reaction on the epoxide ring is occurring during (or thanks to) the gelification process, while it doesn't affect at all the fraction of soluble GPTMS.

According to the NMR shift, the most probable explanation is the formation of a 5-member ring due to the nuclephilic attack of the SiO- to the epoxide, as reported in the following scheme.

127
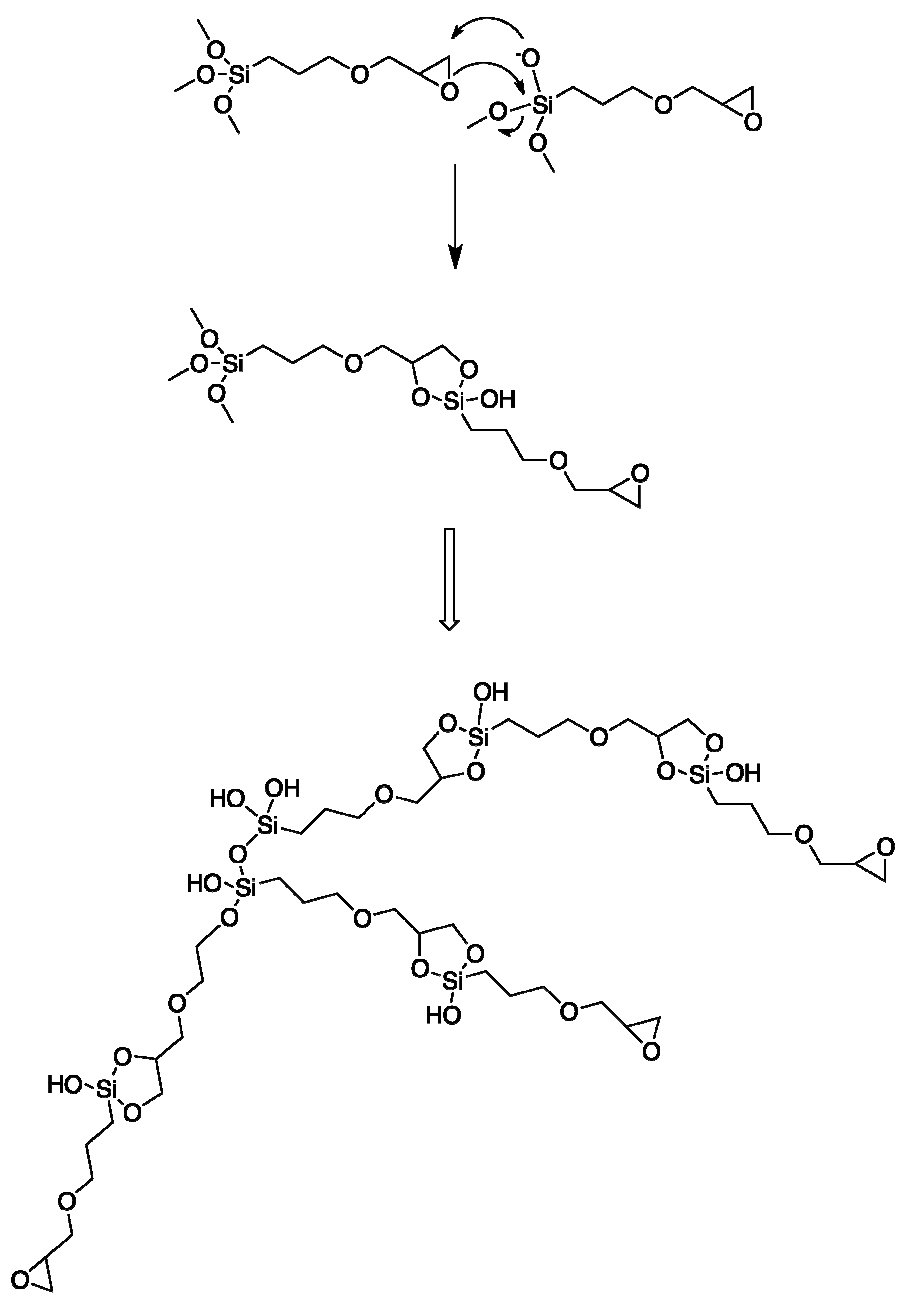
A second explanation could be that in such basic conditions the fast gelification rate brings the epoxides groups close one to each other, thanks to the Si-O-Si bridges. Once a ring has been opened by basic catalysis, the O⁻ could attack the closest epoxide ring, as reported in the following scheme.
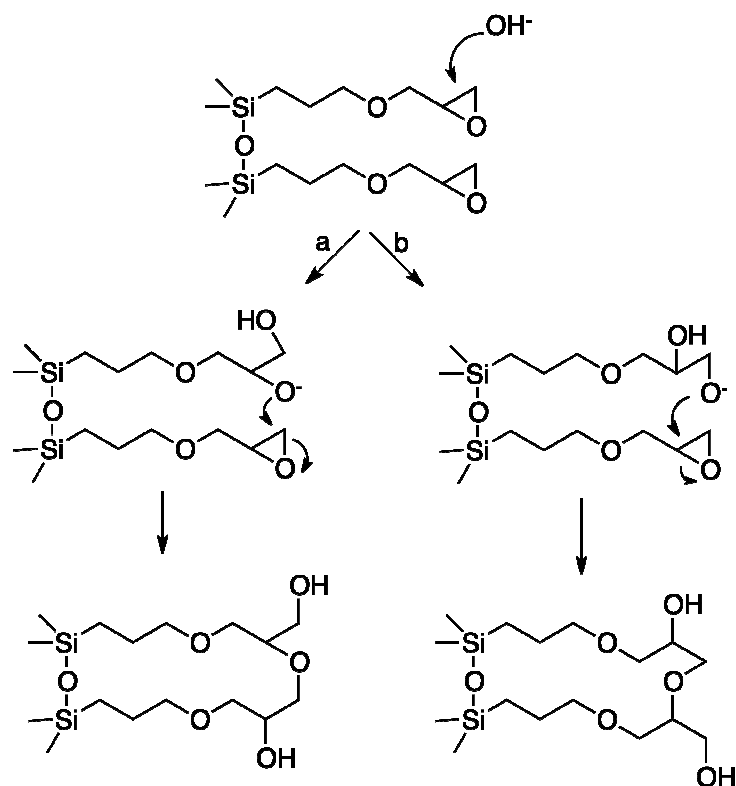
The other parameter that has been taken into account by NMR is the hydrolysis of the silyl-methoxy groups.

At acidic pH (2 and 5), already at t_0, both ^{1}H and ^{13}C NMR showed a complete hydrolysis of the methoxy groups, with consequent formation of MeOH.

At pH 7, as we already observed for the epoxide, also the methoxy hydrolysis is much slower, in fact at t_0 no methanol is detected, while after 3 hours the 77% is hydrolysed and after 28 hours only the MeOH signal is present.

At pH 9 at t_0, about 10% of methoxy groups has been hydrolysed, and in 2.5 hours the hydrolysis is complete.

At pH 11 the hydrolysis is immediate as in acidic conditions, so already at t_0 only methanol is detected.

It's very important to observe that at neutral or acidic conditions, no gelification or precipitation was detectable within 4 days, while at basic pH as soon as the methoxy groups are hydrolysed, Si-O-Si bridges occur, with consequent gelification and this process becomes drastically faster increasing the pH.

This could be easily explained considering that the Si-O$^-$ groups that are present at basic pH are much more nucleophile than Si-OH groups.

These data lead to some important considerations:

> 1.   In order to functionalize the epoxide group in GPTMS, slightly acidic conditions (i.e. pH 5) are suggested, because at neutral pH the catalysis will be too slow, while increasing too

much the acidity can make the hydrolysed epoxide the predominant species.

2. At basic conditions the gelification process is the dominant factor, and the opening of the epoxide ring seems to be caused from intra-molecular reactions between condensed GPTMS molecules.

Moreover the gelification is so fast that can compete with a functionalization of the epoxide in solution.

According to these observations, let's consider a practical example, in which we want to functionalize GPTMS with a basic nucleophile (i.e. amine).

If we add GPTMS to an amine solution (basic pH) and then we bring the solution at slightly acidic pH or, if we first adjust the pH of the amine solution and then we add the GPTMS, we could expect two different results, in terms of molecular composition and therefore of material's property.

In the first case the GPTMS could experiment already in the beginning a gelification process, without being functionalized with the amine and this will depend on the basicity of the starting solution and on the time required to reach neutral/acidic pH. In these conditions intra-molecular epoxide condensation may be possible.

In the second case we could avoid an immediate gelification and hopefully we could functionalize the epoxide with the desired nucleophile before the formation of the solid material.

Chapter 5

5. Conclusions

During PhD period were been development different strategies for biomaterials functionalization. Particular attention was drawn on the functionalisation method and on the presence/absence of spacer arms between the material surface and the biomolecule. Detailed studies of biological responces flanked by NMR conformational studies on the surface immobilised molecules will give a deep knowledge of the requirments needed for smart biomaterial design. To date, only a couple of examples are reported in the literature on this issue, hence this study will be of valuable interest for tissue engineering applications.

In addition, a novel approach has been used in this project: material surfaces have been decorated with small biomolecules This aspect is particularly innovative since to date most studies report the use of whole proteins and polysaccharides. The use of small biomolecules will guarantee reduced costs of the functionalized materials. This can be a key issue for the development of biomaterial for large scale use. Furthermore, despite the relevant biological roles of carbohydrates, very few studies on the use of small sacchardic epitopes have been reported for the funcionalisation of biomaterials. We expect that the fundamental knowledge gained from this issue will have broad

131

significance over the development of tissue engineering and novel smart biomaterials.

Thus, througt surface decoration with small biomolecules different kind of smart biomaterials were obtained, featured by modification and tuning of their physico-chemical properties. All the materials were characterised in term of their functionalisation by different physical methods (Raman spectroscopy, FTIR, fluorescence, NMR, contact angle measurements, XPS). Preliminary biological response of such materials is in due course, and will give informations on cell adhesion, differentiation and proliferation in order to characterize the scaffolds for bone and cartilage tissue regeneration applications.

Chapter 6

Materials and Methods

6.1. Biomolecules

6.1.1 C-Nautriuretic Peptides (CNP)

Synthesis

Purification of peptides was performed by preparative reversed phase HPLC on a Jasco HPLC system, model PU-2080 PLUS (Intelligent isocratic HPLC, High pressure binary gradient Pump) equipped with a Merck LiChrosper 100 RP18 column (250 310 mm2; 10 lm), and eluting with a flow rate of 5 mL min⁻1 with eluent A (0.1% TFA in water) and eluent B (0.1% TFA in 90% aq acetonitrile). Analytical HPLC purity checks were performer using a Merck LiChrosper 100 RP18 column (250 3 4 mm2 ; 5 lm), eluting at a flow rate of 1 mL min _1 and with the same eluent system. Detection was at 280 nm. The purified peptides were characterized by RP-HPLC, LC/MS/MS system Q-TRAP AB Applied Biosystem. Purification of the crude peptides was performed by preparative scale HPLC (eluent: linear gradient 0–30% eluent B in eluent A over 30 min afforded 13 mg of peptide 1 (60% yield) and 14 mg of peptide 2 (65% yield). The purity of both peptides was checked by analytical HPLC (eluent: linear gradient 0–30% eluent B in eluent A; analysis time 30 min, tR ¼ 9.58

min for peptide 1, and tR ¼ 9.9 min for peptide 2, respectively).
Peptide 1: Exact mass: calcd 406.50, found m/z (M + H) 407.50.
Peptide 2: Exact mass: calcd 350.39, found m/z (M + H) 351.39.

6.1.2 Propargyl glycosides

Reactions were carried out using commercially available starting
materials and solvents without further purification. All solvents were
dried over molecular sieves, for at least 24 h prior to use. Thin-layer
chromatography (TLC) was performed on Silica Gel 60 F_{254} plates
(Merck) charring with a solution containing concd. $H_2SO_4/EtOH/H_2O$
in a ratio of 5:45:45 or with an oxidant mixture composed of
$(NH_4)Mo_7O_{24}$ (21 g), $Ce(SO_4)_2$ (1 g), concd. H_2SO_4 (31 mL) in water
(500 mL). Flash column chromatography was performed on silica gel
230–400 mesh (Merck). NMR spectra were recorded at 400 MHz (^{1}H)
and 100.6 MHz (^{13}C) on a Varian Mercury instrument. Chemical
shifts are reported in ppm downfield from TMS as an internal
standard; *J* values are given in Hertz. For all compounds assignments
of the ^{1}H NMR spectra were based on 2D proton–proton shift-
correlation spectra.

6.1.2.1. Ultrasound assisted glycosylation

H_2SO_4–silica was prepared according to ref.[141] The starting material
(1 mmol) was suspended in the acceptor alcohol (5 mmol) and stirred

at 40 °C in ultrasound bath for 30 min. After this time, the free sugar is almost completely dissolved; at this point H_2SO_4–silica (60 mg activated silica/mmol sugar) was added. Ultrasonication was continued till the disappearance of the starting material (15 mins-2 h), checked by TLC. The reaction mixture was recovered by filtration on a silica pad, washing with ethanol. The filtrated were evaporated and the residue (glycoside) was washed twice with diethyl ether in order to remove the unreacted acceptor (propargyl alcohol or 2-azidoethanol). Only glycosylation of lactose required longer times (12 h) and 15 mmol of alcohol acceptor per mmol of disaccharide.

6.1.2.2. Acetylation procedure

An analytical sample of the glycoside was dissolved in dry pyridine and 1.1 equiv Ac_2O per free OH was added. After complete consumption of the starting material, the mixture was diluted with EtOAc, then extracted twice with 5% aq. HCl. The organic layers were collected, dried over dry Na_2SO_4, filtered and concentrated to dryness. The residue was purified by flash chromatography using Petroleum Ether/EtOAc mixtures as eluent.

6.1.2.3. Chemical characterization

All compounds have been characterized by NMR spectroscopy as their peracetylated derivatives. Glycosides **1-5**, **7**, **9-13** and **15-16** have been previously characterized and NMR data are in perfect agreement

with those already reported (references to literature are reported in Tables 1 and 2, next section). Key data are given for unknown compounds.

Propargyl 2-acetamido-3,4,6-tri-O-acetyl-2-deoxy-□-D-mannopyranoside obtained by acetylation of compound **3.6**:

^{1}H NMR (CDCl$_3$, 400 MHz) δ: 5.42 (d, 1H, J=3.7), 5.38. (bs, 1H), 4.91 (t, 1H, J=9.7), 4.82 (bs, 1H), 4.44-4.31 (m, 5H), 4.12 (d, 1H, J=9.7) 2.71 (bs, 1H), 2.14, 2.03, 2.02, 1.98 (4s, 12H); ^{13}C NMR (CDCl$_3$, 101 MHz) δ: 172.3, 170.6, 170.2, 170.0, 102.5, 79.8, 75.8, 71.0, 70.4 69.3 62.6, 59.5, 53.8, 20.8 20.3, 20.3, 19.8; Exact mass-Calcd for C$_{17}$H$_{23}$NO$_9$: 385.37; found m/z (M + H) 386.35.

Propargyl 2',3',4',6',2,4,6-hepta-*O*-acetyl-α-D-lactoside obtained by acetylation of compound **3.8**:

^{1}H NMR (CDCl$_3$, 400 MHz) δ: 5.49 (t, 1H, J=10.3), 5.40-5.32 (m, 1H), 5.28-5.21 (m, 2H), 5.10 (dt, 1H, J=10.3, 3.3), 5.01 (t, 1H, J=10.3), 4.91 (dd, 1H, J=10.3, 3.3), 4.76 (d, 1H, J=10.3), 4.36 (d, 1H, J=2.0), 4.32-4.25 (m, 3H), 4.20-4.06 (m, 3H), 3.75-3.71 (m, 1H), 2.45 (t, 1H, J=2.4), 2.18-1.98 (m, 21H); ^{13}C NMR (CDCl$_3$, 101 MHz) δ: 170.0, 169.9, 169.7, 169.7, 169.4, 168.9, 168.6, 98.3, 94.8, 78.5, 75.9, 73.0, 72.1, 71.3, 70.7, 70.1, 68.6, 68.5, 68.0, 62.0, 61.9, 56.2, 21.0, 21.0, 20.9, 20.9, 20.8, 20.8, 20.8; Exact mass-Calcd for C$_{29}$H$_{38}$O$_{18}$: 674.60; found m/z (M + H) 675.61.

136

2'-Azidoethyl 2-acetamido-3,4,6-tri-*O*-acetyl-2-deoxy-☐-D-mannopyranoside obtained by acetylation of compound **3.14**:

^{1}H NMR (CDCl$_3$, 400 MHz) ☐: 5.98 (bs, 1H), 5.53 (dd, 1H, J=8.4, 2.9), 5.42 (d, 1H, J=2.9), 5.18-5.09 (m, 2H), 4.25 (dd, 1H, J=12.5, 2.9), 4.08 (dd, 1H, J=12.4, 5.7), 3.96-3.87 (m, 2H), 3.68 (ddd, 1H, J=12.4, 6.5, 2.9), 3.48-3.33 (m, 2H), 2.14, 2.08, 2.05, 2.02 (4s, 12 H); ^{13}C NMR (CDCl$_3$, 101 MHz) δ: 173.2, 172.3, 171.0, 171.0, 105.2, 73.1, 70.3, 69.5, 68.6, 68.0, 62.1, 50.7, 21.8, 21.2, 21.2, 20.7; Exact mass Calcd for C$_{16}$H$_{24}$N$_4$O$_9$: 416.38; found m/z (M + H) 417.39.

6.1.3 C-Glycosides

Glucose and galactose *C*-glycosides were obtained from the corresponding methyl-☐-D-2,3,4,6-tetra-*O*-benzyl-glycopyranoside, in a three steps sequence, involving the acid-catalysed *C*-glycosylation reaction with allyltrimethylsilane and boron trifluoride etherate in dry acetonitrile to compound **3.16** (*a,b*),[164] followed by regiospecific hydroxylation with 9-BBN to the primary alcohol **3.17** (*a,b*),[165] and final oxidation with TEMPO[166] to the corresponding carboxylic acid **2.11** and **2.12**[2,](**Scheme 3.1**).

On the other hand, fucose *C*-glycoside was obtained from 2,3,4-tri-O-benzyl-L-fucopyranose as reported in the literature.[167] Introduction of the required carboxylic function was performed with the same

reaction sequence as described before affording acid **2.13**[168] (**Scheme 3.2**).

6.1.3.1 Synthesis

General procedure for hydroboration reaction: To a stirred solution of ☐-allyl-*C*-glycoside (1.090 mmol) in anhydrous THF (3 ml) at 0ºC and under argon was added a 0.5 M solution of 9-BBN in THF (6.6 mL, 3.3 mmol) via a syringe. The solution was allowed to warm to room temperature. After 2h the reaction mixture had cooled to 0°C, 0.186 mL ethanol was added, dropwise, followed by 0.478 mL of NaOH 4M. The solution was cooled to 0ºC, and 35% hydrogen peroxide (0.478 ml) was added, dropwise, then to the resulting suspension was added brine and diethyl ether. The organic layer was collected, and the brine layer was re-extracted, carefully, into further diethyl ether. All organic layers were combined, washed with brine, dried and concentrated under vacuum to afford the corresponding primary alcohol.

General procedure for TEMPO oxidation: To a stirred suspension of primary alcohol (1.131 mmol) in $NaHCO_3$ saturated solution (2.268 mL), were added a 0.5 M solution of KBr in H_2O (0.454 mL, 0.227 mmol) and a 0.1 M solution of TEMPO in CH_3CN (2.27 mL, 0.227 mmol). NaOCl (5.83 mL, 0.35 M) was added dropwise. The aqueous layer was acidified with 5 mL of HCl 5% and extracted five times

with EtOAc. The organic layer was dried on sodium sulfate, filtered and concentrated under vacuum to afford the corresponding carboxylic acid.

6.1.3.2 Characterization

Selected NMR data for compound **3.17a**:[2] ^{1}H NMR (400 MHz, CDCl$_3$): δ = 1.65 (app sex, 2 H, J = 6.8 Hz), 1.79 (m, 2 H), 1.94 (brs, 1 H), 3.55 (m, 2 H), 3.66 (m, 4 H), 3.77 (m, 2 H), 4.05 (m, 1 H), 4.47 (app t, 2 H, J = 12.4 Hz), 4.60 (d, 1 H, J = 12.4 Hz), 4.61 (d, 1 H, J = 12.0 Hz), 4.70 (d, 1 H, J = 11.6 Hz), 4.80 (app t, 2 H, J = 10.8 Hz), 4.92 (d, 1 H, J = 11.2 Hz), 7.10-7.15 (m, 2 H), 7.20-7.31 (m, 18 H).

Selected NMR data for compound **3.17b**:[2] ^{1}H NMR (500 MHz, CDCl$_3$): δ = 1.61 – 1.64 (m, 3 H), 1.72 (m, 1 H), 2.27 (br s, 1 H), 3.57 – 3.64 (m, 2 H), 3.65 – 3.70 (m, 1 H), 3.74 (dd, 1 H, J = 3.0, 7.5 Hz), 3.83 (m, 2 H), 3.98 (t, 1 H, J = 3.0 Hz), 4.00 – 4.03 (m, 2 H), 4.48 (d, 1 H, J = 12.0 Hz), 4.54 (app d, 2 H, J = 12.0 Hz), 4.58 (d, 1 H, J = 11.5 Hz), 4.65 (app d, 2 H, J = 12.5 Hz), 4.74 – 4.77 (m, 2 H), 7.28 – 7.35 (m, 20 H).

Selected NMR data for compound **3.19**: [169] ^{1}H NMR (500 MHz, CDCl$_3$): δ = 1.29 (d, 3 H, J = 6.6 Hz), 1.60 (m, 4 H), 2.05 (brt, 1 H, J = 5.6 Hz), 3.61 (m, 2 H), 3.77 (m, 3 H), 3.97 (m, 2 H), 4.49 – 4.78 (m, 6 H), 7.26 – 7.37 (m, 15 H).

Selected NMR data for compound **3.11**:[2] ^{1}H NMR (300 MHz, CDCl$_3$): δ = 2.06 (m, 2 H), 2.52 (m, 2 H), 3.65 (m, 2 H), 3.75 (m, 2 H), 3.88 (m, 2 H), 4.05 (m, 1 H), 4.49 (d, 1 H, *J* = 10.8 Hz), 4.52 (d, 1 H, *J* = 12.3 Hz), 4.64 (d, 1 H, *J* = 12.3 Hz), 4.66 (d, 1 H, *J* = 11.4 Hz), 4.72 (d, 1 H, *J* = 11.7 Hz), 4.83 (d, 1 H, *J* = 10.8 Hz), 4.84 (d, 1 H, *J* = 10.8 Hz), 4.96 (d, 1 H, *J* = 10.8 Hz), 7.13 (m, 2 H), 7.20-7.35 (m, 18 H).

Selected NMR data for compound **3.12**: [2] ^{1}H NMR (400 MHz, CDCl$_3$): δ = 1.95 – 2.20 (m, 2 H), 2.37 – 2.44 (m, 1 H), 2.49 – 2.57 (m, 1 H), 3.65 – 3.69 (m, 1 H), 3.76 – 3.83 (m, 2 H), 3.91 (m, 1 H), 4.02 – 4.06 (m, 3 H), 4.48 – 4.63 (m, 4 H), 4.67 – 4.86 (m, 4 H), 7.32 – 7.36 (m, 20 H).

Selected NMR data for compound **3.13**:[5] ^{1}H NMR (400 MHz, CDCl$_3$): δ = 1.85 (d, 3 H, *J* = 6.5 Hz), 2.42 – 2.69 (m, 2 H), 2.92 – 3.10 (m, 2 H), 4.33 – 4.39 (m, 2 H), 4.49 (brs, 2 H), 4.64 (dt, 1 H, *J* = 3.7, 7.8 Hz), 5.15 – 5.43 (m, 6 H), 7.85 – 8.01 (m, 15 H).

6.2 Materials

6.2.1 Hydroxyapatite 3D: sample molecules

Water unsoluble molecules (compounds 2.1-2.2)

A sample of HA-COOH (COOH functionalized hydroxyapatite) was immersed in dry dimethylformamide (DMF, 1 mL), containing DCC (dicyclohexyl-carbodiimide, 0.5 M) and *N*-hydroxysuccinimide (NHS, 0.5 M), and carboxylic groups were activated as succinimidyl esters, as depicted in Scheme 2.1. The mixture was stirred under argon atm for 2 h, then the liquids removed and the scaffold washed with fresh DMF. A 0.5 M solution in dry DMF (1 mL) containing the biomolecule was added to the scaffold and the suspension was stirred for 24 h. The scaffold was thoroughly washed with ethyl acetate (EtOAc) and subsequently petroleum ether, and finally dried under vacuum overnight.

Water soluble molecule (compound 2.3)

The scaffold HA-COOH was immersed in distilled H_2O containing 1-ethyl-3-(3-dimethylaminopropyl)carbodiimide (EDC, 0.5 M) and *N*-hydroxysuccinimide (NHS, 0.5 M) and carboxylic groups were activated as succinimidyl esters, as depicted in Scheme 2.1). The suspension was stirred for 2 h, then the liquids removed and the scaffold washed with fresh distilled H_2O. A 0.5 M solution in distilled

H$_2$O (1 mL) containing the biomolecule was added to the scaffold and the suspension was stirred for 24 h. The scaffold was thoroughly washed with water, then ethanol (EtOH) and finally dried under vacuum overnight.

6.2.2 Hydroxyapatite 3D: CNP

The scaffold HA-COOH was immersed in distilled H$_2$O containing 1-ethyl-3-(3-dimethylaminopropyl)carbodiimide (EDC, 0.5 mM) and *N*-hydroxysuccinimide (NHS, 0.5 mM) and carboxylic groups were activated as succinimidyl esters, as depicted in Scheme 2.2. The suspension was stirred for 2 h, then the liquids removed and the scaffold washed with fresh distilled H$_2$O. A 0.5 mM solution in distilled H$_2$O (1 mL) containing the bifunctional peg was added to the scaffold and the suspension was stirred for 24 h. The scaffold was thoroughly washed with water, and finally dried under vacuum overnight. Pegylated scaffold was immersed in distilled distilled H$_2$O containing 1-ethyl-3-(3-dimethylaminopropyl)carbodiimide (EDC, 0.5 mM) and *N*-hydroxysuccinimide (NHS, 0.5 mM) and carboxylic groups were activated as succinimidyl esters, as depicted in Scheme 2.2.. The suspension was stirred for 2 h, then the liquids removed and the scaffold washed with fresh distilled H$_2$O. A 0.5 mM solution in distilled H$_2$O (1 mL) containing the CNP peptides was added to the scaffold and the suspension was stirred for 24 h. The scaffold was

thoroughly washed with water, and finally dried under vacuum overnight.

6.2.3 Hydroxyapatite granules: Pegylation

General. Chemicals were purchased by Sigma-Aldrich or Merck and used without any further purification. Concanavalin A was purchased by Invitrogen. Solvents were dried over molecular sieves, for at least 24 h prior to use. When dry conditions were required, the reaction was performed under Ar atmosphere.

Difunctionalised triethylene glycol was synthesised according to Bertozzi et al.[13]

The propargyl □-glucoside was obtained in one step following a published procedure on fully deprotected glucose.[22] Activation of 4 (79 mg, 0.42 mmol) was performed by DIC (185 mg, 1.47 mmol) in dry THF (1.23 mL) for 2 h. The solution containing activated 4 was used directly for HA functionalisation.

6.2.3.1 HA decoration. Hydroxyapatite granules (0.2 g) were suspended in the solution containing activated **2.10** in dry THF and kept stirring for 12 h at room temperature; the quantity of **2.10** was calculated in order to have 0.24 mol of reactant *per* 100 g of HA granules.[12] Finally, the solvent was removed by filtration and HA washed vigorously with THF, MilliQ water and acetone.

Click reaction was performed using 0.03 M stock solutions of propargyl ☐-d-glucopyranoside, $CuSO_4 \cdot 5H_2O$ and sodium ascorbate in milliQ water. The cupric sulfate solution (0.100 mL, 0.003 mmol, 5% in respect to the saccharide) and the ascorbate solution (0.300 mL, 0.009 mmol, 15 mol % in respect to the saccharide) were pre-mixed and stirred until obtaining yellow solution. The yellow solution was then added to the HA-N_3 suspended in the saccharide solution (2 mL, 0.06 mmol). The reaction was stirred at room temperature for 24 hours, then the solvents removed by filtration and the material washed vigorously with MilliQ water and acetone. In order to avoid the non-specific adsorption of **2.10** on the HA surface, the samples were soaked in MilliQ water for 1 h at room temperature and then washed again, with MilliQ water and acetone, and finally dried at room temperature.

6.2.3.2 Lectin binding assay. Glucosylated HA (HA-Glc) was exposed to a solution containing lectin (20 μg mL^{-1}) in phosphate-buffered saline (PBS) for 60 min at room temperature followed by successive rinses in PBS, phosphate buffered saline diluted to 50% v/v with deionized water, and twice with deionized water.[170]

6.2.4 HA granules Silanization

General. All solvents were dried over molecular sieves, for at least 24 h prior to use. When dry conditions were required, the reaction was

performed under Ar atmosphere. Thin-layer chromatography (TLC) was performed on silica gel 60F$_{254}$ coated glass plates (Merck) with UV detection when possible, charring with a conc. H$_2$SO$_4$/EtOH/H$_2$O solution (10:45:45 v/v/v), or with a solution of (NH$_4$)$_6$Mo$_7$O$_{24}$ (21 g), Ce(SO$_4$)$_2$ (1 g), conc. H$_2$SO$_4$ (31 mL) in water (500 mL) and then heating to 110°C for 5 min. Flash column chromatography was performed on silica gel 230-400 mesh (Merck). All reported compounds have been previously synthesised and characterized; here we present only selected NMR data.

6.2.4.1 Hydroxyapatite functionalization (via APTES)

General procedure for grafting hydroxyapatite : granules were heated at 160°C for 24 h and under vacuum at room temperature to remove any water attached to the surface. Silanisation of hydroxyapatite was carried out by immersing 0.400 mg of granules in a 1 M solution of APTES (0.900 mL, 3.846 mmol) in anhydrous hexane (4 ml; 1 ml of APTES solution *per* 0.1 g of hydroxyapatite) for 3 h while stirring. The resulting suspension was washed with EtOAc and hexane several times and granules were dried at mild heat under vacuum for 24 h. Carbohydrates were finally supported on hydroxyapatite samples (–NH$_2$ functionalised, CHA-APTES, see Scheme 2.5 in the main text) as follows: a 0.065 M solution of compounds 2.1**1**-1**3** in dry THF was prepared (1 ml of solution *per* 0.1 g of hydroxyapatite), then NHS (5 equiv based on the carbohydrate) and DIC (5 equiv based on the carbohydrate) were sequentially added. The mixture was stirred for 1

145

hour, then added to CHA-APTES. The suspension was stirred overnight, then the functionalized CHA (CHA-2.11, CHA-2.12 and CHA-2.13 respectively) was washed thoroughly with EtOAc and hexane and finally essicated under vacuum.

6.2.5 Polypropylene

6.2.5.1. Preparation of the triflyl azide stock solution

After sodium azide (68 mg, 1.05 mmol) was dissolved in water (0.175 mL), then an equal volume of toluene was added (0.175 mL) was added. The biphasic mixture was cooled to 0° C under vigorous stirring and triflic anhydride (0.089 mL, 0.525 mmol) was added dropwise; the mixture was kept under vigorous stirring for further 30 min at 0° C, then temperature was raised to 10° C, and kept stirring for additional 2 h. A satd aq. solution of $NaHCO_3$ was added dropwise until gas evolution had stopped. The two phases were separated and the aqueous layer was extracted twice with toluene (2 x 0.175 mL). The combined organic layers gave a stock TfN_3 solution that was used directly in the subsequent diazo transfer reaction.

6.2.5.2. Typical procedure for the diazo transfer reaction

The reactions were carried out in a monophasic solvent mixture of H_2O/TfN_3 in Toluene/MeOH 1/1.7/6.7. The total volume used was 1.4

mL (0.150 mL/0.250 mL/1 mL), determined in order fully cover the polypropylene membrane, fitted in a 2 mL screw capped vial. Thus the amino functionalised PP membrane (1.1 cm x 0.26 cm) was suspended 0.150 mL of milliQ water containing $NaHCO_3$ (39 mg, 0.465 mmol) and $CuSO_4 \cdot 5H_2O$ (1.1 mg, 0.005 mmol); triflic azide stock solution (0.250 mL) was added, followed by the addition of methanol (1 mL). The blue mixture was mechanically stirred at room temperature for 24 h. Then the solvents were removed and the azido membrane was sequentially washed with toluene, water and methanol and finally dried at 50° for 10 min.

6.2.5.3. Click reaction

0.01 M stock solutions of propargyl 2-acetamido-2-deoxy-□-D-glucopyranoside, $CuSO_4 \cdot 5H_2O$ and sodium ascorbate were prepared in milliQ water. The cupric sulfate solution (5 mol % in respect to the saccharide, 0.040 mL, 0.0004 mmol) and the ascorbate solution (15 mol % in respect to the saccharide, 0.120 mL, 0.0012 mmol) were pre-mixed and stirred until obtaining yellow solution. The yellow solution was then added to the azido-PP membrane suspended in the saccharide solution in (0.800 mL, 0.008 mmol) in a screw cap vial. The reaction was stirred at room temperature for 24 hours, then the solvents were removed and the membrane was thoroughly washed with water and methanol and finally dried at 50° for 10 min.

6.2.6 Polycaprolactone

6.2.6.1 PCL: one step procedure

Aminolysis was conducted by immersing the PCL scaffold in 0.500 mL of 0.5 M glucosamine solution in milliQ water containing and NaHCO$_3$ (1 eq). The suspension was stirred for 30 min at 37° C. After aminolysis treatment, the samples were washed with 0.500 mL of deionized water 5 times x 10 min. Subsequently, the samples were dried in a vacuum desiccator at room temperature for 24 h.

6.2.6.2 PCL: functionalization via linker

- *Hexanediamine*

Aminolysis was conducted by immersing the PCL scaffold in a 10% (w/w) 1,6-hexanediamine solution under stirred for 30 min at 37° C. After aminolysis treatment, the samples were washed with 500 µL deionized water 5 times x 10 min. Subsequently, the samples were dried in a vacuum desiccator at room temperature for 24 h.

- *Cysteine*

Aminolysis was conducted by immersing the PCL scaffold in 0.500 mL of 0.5 M cysteine solution in milliQ water containing and NaHCO$_3$ (2 eq). The suspension was stirred for 30 min at 37° C. After aminolysis treatment, the samples were washed with 0.500 mL

of deionized water 5 times x 10 min. Subsequently, the samples were dried in a vacuum desiccator at room temperature for 24 h.

6.2.7 Collagen

6.2.7.1 Film Preparation

Insoluble collagen (3.5 g) (Opocrin, lotto 1028203) was soaked in 25 mL of H_2O. The mixture was homogenized in a Waring blender for 90 sec with ice cooling. 20 mL of this suspension was added per tissue culture Petri dish (Corning) and allowed to dry at room temperature, in hood to form a transparent film. The films were washed with and with distilled water and then dried in a hood.

6.2.7.2 Collagen treated surface functionalization

The film collagen-COOH was immersed in distilled H_2O containing 1-ethyl-3-(3-dimethylaminopropyl)carbodiimide (EDC, 0.5 M) and *N*-hydroxysuccinimide (NHS, 0.5 M) and carboxylic groups were activated as succinimidyl esters. The suspension was stirred for 30 min, then the liquids removed and the film washed with fresh distilled H_2O. A 0.5 M solution in CH_3CN (1 mL) containing dansyl hydrazine was added to the film and the suspension was stirred for 1 h. The scaffold was thoroughly washed with water, then ethanol (EtOH) and finally dried under hood overnight

6.2.8. Hybrid Materials

The reaction procedure for the synthesis of the hybrid organic/inorganic material 35wt% dPEG with 65 wt% SiO_2 is described below. The hybrid was produced with dPEG:GPTMS ratio 1:2 and ratio 1:4. All materials were purchased from Sigma-Aldrich.

6.2.8.1 Hybrid dPeg:GPTMS 1:2

Functionalization reaction

2g dPEG (1,333 mmol) was dissolved in 8 mL of distillated water under stirred. To the dissolved dPEG solution 0,619 mL of GPTMS (2,666 mmol) was added dropwise. Under stirred was added HCl 2N until pH 6. The solution was stirred for 2 h at room temperature.

Reaction of organic and inorganic

In a separate beaker 1,184 mL of deionised water, 0.394 mL of 1 N hydrochloric acid and 3,804 mL of tetraethyl orthosilicate (TEOS) were dissolved in order and left to react for 1 h. The reacted inorganic precursor solution was then added to the functionalised dPEG solution and left mixing for 2 h.

A 3.5 ml aliquot of this solution was poured into moulds (15 cc-29 d, 38 h, Teflon container) The samples were immediately sealed and transferred to a heated oven. The sealed samples were aged at 40 _C

for 3 days followed by opening the moulds to dry at 60 C until completely dry (8 days).

6.2.8.2 Hybrid dPeg:GPTMS 1:2

Functionalization reaction 1:4

2g dPEG (1,333 mmol) was dissolved in 8 mL of distillated water under stirred. To the dissolved dPEG solution 1,260 mL of GPTMS (5,332 mmol) was added dropwise. Under stirred was added HCl 2N until pH 6. The solution was stirred for 2 h at room temperature.

Reaction of organic and inorganic

In a separate beaker 1,184 mL of deionised water, 0.394 mL of 1 N hydrochloric acid and 3,804 mL of tetraethyl orthosilicate (TEOS) were dissolved in order and left to react for 1 h. The reacted inorganic precursor solution was then added to the functionalised dPEG solution and left mixing for 2 h.

A 3.5 ml aliquot of this solution was poured into moulds (15 cc-29 d, 38 h, Teflon container). The samples were immediately sealed and transferred to a heated oven. The sealed samples were aged at 40 _C for 3 days followed by opening the moulds to dry at 60 C until completely dry (8 days).

6.2.8.3 Characterization

Electron microscopy studies.

A LEO 1525 scanning electron microscope (SEM) equipped with a GEMINI field emissioncolumn was used to image the hybrid fracture surface. All samples were ground to powder in liquid nitrogen, mounted on sticky carbon tape and sputter coated with chromium to a maximum thickness of 15 nm before imaging. Images were collected on the in-lens secondary electron detector with an operating voltage of 5 kV and a working distance of 5–8 mm.

Scaffold compression testing

Compression testing (Instron 5866) was carried out on right parallel piped scaffolds with a width/thickness ratio of 2:1 (n=5). A 500 N load cell was used for testing, with a compression extension speed of 0.5 mmmin-1.

6.2.8.4 Reactivity of GPTMS as a function of pH

General methods

Reactions were carried out using commercially available starting materials and solvents without further purification.

NMR spectra were recorded at 400 MHz (^{1}H) and 100.6 MHz (^{13}C) on a Varian Mercury instrument. Chemical shifts are reported in ppm downfield from TMS as an internal standard; *J* values are given in

Hertz. For all compounds assignments of the ^{1}H NMR spectra were based on 2D proton–proton shift-correlation spectra.

132 mL of GPTMS are dissolved in 0,7 mL of a D_2O solution at pH 2, 5, 7, 9, 11 directly in the NMR tubes. GPTMS solutions were prepared using Deuterium cloride (35 wt% solution in D_2O, 99 atom %D) and Sodium deuteroxide (40 wt.% solution in D2O, 99.5 atom %D) until desired pH values.

The solution is stirred and a ^{1}H NMR and then a ^{13}C APT NMR spectra are recorded. The NMR tubes are kept, at room temperature, under gentle mixing and checked at different reaction's intervals.

[1] Ratner BD. and Bryant SJ (2004) Annu. Rev. Biomed. Eng. *6*, 41–75.
[2] Huebsch N and Mooney DJ (2009) Nature *462(7272)*, 426–432.
[3] Balasundaram G and Webster TJ (2006) J. Mater. Chem. *16* 3737–3745.
[4] Leeuwenburgh SCG et al (2008) Biomaterials *29* 3047–3052.

[5] Langer R and Tirrell D (2004) Nature *428*, 487-492.

[6] Yurchenco PD et al (1994) Eds. Extracellular Matrix Assembly and Structure (Academic, San Diego)

[7] van Hest JCM and Tirrell DA (2001) Chem. Commun. 19, 1897–1904.

[8] Bacáková L et al (2004) Physiol Res *53*, Suppl 1:S35-45.

[9] Gao J et al (2006) PNAS *103*, 16681-16686.

[10] Fan VH et al (2007) Stem Cells *25*, 1241-1251.

[11] Sahni A et al (1999) J Biol Chem *274*, 14936-14941.

[12] Gomez N et al (2007) Biomaterials *28*, 271-284.

[13] Alberti K et al (2008) Nat Methods *5*, 645-650.

[14] Daley WP et al (2008) J Cell Sci *121*, 255-264.

[15] Zagris N (2001) Micron *32*, 427.

[16] Gullberg D and Ekblom P (1995) Int. J. Dev. Biol. *39*, 845-854.

[17] Scott JE (1995) J. Anat. *187,* 259-269.

[18] Aumailley M and Gayraud B (1998) J. Mol. Med. *76*, 253-265.

[19] Wallner EI et al (1998) Am. J. Physiol. *275*, F467-477.

[20] Behonick DJ and Werb Z (2003) Mech. Dev. *120*, 1327-1336.

[21] Stevens MM et al (2005) Science *310* 1135-1138.

[22] Accouns of chemical research – Special Issue on Theranostic Nanomedicine 2011 *Volume 44*, 841-1134.

[23] Advanced Drug Delivery Reviews 62 (2010) 1052–1063 MacKay

[24] Wang AZ et al (2011) Annu. Rev. Med. doi: 10.1146/annurev-med-040210-162544.

[25] Xu T et al. (2007) Mat Sci Engin C *27*, 579–594.

[26] Langer K et al (2000) Journal Pharm Biopharm 303-307.

[27] Goddard JM and Hotchkiss JH (2007) Prog Pol Sci *32*, 698-725.

[28] Whittlesey KJ and Shea LD (2004) Exp Neurol *190*, 1-16. Simmons CA et al (2004). Bone *35*, 562-569. Kroese-Deutman et al (2005) Biomaterials *26*, 1131–1138.

[29] Lutolf MP 2003. Cell responsive synthetic hydrogels. *Adv. Mater.* 15, 888-892.

[30] Zhang, Y et al. (2000). J. Neurosci. *20*, 5671–78.

[31] Kuhl PR and Griffith-Cima LG (1996). Nat. Med. *2*, 1022–1027.

[32] Kirkwood K. et al (2003). J. Oral Implantol. *29*, 57–65.

[33] Karageorgiou V et al (2004). J. Biomed. Mater. Res. A *71*, 528–37.

[34] Zisch AH. et al (2003). FASEB J. *17*, 2260–2262.

[35] Lee AC et al (2003). Exp. Neurol. 184, 295–300.

[36] Taylor SJ and McDonald JW (2004). J. Control. Release *98*, 281-94

[37] Seliktar D et al (2004) J. Biomed. Mater. Res. A *68*, 704–716.

[38] Dinbergs ID et al (1996). J. Biol. Chem. 271, 29822–29829.

[39] Hersel U (2003) Biomaterials *24*, 4385-415.

[40] La Ferla B.et al (2009) Synlett *14*, 2325–2327.

[41] Dubruel P. et al (2006). Surface Science *600*, 2562-2571.

[42] Xu T et al (2007) Mat Science Engin *27*, 579-594.

[43] Favia P et al (2002) J Photopolym Sci Technol *15*, 341-350.

[44] Lutolf MP and Hubbel JA (2005) Nature Biotech, *23*, 47-55.

[45] Stoop R. (2008) Injury 39, 77-87

[46] Singh A and Elisseeff J (2010) J. Mater. Chem., 2010, 20, 8832-8847.

[47] Zanini S et al (2009) Chem. Plasma Process. 29, 535–547.

[48] Ivanov et al (1996)Surf. Interf. Anal. 24, 251–262

[49] Pimentel E (1994) Handbook of growth factors. Boca Raton, FL: CRC Press

[50] Nakajima N and Ikada Y (1995) Bioconj. Chem. *6*, 123–130.

[51] Neises and Steiglich W (1990) Org. Synth. Coll. *7*, 93–95

[52] Cipolla L et al (1997) J. Org. Chem. 62, 6678.

[53] Zurlinden K et al (2005) Mat wiss u Werkstoff tech *36*, 820-827.

[54] Baeza A et al (2010) Acta Biomater *6*, 743-749.

[55] Bertozzi CR and Bednarski MD (1991) J. Org. Chem. *56*, 4326-4329.

[56] Bragd PL et al (2004) Topics Catal. *27*, 49-66.

[57] Moses JE and Moorhouse AD (2007) Chem. Soc. Rev. *36*, 1249-1262.

[58] Tornoe CW et al (2002) J. Org. Chem.*67*, 3057-3064.

[59] Nandivada H et al (2007) Adv. Mater. *19*, 2197-2208.

[60] Fournier D et al (2007) Chem. Soc. Rev. 36, 1369-1380.

[61] Damiron D et al (2009) J. Polym. Sci. Part A: Polym. Chem. *47*, 3803-3813.

[62] Cummins D et al (2009) Soft Matter *5*, 804-811.

[63] Dirks AJ et al (2007) QSAR Comb. Sci. *26*, 1200-1210.

[64] Shaikh, N.; Russo, L.; Cipolla, L.; Nicotra, F.(2010) Mol. Diver. DOI: 10.1007/s11030-010-9281-9282.

[65] Susi H and Byler DM (1986). Methods Enzymol. *130,* 290-311.

[66] Kolb HC et al. (2001) Angew. Chem. Int. Ed. *40*, 2004-2021.

[67] Nandivada H et al (2007*)* Adv. Mater 19, 2197-2208.

[68] Fournier D et al (2007) Chem. Soc. Rev *36*, 1369-1380.

[69] Remzi Becer C et al (2009) Angew. Chem. Int. Ed. *48*, 4900-4908.

[70] Moses JE and Moorhouse AD (2007) Chem. Soc. Rev. *36*, 1249-1262.

[71] Tornoe CW et al (2002) J. Org. Chem. *67*, 3057.

[72] Iha RK et al (2009) Chem. Rev. *109*, 5620-5686.

[73] Vogt AP and Sumerlin BS (2010) Macromolecules 43, 1-13.

[74] Damiron D et al. (2009) J. Polym. Sci. Part A: Polym. Chem. *47*, 3803-3813.

[75] Cummins D et al (2009) Soft Matter *5*, 804-811.

[76] van Delft FL et al (2007) QSAR Comb. Sci *26*, 1200-1210.

[77] Tsarevsky NV (2010) J. Polym. Sci. Part A: Polym. Chem. 48, 966-974 .

[78] Akhrass S et al (2009) Soft Matter *5*, 586-592.

[79] Lutz JF et al (2009) Macromol. Rapid Commun. *26*, 514-518.

[80] Lee RS and Huang YT J. (2008) Polym. Sci. Part A: Polym. Chem. *46*, 4320-4331.

[81] Tsarevsky NV et al (2007) Macromolecules *40*, 4439-4445.

[82] Siow, KS et al (2006) Plasma Process. Polym. *3*, 392-418.

[83] Desmet T et al (2009) Biomacromol. *10*, 2351.

[84] Zanini S et al (2007) Plasma. Chem. Plasma. Proc. *27*, 446-457.
[85] Zanini S et al (2010) J. Colloid. Interface Sci. 341, 53-58.
[86] Riccardi C et al (2010) New J. Phys. *12*, 073008.
[87] Borcia G et al (2003) Plasma Sources Sci. Technol. *12*, 335-344.
[88] Borcia G et al (2004) Appl. Surf. Sci. *221*, 203-214.
[89] Morent R et al (2008) Surf. Interface Anal. *40*, 597-600.
[90] De Geyter N et al (2008) Surf. Interface Anal. *40*, 608-611.
[91] Morent R et al (2008) Surf. Coat. Technol. 202, 3427-3449.
[92] De Geyter N et al (2007) Surf. Coat. Technol. *201*, 7066-7075.
[93] Titz A et al (2006) Tetrahedron Lett. *47*, 2383-2385.
[94] van Dongen SFM et al (2009) Bioconj. Chem. *20*, 20-23.
[95] Ghasemi M et al (2007) Langmuir *23*, 11554-11561.
[96] Wang MJ et al (2003) Langmuir *19*, 8325-8320.
[97] Ivanov VB et al (1996) Surf. Interface Anal. *24*, 257-262.
[98] Siow KS et al (2006) Plasma Process. Polym. *3*, 392-418.
[99] Radhakrishnan C et al (2006) Langmuir *22*, 5018-5024.
[100] Esaki K et al (2009) Biomacromol. *10*, 1265-1269.
[101] Acharya C et al (2008) Biomaterials 29, 4665-4675.
[102] Raman R et al (2005) Nat. Methods *2*, 817-824.
[103] Harris LG et al (2009) J. Am. Chem. Soc. *131*, 7755-7761.
[104] Fukui S et al (2002) Nat. Biotechnol. *20*, 1011-1017.

[105] Yeoh KK et al (2009) Carbohydr. Res. *344*, 586-591
[106] Causa F et al (2010) Langmuir *26*, 9875–9884
[107] France RM and Short RD (1997) J. Chem. Soc., Faraday Trans. *93*, 3173–3178.

[108]. Potter LR et al (2009) Handb Exp Pharmacol 341-366.
[109]. Sudoh T (1998) Nature *332*, 78–81.
[110]. Sudoh T (1990) Biochem Biophys Res Commun *168*, 863–870.
[111]. Woods A et al (2007) Endocrinol *148*, 5030–5041.
[112]. Schweitz H et al (1992) J Biol Chem *267*, 13928–13932.
[113]. Potter LR et al (2006) Endocr Rev 2006, *27*, 47–72.
[114]. He XL et al (2006) J Mol Biol *361*, 698–714.
[115]. Potter LR (2005) Front Biosci *10*, 1205–1220.
[116]. Anand-Srivastava MB (2005) Peptides *26*, 1044–1059.
[117]. Olney RC (2006) Growth Horm. IGF. Res. *16*, Suppl. A, S6–14.
[118]. Pejchalova K et al (2007) Mol Genet Metab *92*, 210–215.
[119]. Teixeira CC (2008) Dev Biol *319*, 171–178.
[120]. Candace YW (2007). Heart Fail Rev *12*, 131–142.
[121]. Gardner DG et al (2003) Trends Endocrinol Metab *14*, 411–416.
[122]. Golembo M et al (2008) US 2008/0194682.
[123] Shaikh N et al (2010) Pept Sci. *94* 213–219.
[124] Moffatt P and Thomas GP (2009) Cell Mol Life Sci *66*, 1135–1139.

[125] Papaleo E et al (2010) J. Mol. Graph. Model. 28, 834-841.

[126]. Franceschi RT et al (1985) J Cell Physiol 123, 401–409.

[127]. Rodan SB et al (1987) Cancer Res *47*, 4961–4966.

[128]. Revazova ES et al (1988) Exp Biol Med *106*, 471–472.

[129]. Schedlich LJ et al (2007) Mol Endocrinol *21*, 2378–2390.

[130]. Nishida Y et al (2005) Exp Cell Res *307*, 194–203.

[131]. Takarada M et al (1996) *63*, 375–386.

[132]. Hosono K et al (2007) Am J Pathol *171*, 274–286.

[133]. Franz-Odendaal T., et al (2006) Develop Dynam *235*, 176–190.

[134]. Suda M et al (1998) Proc Natl Acad Sci USA *95*, 2337–2342.

[135]. Yasoda A et al (2004) Nat Med *10*, 80–86.

[136]. Mackie EJ and Ramsey SJ (1996) Cell Sci *106*, 1597–1604.

[137]. Suda M et al (1999) Calcif Tissue Int *65*, 472–478.

[138] Alan T and Tufan AC (2008) J Cell Biochem *105*, 227–235.

[139] Agui T (1992) Endocrinology *130*, 2487–2494.

[140] Gabius HJ (2009) The sugar code: fundamentals of glycoscience. Ed Wiley-Blackwell.

[141] Moorhouse AD, Moses JE (2008). Chem Med Chem 3, 715–723.

[142] a) Sun X-L et al (2006) Bioconj Chem 17, 52-57; doi: 10.1021/bc0502311 b) Devaraj NK et al (2005) J Am Chem Soc *127*, 8600-8601; c) Collman J et al (2004) Langmuir 20, 1051-1053. d) Lummerstorfer T and Hoffmann H (2004) J Phys Chem B 108, 3963-3966.

[143] Hölemann A and Seeberger PH (2004) Curr Opin Biotechnol *15*, 615–622

[144] a) Bornaghi LF and Poulsen S-A (2005) Tetrahedron Lett *46*, 3485–3488. b) Kappe CO (2004) Angew Chem Int Ed *43*, 6250–6284; (c) Heard DD and Barker R (1968) J Org Chem *33*, 740–746; d) Ferrier RJ and Hatton LR (1968) Carbohydr Res 6, 75–86; e) Freudenberg K (1966) Adv Carbohydr Chem. *21*, 2–38.

[145] Ferrières V et al (1995) Tetrahedron Lett *36*, 2749-2752.

[146] Sanki AK and Mahal L (2006) Synlett 455-459.

[147] Roy B and Mukhopadhyay B (2007) Tetrahedron Lett *48*, 3783–3787.

[148] Yeoh KK et al (2009) Carbohydr Res *344*, 586–591.

[149] Miller N (2010) Org Lett *12*, 1375-1376.

[150] Liu CZ and Czernuszka JT (2007) Mater. Sci. Technol. *23*, 379–391 b) Jones JR et al (2006) Biomaterials 27, 964–973. c) Jones JR et al (2006) *Philos. Trans. R. Soc., A, 364*, 263–281.

[151] Place ES et al (2009) Chem.Soc. Rev. *38*, 1139–1151. b) Place ES et al (2009) Nat. Mater *8*, 457–470.

[152] Poologasundarampillai G et al (2010) J. Mater. Chem., 2010, 20, 8952-8961

[153] Hench LL et al.(2002) Science *295*, 1014-1017.

[154] Jones JR et al (2006) Biomaterials *27*, 964-973.

[155] Valliant EM and Jones JR (2011) Soft Matter *7* 5083 - 5095.

[156] Mahony O et al (2010) Advanced Functional Materials *20*, 3835-3845

[157] Innocenzi P and Kidchob T (2005) Journal of Sol-Gel Science and Technology *35*, 225-235.
[158] Robertson MA et al (2003) J Sol-Gel Sci Tech, *26,* 291.
[159] Costa E et al (2008) J Mater Sci *43*, 494–502.
[160] John C (2000) Encyclopedia of Analytical Chemistry R.A. Meyers (Ed.) 10815–10837**.**
[161] Sanchez G et al (2001) Chem. Mater. *13* 3061–3083. b) Livage J and Sanchez C (1992) J. Non-Cryst. Solids *145*, 11–19.
[162] Kelts LW and Armstrong NJ (1989) J. Mater. Res. 423–433.
[163] Maly M (2008) Molecular Simulation *34*, 1215–1236.
[164] Hosomi A et al (1984) Tetrahedron Lett *22***,** 2383.
[165] Cook BN et al (2000) J. Am. Chem. Soc. *122*, 8612-8622.
[166] Huang L et al (2006) Chem. Eur. J. *12*, 5246-5252.
[167] La Ferla B et al (2009) Tetrahedron: Asymm. *20*, 744-761.
[168] Tang PC et al (1996) Glycomed Inc. US5508387.
[169] Uchiyama T (1996) Bioorgan. Med. Chem. *4*, 1149-1165.
[170] Harris LG et al (2009) J. Am. Chem. Soc. *131*, 7755-7761.